Wind Power Plant Control Optimisation with Embedded Application of Wind Turbines and STATCOMs

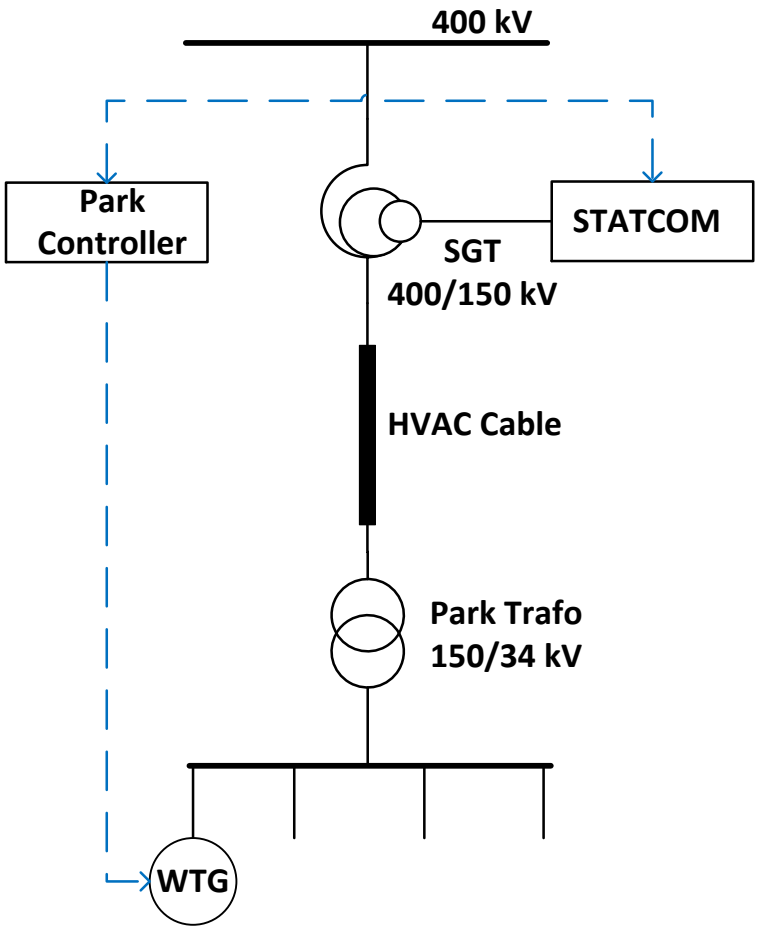

Master Thesis
EPSH4-1035 / WPS4-1056

DEPARTMENT OF ENERGY TECHNOLOGY
AALBORG UNIVERSITY

AALBORG UNIVERSITY
Department of Energy Technology
Pontoppidanstræde 101
DK-9220 Aalborg
Denmark
Web address: http://www.et.aau.dk

Printed in Denmark by UniPrint
ISBN: 978-87-92846-55-6

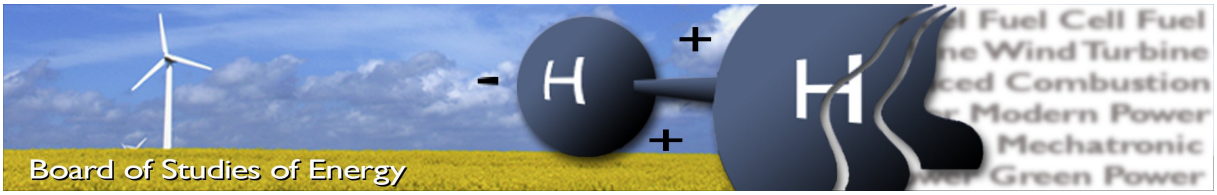

Title:	Wind Power Plant Control Optimisation with Embedded Application of Wind Turbines and STATCOMs
Semester:	10
Semester theme:	Master Thesis
Project period:	01/02/15 - 03/06/15
ECTS:	30
Supervisor:	Florin Iov
Project group:	EPSH4-1035 and WPS4-1056

Lennart Petersen

Fitim Kryezi

Copies:	7
Pages, total:	139
Appendix:	A-B
Supplements:	CD-ROM

SYNOPSIS:

The increasing tendency of installing larger wind power plants as replacement for conventional power generation into the power system leads to the responsibility of wind power plants to control the node voltages. The focus of this project is placed on the development of a wind power plant model for control analysis as well as the design and tuning process of one voltage control architecture. An exemplary wind power plant located in United Kingdom and the corresponding grid code requirements are used as a base case. First, various possible voltage control philosophes are investigated and their advantages and disadvantages characterized. Subsequently, small-signal models of a single wind turbine and the whole wind power plant are developed, being appropriate for voltage control assessment. The functionality of the wind turbine model is verified by means of Eigenvalue analysis and validated against numerical EMT simulations. The wind power plant model is validated by means of load flow simulations. The final design and tuning process of the voltage controller results in a guidance, proposed for this particular control architecture. It provides qualitative outcomes regarding the impact of system delays, grid conditions and various operating conditions of the wind power plant, with and without incorporation of STATCOMs.

Keywords: Wind turbine generator, Offshore wind power plant, Power system, Voltage control, State-space model, Grid codes

By signing this document, each member of the group confirms that all group members have participated in the project work, and thereby all members are collectively liable for the contents of the report. Furthermore, all group members confirm that the report does not include plagiarism.

Abstract

This thesis deals with the topic of voltage control assessment in large wind power plants, with the main focus on embedded application of both wind turbines and STATCOM.

The increasing amount of wind power generation in both transmission and distribution grids has forced the wind power plants to take over the past responsibility of conventional generation to control the node voltages adequately. This has also engaged different countries to tighten their grid codes requirements in this regard. Nowadays, voltage control at the point of common coupling of a wind power plant is realized by an overall controller which provides voltage or reactive power reference signals to the wind turbines. However, their contribution is limited due to reactive power capability limits and, in case of offshore wind power plants, large distances to the connection point. A way of dealing with this issue is by integrating fast acting devices such as STATCOMs, which are capable of supporting the voltage with fast dynamic responses.

Such sophisticated approach for voltage control requires high-performance and robust solutions, smoothly incorporating all plant controllers. It is important to investigate how the involved grid connected converters can be included to provide a stable control solution for different operational scenarios in order to fulfill the dynamic requirements. This aspect even reinforces the need of investigating the final tuning process and control philosophy adjustment, as the implementation of STATCOMs has not yet been investigated thoroughly in previous control studies regarding wind power plants.

Consequently, the first part of the studies focuses on the possible voltage control philosophes in wind power plants. In form of a state-of-the-art analysis, various architectures for different control levels such as main controller, dispatch function and wind turbine controller are investigated and their advantages and disadvantages emphasized. It is ascertained that control performance is dependent on the overall coordination of those control levels with respect to factors such as grid code demands, grid stiffness, communication delays and integrated reactive power generating units. However, the selected control architecture for this study is based on a centralized system, where the voltage control is managed only on plant level and the wind turbines and STATCOMs regulate their reactive power supply to fulfill the central control target. The voltage at the point of common coupling is controlled

according to a slope characteristic and an additional reactive power control loop is applied for taking into account the reactive power losses within the plant.

The main body of the work is devoted to the model development of the whole wind power plant system being appropriate for control analysis, which is done without usage of already built-in models. A large focus is laid on the state-space representation of full-scale converter (type-4) wind turbines and STATCOMs, since they determine the most significant dynamics of the plant. It is proved by Eigenvalue analysis that only the dynamics of the outer reactive power controller are relevant with respect to the bandwidth of the overall voltage control. The model functionality is successfully validated against a numerical EMT model, with the outcome that the linearized state-space model provides adequate results, even in the case of larger reactive power changes. The small-signal model of the whole plant is successfully validated by means of load flow simulations, thus it delivers satisfying outcomes regarding the voltage states of the network. In this way, the dynamic behaviour within the wind power plant is assessable with respect to voltage control, which enables the implementation of various dispatch strategies to analyze reactive power contribution of the individual wind turbines and STATCOMs.

Finally, the design and tuning process of the plant voltage controller provides qualitative outcomes regarding the impact of system delays, grid conditions and various operating conditions of the wind power plant. Time delays caused by the communication network and control sampling deteriorate the control performance and can be improved sufficiently by use of predictive controllers. The influence on different grid stiffnesses needs to be studied in combination with the specified slope characteristic of the voltage controller, as both of them determine the open-loop gain of the control system and in this way the control performance regarding overshoot, rise and settling time. The time constant of the voltage controller should be selected according to the bandwidth of the remaining system in order to provide a decent response time. However, tendentially weak grids and flat slope characteristics complicate the fulfillment of overshoot and settling time requirement of the reactive power output response. In this case, enhancing the control time constant can compensate for those concerns, though the rise time demand will be the crucial criteria to bear in mind. Different operating conditions of the plant affect the control performance in minor ways, so that the tuning process should account some margins to ensure grid code compliance for all operating scenarios. However, it should be regarded for the control design and tuning whether voltage control is realized with or without STATCOMs, since both scenarios exhibit significant differences regarding overshoot of reactive power output.

All the observations made during the assessment studies are collected to provide a first guidance of how to design and tune the particular voltage control architecture considered in this study.

Preface and Acknowledgements

This project is written by the members of group EPSH4-1035 / WPS4-1056 as Master Thesis project at the Department of Energy Technology of Aalborg University. This document is a project report about wind power plant control optimisation with embedded application of wind turbines and STATCOMs. This project was proposed by the Danish energy company DONG Energy. It has been drawn up during the period of 1st February to 3rd June of 2015.

The results of this project will be used in the Danish *RePlan* project „Ancillary Services from Renewable Power Plants“ (PSO Project number: 2015-12347). The authors would

like to thank their supervisor from Aalborg University, **Florin Iov**, for all his guidance and support during this project. Furthermore, the authors express their appreciation and acknowledge the contribution of **Lukasz Hubert Kocewiak** and **Mikkel Peter Sidoroff Gryning** from DONG Energy in providing data and feedback during this project.

Following software tools are used in order to accomplish this project:

- PowerFactory - for power flow simulations
- MATLAB - for small-signal and control analysis
- PLECS - for EMT simulations

Reader's guide: The used information to accomplish this project has been found in literature, reports, web pages, lectures and information from the supervisor. Throughout the project it will be referred to these sources, which can be found in the Bibliography. The citation style is referred to the IEEE method, which puts the number of the reference in square brackets. Figures, equations and tables are labelled with the number of the chapters they are located at. The CD attached in the report contains the following: PDF version of project report, figures and references.

Contents

List of Figures

List of Tables

Nomenclature

Acronym	Description
AQR	Automatic Reactive Power Regulator
AVR	Automatic Voltage Regulator
CC	Current Control
CT	Current Transformer
ECS	Export Cables
FACTS	Flexible AC Transmission System
FRT	Fault Ride Through
GSC	Grid Side Converter
GT	Grid Transformer
HF	Harmonic Filters
HV	High Voltage
IGBT	Insulated Gate Bipolar Transistors
LV	Low Voltage
MIMO	Mulitple Input Multiple Output
MO	Modulus Optimum
MSR	Mechanically Switched Reactor
MV	Medium Voltage
NETS	National Electricity Transmission System
NGET	National Grid Transmission System
PCC	Point of Common Coupling
PF	Power Factor
PI	Proportional and Integral Controller
PMSG	Permanent Magnet Synchronous Generator
POC	Point Of Connection
RMS	Root Mean Square

Acronym	Description
SCR	Short-Circuit Ratio
SG	Synchronous Generator
SISO	Single Input Single Output
SO	Symmetrical Optimum
STATCOM	Static synchronous compensator
STG	Supergrid Transformers
SVM	Space Vector Modulation
TSO	Transmission System Operator
UK	United Kingdom
VSC	Voltage Source Converter
VT	Voltage Transformer
WPP	Wind Power Plant
WTG	Wind Turbine Generator

List of Symbols

Symbol	Description	Unit
Φ	Right eigenvectors of the system matrix	-
Ψ	Left eigenvectors of the system matrix	-
φ	Intermediate state variables	-
δ_{POC}	Voltage angle at POC	deg
δ_{PCC}	Voltage angle at PCC	deg
ζ	Damping ratio	-
λ	Eigenvalue	-
τ	Time constant	s
ω_b	Bandwidth angular velocity	$\frac{\text{rad}}{\text{s}}$
ω	Electrical angular velocity of grid voltage	$\frac{\text{rad}}{\text{s}}$
$\mathbf{A}$	System state matrix (state-space method)	-
$\mathbf{B}$	Input matrix (state-space method)	-
B_{shunt}	Shunt susceptance	S
B	Susceptance	S
$\mathbf{C}$	Output matrix (state-space method)	-
$\mathbf{D}$	Feed-forward matrix (state-space method)	-
f_b	Bandwidth frequency	Hz
$F_m(s)$	Transfer function of grid meter	-
$F_{AVR}(s)$	Transfer function of AVR	-
$F_{AQR}(s)$	Transfer function of AQR	-
$F_{del}(s)$	Transfer function of time delay	-
G	Conductance	S
G_p	Internal plant model of delay-free response	-
G_m	Gain margin	dB
$G_{Q^*_{WTG}Q_{WTG}}(s)$	Transfer function of WTG	-

Symbol	Description	Unit
$G_{Q_{out}^{WPP}Q_{PCC}}(s)$	Transfer function of WPP for AQR design	-
$G_{Q_{ref}^{WPP}V_{PCC}}(s)$	Transfer function of WPP for AVR tuning	-
i_{ACdq}	WTG dq-axis current	A
I	Identity matrix (state-space method)	-
$I_{q,ref}$	WTG q-axis current reference	A
$I_{d,ref}$	WTG d-axis current reference	A
I_{SG}	Output current of synchronous generator	A
I_{grid}	Short-circuit current of external grid	A
$\bar{I}_i$	Complex current injection to i-th bus of WPP	A
k_1, k_2	Coefficients for symmetrical optimum	-
K	Contribution factor for reactive power	-
K_{PO}	Slope gain of AVR	$\frac{\text{Mvar}}{\text{pu}}$
K_{FF}	Gain of AQR feed-forward loop	-
$K_{I,DC}$	Integral gain of DC voltage controller	$\frac{\text{A}}{\text{Vs}}$
$K_{P,DC}$	Proportional gain of DC voltage controller	$\frac{\text{A}}{\text{V}}$
$K_{I,Q}$	Integral gain of reactive power controller	$\frac{\text{A}}{\text{var·s}}$
$K_{P,Q}$	Proportional gain of reactive power controller	$\frac{\text{A}}{\text{var}}$
$K_{I,idq}$	Integral gain of current controller	$\frac{\text{V}}{\text{As}}$
$K_{P,idq}$	Proportional gain of current controller	$\frac{\text{V}}{\text{A}}$
K_p	Gain of AQR	-
K_{plant}	Plant gain	-
K_T	Open-loop gain of overall system	-
L	WTG series inductance	mH
OS	Overshoot	%
p_{ki}	Participation factors	-
P_i	Participation matrix	-
PF_{ref}^{TSO}	Power factor reference signal by TSO	-
P_{meas}^{WPP}	Measured WPP power factor	MW
P_{av}^{WTG}	WTG available active power	MW
P_{SG}	Active power output of synchronous generator	MW
P_{WTG}	Active power output of WTG	MW

Symbol	Description	Unit
P_{WPP}	Wind power plant active power output	MW
P_{copper}	Transformer copper losses	kW
P_m	Phase margin	°
Q_{ref}^{TSO}	Reactive power reference signal by TSO	Mvar
Q_{meas}^{WPP}	Measured WPP reactive power	Mvar
Q_{ref}^{WPP}	Reactive power reference signal by AVR	Mvar
Q_{out}^{WPP}	Reactive power reference signal by main controller	Mvar
Q_0	Reactive power offset of WPP	Mvar
$\triangle Q_m$	Reactive power correction of WPP model	Mvar
Q_{ref}^{WTG}	WTG reactive power reference signal	Mvar
Q_{av}^{WTG}	WTG available reactive power	Mvar
Q_{WTG}	Reactive power output of WTG	Mvar
Q_{PCC}	Reactive power output at PCC	Mvar
Q_{shunt}	Reactive power of shunt capacitor	Mvar
R_c	Core loss resistance of transformer	Ω
R_T	Short circuit resistance of transformer	Ω
R_{grid}	Grid resistance	Ω
SCR_{min}	Minimum short-circuit ratio	-
SCR_{max}	Minimum short-circuit ratio	-
S_r^{WTG}	WTG apparent power rating	MVA
S_{rT}	Transformer rated power	MVA
S_{grid}	Short-circuit power	MVA
t_d	Delay time	s
t_r	Rise time	s
t_s	Settling time	s
T_m	Time constant of grid meters	s
T_{com}	Communication delay	s
T_s	Sampling time	s
T_i	Time constant of AQR	s
T_{PO}	Time constant of AVR	s
T_1	Dominant time constant of WPP	s
u	Input vector (state-space method)	-

Symbol	Description	Unit
u_k	Short-circuit voltage of transformer	%
v_{ACdq}	dq-axis voltage at AC terminal of GSC	kV
v_{POCdq}	dq-axis voltage at POC	kV
V_{rT}	Rated voltage of transformer	kV
V_{ref}^{TSO}	Voltage reference signal by TSO	kV
V_{meas}^{WPP}	Measured WPP voltage	kV
V_{out}^{WPP}	Voltage reference signal by WPP main controller	kV
V_{ref}^{WTG}	WTG reference voltage	kV
V_{comp}	Compensator voltage of STATCOM	kV
V_{grid}	Grid voltage	kV
V_{DC}	DC-link voltage	kV
$\bar{V}_i$	Complex voltage at i-th busses of WPP	kV
ΔV_{SS}	Voltage deviation of state-space model	kV
ΔV_{LF}	Voltage deviation of load-flow simulation	kV
x	State vector (state-space method)	-
X_m	Magnetizing reactance of transformer	Ω
X_T	Short-circuit reactance of transformer	Ω
X_{grid}	Grid reactance	Ω
y	Output vector (state-space method)	-
Y_{ij}	Non-diagonal elements of network admittance matrix	-
Y_{ii}	Diagonal elements of network admittance matrix	-
Z_T	Short-circuit impedance of transformer	Ω
Z_{grid}	Short-circuit impedance of the external grid	Ω

1 Introduction

1.1 Background in Wind Power Plants

Traditionally the power is generated by large centralized power plants and is delivered to the customers throughout the transmission and distribution grids. However, in recent decades offshore wind power plants (WPPs) are replacing the conventional power generation. This has forced the wind power generation to take over the past responsibility of conventional generation to control the node voltages adequately, meaning that WPPs have to contribute to voltage control. This has also engaged different countries to tighten their grid codes requirements regarding voltage control to be handled by WPPs. The WPPs consist of a large number of wind turbine generators (WTGs) spread over a wide area resulting in different power contribution at the point of common coupling (PCC) due to different wind patterns, which affect the voltage levels. Furthermore, in case of offshore WPPs the distance between WTGs and PCC makes it difficult for the WTGs to contribute to voltage control.

Another major concern when interconnecting a WPP to the power grid is the dynamic stability [12]. In particular, the large penetration of fluctuating wind power generation poses challenges on small-disturbance voltage stability. A way of dealing with this issue is by integrating fast acting Flexible AC Transmission Systems (FACTS), especially Static Synchronous Compensators (STATCOMs), which are capable of supporting the voltage control at the PCC with fast dynamic responses [13, p, 348].

Nowadays, voltage control in WPPs is realized by an overall controller which receives either voltage or reactive power references from the Transmission System Operator (TSO) and provides these reference signals to the WTG units based on the mismatch of reference and measured voltage or reactive power at the PCC.

1.2 Problem Statement

As aforementioned the large penetration of wind power represents new challenges to project developers, WTG manufacturers and TSOs in order to provide robust voltage

control of WPPs connected to different networks within various grid code regimes. In particular, the dynamic requirements of controlling the voltage with a limited time delay, time response and overshoot pose challenges to large offshore WPPs, where the voltage regulating WTGs are located remotely to the PCC. It requires high-performance and robust solutions, smoothly incorporating all controllers within a WPP, which could be characterized by WTGs and possibly STATCOMs.

Hence, it is important to investigate how the involved grid connected converters can be incorporated to provide a stable control solution for different operational scenarios of the WPP in order to fulfill present grid code requirements. This aspect even reinforces the need of investigating the final tuning process and control philosophy adjustment, as the implementation of STATCOMs has not yet been investigated thoroughly in previous control studies of WPPs.

Factors such as grid stiffness, present communication delays and operational modes of the WPP affect the overall control performance, where flexible changes in control modes may benefit the WPP control performance. As United Kingdom (UK) is one of the emerging markets for offshore WPPs, exhibiting challenges due to possibly long cable connections and tendentially incorporating STATCOMs, the study applies the UK grid as a base case. [14]

1.3 Objectives

The previously outlined challenges lead to the following objectives acting as success criteria of this project.

1.3.1 Main Objectives

1. Investigation of possible voltage control philosophes in WPPs and evaluation of their advantages and disadvantages;
2. Model development of the whole WPP system being appropriate for small-signal analysis;
3. Definition of a guideline to design and tune the WPP controllers for incorporation of WTGs and STATCOM to provide a robust and flexible design, taking into account the specified grid code requirements

1.3.2 Tasks

In order to achieve each of the main objectives previously stated, it is necessary to first accomplish several tasks.

For the Main Objective 1:

- Perform state-of-the-art studies of typical WPP control strategies including various control layers within the WPP;
- Assess their advantages and disadvantages for various WPP configurations and control coordinations.

For the Main Objective 2:

- Determine the required specifications for modelling components and the whole system;
- Create a linearized model of the WPP network being applicable for analysis of control performance;
- Verify and validate the model performance with respect to the dynamic behaviour being relevant for assessing voltage control aspects.

For the Main Objective 3:

- Ascertain the relevant grid code requirements in UK and their impact on WPP control performance;
- Define simulation scenarios, test cases and their evaluation criteria;
- Design the components of one selected voltage control architecture taking into account specified design criteria;
- Tune the designed voltage controller with respect to the grid code requirements and selected test cases.

1.4 Scope and Limitations

As aforementioned in the problem statement, large WPPs become more complex in their design and structure, which increases the challenges regarding voltage control. The offshore WPP considered in the present work has a rated power of 210 MW and is connected to the transmission system at a voltage level of 275 kV. The layout is based on an existing WPP and it is equipped with two STATCOMs for reactive power support.

The PCC, which is the point where the power is exchanged with the grid, is in this study considered to be on the primary side of the super grid transformer (SGT), since it is the most common location.

The slope of the voltage controller is assumed to be fixed during the WPP operation, since this is normally defined by the TSO. If by any circumstances the TSO decides to change the slope, the controller should be capable to adapt to its changes by reparametrisation.

Node voltages are considered to be a local quantity, compared to frequency which has to be evaluated in global perspective. In this way, it is not possible to control certain node voltages from any point in the system and voltage control can only be achieved by reactive power compensation units in immediate surroundings. Thus, for the purpose of this project it is not necessary to represent the remote electrical network of the WPP connection, which means the external grid can be represented as Thevenin equivalent.

The corresponding grid impedance may suffer unexpected changes, hence the TSO normally provides a minimum and maximum short-circuit ratio SCR_{min} and SCR_{max} being valid for a particular point of connection.

The interaction between voltage controller and active power are not considered in this work, since active power is assumed to be constant during the occurrence of voltage disturbances. Furthermore, in this study only small disturbances are considered, which fall in the range of normal operating voltages of $\pm 10\,\%$. Abnormal conditions as occuring during faults are not part of this project's objectives.

Following limitations are stated for the project scope:

- The impact of neighbouring WPPs on the voltage control is not investigated;
- Voltage control interactions inside the WPP are not considered;
- The dynamic actions and control of mechanically switched devices are disregarded and assumed to operate in steady-state;
- Transient analyses are not performed, since the behaviour of large disturbances of the system is out of the scope. Hence, grid code requirements such as fault-ride through (FRT) are not taken into account;
- The network representation is assumed to be symmetric and balanced;
- The WPP consists of only type-4 WTGs, i.e. full-scale converter connected WTGs;
- The analysis is applied for the UK grid using the corresponding grid code which might differ from the requirements in other countries;

1.5 Content of Report

The chapters of this document present the following content:

Chapter 2: Wind Power Plant Reactive Power and Voltage Control Strategies This chapter gives a literature review of the main topics of this project in form of a state-of-the-art analysis. The technical coherences and present strategies regarding reactive power and voltage control in WPPs are outlined. Furthermore, a state-of-the-art regarding modelling of WPPs for control analysis is provided, as well as a brief introduction to the characteristics of a STATCOM regarding voltage control.

Chapter 3: Small-Signal Analysis Methodology This chapter introduces the methodology for small-signal analysis in form of a state-of-the-art analysis. Subsequently, the general approach for modelling and analysis of state-space systems is discussed and some performance criteria of small-signal analysis are explained.

Chapter 4: System Characterization This chapter is dedicated to the description of the studied WPP and to the definition of scenarios and evaluation criteria. The general requirements and specifications for different assessment studies are obtained through generic guidelines as well as the UK grid code.

Chapter 5: System Design The theory and assumptions for modelling the different components of the WPP are exposed in this chapter. The WTGs, STATCOMs, the network components such as cables, transformers and external grid as well as the WPP control are modelled according to the purpose of this study. Furthermore, a verification of the WTG model is conducted.

Chapter 6: Model Validation In this chapter a validation process of the small-signal models for WTG and WPP network, developed in chapter 5, is perfomed by means of existing reference models.

Chapter 7: Design and Tuning of Voltage Control This chapter deals with the design and subsequent tuning of the WPP voltage control. Subsequently, a performance analysis of voltage control is conducted to evaluate the influence of the SCR on the system behaviour. All observations are collected to provide a guidance how to design and tune the particular voltage control architecture considered in this study.

2 Wind Power Plant Reactive Power and Voltage Control Strategies

In this chapter the technical coherences and present strategies regarding reactive power and voltage control in WPPs are outlined. First, in section 2.1 an overview of the different WPP control levels is provided. In section 2.2 the state-of-the-art of various architectures for the WPP main controller is summarized by recent publications, likewise for the dispatch function block in section 2.3. Present control strategies on the WTG level are presented in section 2.4, before it is elaborated on the coordination of the different WPP control levels in section 2.5. Section 2.6 provides the state-of-the-art regarding modelling of WPPs for control analysis and section 2.7 finally introduces the characteristics of a STATCOM regarding voltage control.

2.1 Wind Power Plant Control Levels

The WPP control structure in general is defined by two control levels: the WPP control level and the WTG control level. In Fig. 2.1 the WPP levels for reactive power control are depicted, where the WPP control level is further subdivided into a *Main Controller* and a *Dispatch function*.

The TSOs demand reactive power support in several ways, which define the different control strategies to be implemented at WPP control level:

- *Reactive power control* (Q_{ref}^{TSO})
- *Power factor control* (PF_{ref}^{TSO})
- *Voltage control* (V_{ref}^{TSO})

Reactive power control receives a reference signal Q_{ref}^{TSO} by the TSO, which has to be obtained at the PCC. It has a disadvantage during fast and large active power changes (e.g. due to wind speed changes below rated power), since also active power flows affect the voltage levels. Hence, the TSO has to adjust the reactive power setpoint and the

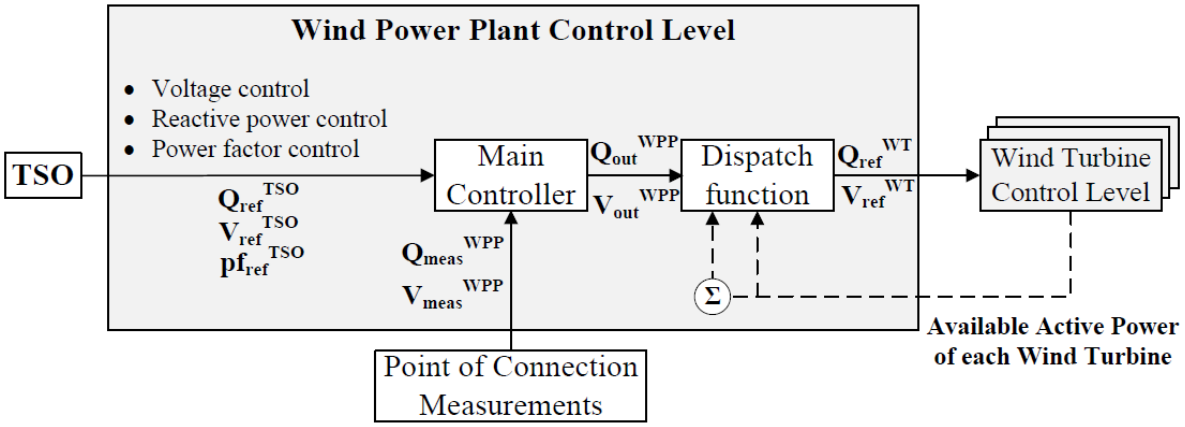

Fig. 2.1: Reactive power and voltage control levels within a wind power plant [1]

WPP controller has to obtain the reactive power output in a fast way in order to maintain the voltage level at the PCC. Reactive power control is commonly used in transmission systems with large synchronous generators providing constant active power output, but also has to be realized by WPPs. [15]

Power factor control is achieved by adjusting the reactive power according to the actual active power of the WPP in order to obtain the reference signal PF_{ref}^{TSO}. Therefore, it is referred to a passive reactive power control. It is even more influenced by active power changes, as they lead to permanent setpoint changes of reactive power. Both reactive power and power factor control originate from industrial applications of synchronous machines and generators in distribution systems, where the voltages are typically controlled by the utility as for instance with on-load tap changing transformers (OLTCs). But in transmission systems superior voltage support is required by generating units to maintain the stability of the system. [15]

This is achieved by the *voltage control* strategy, where a given reference voltage V_{ref}^{TSO} is to be obtained independent on active power impacts. In this way, it constitutes the optimal approach to ensure a consistent voltage level. However, the communication delay within the WPP may lead to undesired, but inevitable voltage changes at the PCC. The voltage control strategy is required by the UK grid code and hence further elaborated in section 2.2 as well as in chapter 4.2. [1, 16]

In order to fulfill the previously explained controls required by the TSO, the *Main Controller* (Fig. 2.1) uses *Point of Connection Measurements* of the related signals (Q_{meas}^{WPP}, V_{meas}^{WPP} and for power factor control also P_{meas}^{WPP}) as depicted in Fig. 2.1. Then, typically PI controllers deliver reference signals (Q_{out}^{WPP} or V_{out}^{WPP}) for the whole WPP. The difference of defining reactive power Q_{out}^{WPP} or voltage reference signals V_{out}^{WPP} to the WPP depends on the outer control loop of the WTGs and is further elaborated in section 2.4.

The *Dispatch function* block handles the distribution of reactive power / voltage reference signals to the WTGs. Various dispatch strategies are investigated in section 2.3. In some cases the available active power of each WTG is required to calculate Q_{ref}^{WTG} or V_{ref}^{WTG}, which are used as input signals for the *Wind Turbine Control Level* (Fig. 2.1). [1]

2.2 Wind Power Plant Main Controller

The *Main Controller* (Fig. 2.1) of the WPP can be composed of an automatic reactive power regulator (AQR) and an automatic voltage regulator (AVR) or a combination of them, depending on the reference signals provided by the TSO and the selected control strategy.

I. Reactive power and power factor control

For reactive power control and power factor control the outer loop is characterized by an AQR. Moreover, in order to maintain the voltage limits at the PCC a voltage control has to be implemented. This can be realized either by a subordinate voltage control loop prior to the AQR (Fig. 2.2 **I.a**) or by an inner loop AVR subsequent to the outer loop AQR (Fig. 2.2 **I.b**).

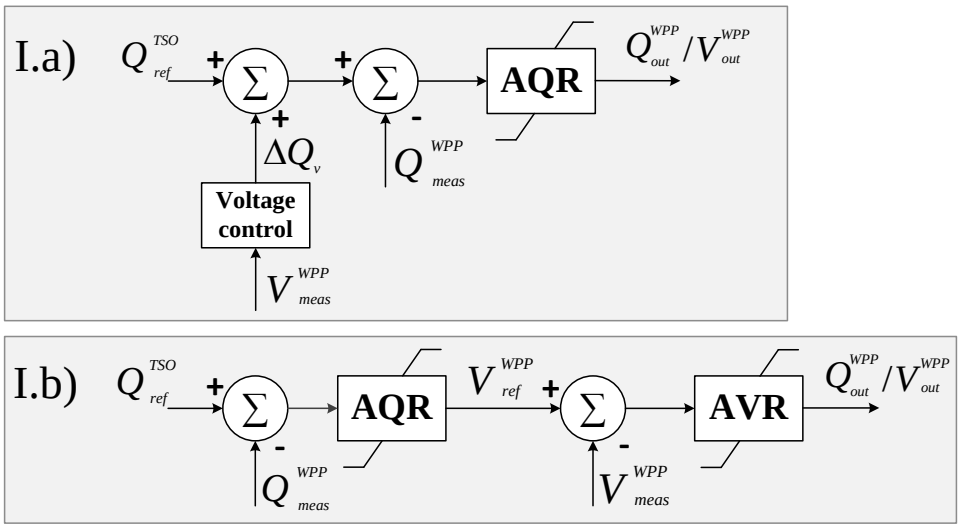

Fig. 2.2: Two strategies for reactive power main controller: (I.a) cascaded AQR and AVR, (I.b) subordinate AVR prior to AQR

The former control strategy modifies the reactive power reference by adding a reactive power correction value according to the voltage control, while the latter control strategy assures that the voltage limits are not violated before trying to reach the reactive power reference. [1]

However, the reactive power main controller is not further elaborated, as the UK grid code used as a reference in this project requires voltage control at the WPP level and its various strategies are explained as follows.

II. Voltage control

Here the outer loop is characterized by an AVR which can be realized by various schemes (Fig. 2.3 II.A - II.C). The AVR provides a reference signal Q_{ref}^{WPP} being used as an input

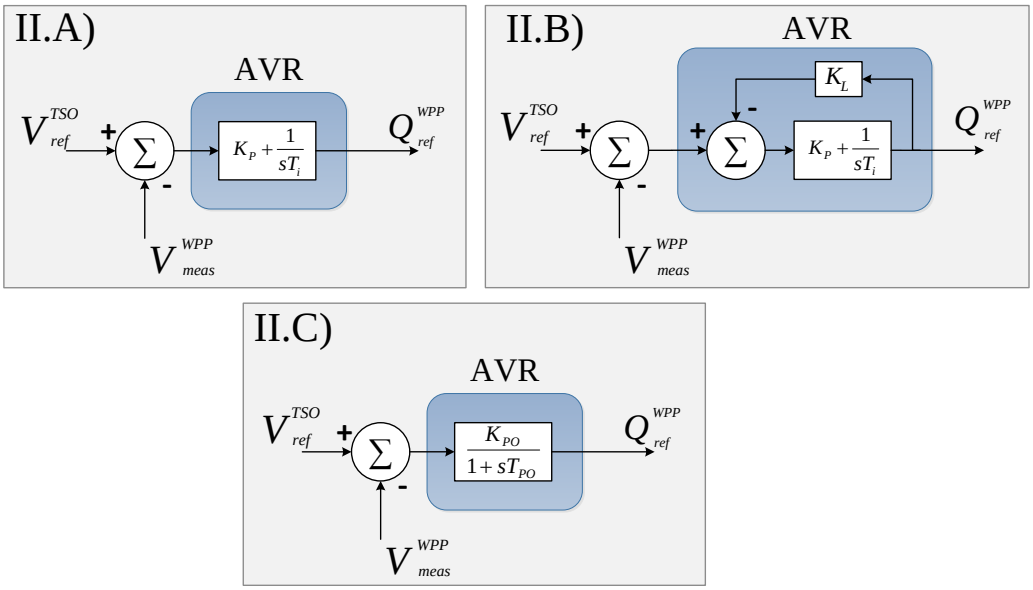

Fig. 2.3: Various schemes of AVR for voltage main controller: (II.A) pure PI controller, (II.B) PI with line drop compensation, (II.C) Slope or proportional control

for the inner loop. The following schemes are possible:

II.A) The most simple approach is a control with proportional and integral components (PI control) which actuates reactive power production in order to obtain exactly the provided V_{ref}^{TSO} (Fig. 2.3 II.A). It provides a tight voltage regulation performance and is commonly applied for WPPs being located remotely and connected to relatively weak grids. A low short-circuit ratio (SCR) causes high over-/undervoltages that can be compensated by a generic PI control. However, in relatively stiff grids (high SCR) this approach leads to constant saturation of the controllers, since reactive power actuation by the WPP is limited, so that V_{ref}^{TSO} might not be reached. Moreover, when multiple WPPs are connected in closed proximity, coordination of voltage control is required. The flat characteristic of PI control (Fig. 2.4 a) can lead to hunting effects, if adjacent WPPs are controlling the voltage in the same way.

II.B) In order to compensate for these aspects, a PI control with line drop compensation can be used, which includes a feedback of its output (Fig. 2.3 II.B). [2, p. 9 ff.][17, p. 285]

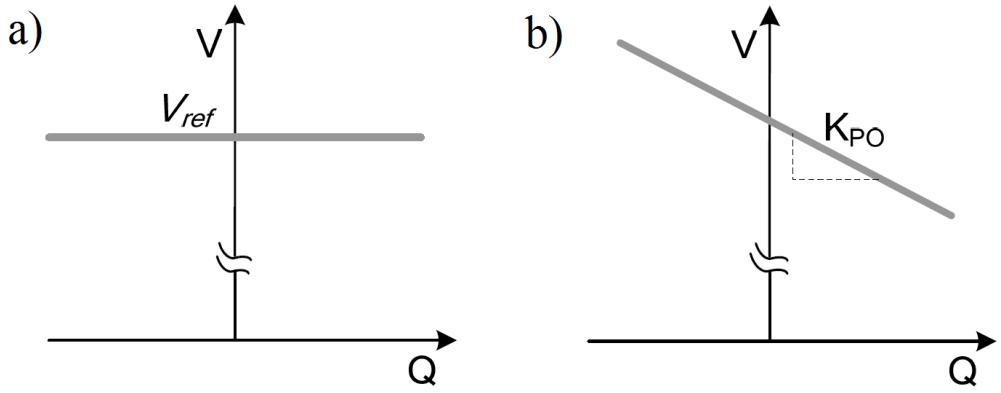

Fig. 2.4: Voltage vs. reactive power characteristics of PI control (a) and slope control (b) [2, p. 11 f.]

II.C) It provides a similar characteristic to a slope or proportional control (Fig. 2.3 II.C), where the gain K_{PO} of the AVR defines the ratio between measured voltage and injected reactive power (Fig. 2.4 b). The difference of both control characteristics in Fig. 2.4 is that for $V \neq V_{ref}$ the PI control (a) would actuacte any reactive power in order to return to $V = V_{ref}$, whereas the slope control (b) actuates a defined amount of reactive power for a certain V. In this way the required reactive power Q_{ref}^{WPP} is known for every measured voltage, so that it is easily manageable how several power plants will share the reactive power injection for a certain voltage disturbance. According to Eq. 2.1 the reactive power injection/absorption can be regulated by either changing the reference voltage (V_{ref}^{TSO}) or the slope gain (K_{PO}), which is defined by Eq. 2.2. Those parameters are given by the TSO (cp. chapter 4.2). A fixed reactive power offset Q_0 can be used to account for reactive power losses within the WPP, when sending the reference signal Q_{ref}^{WPP}.

$$Q_{ref}^{WPP} = Q_0 + \left(\frac{1}{slope}\right) \cdot (V_{ref}^{TSO} - V_{meas}^{WPP}) \tag{2.1}$$

$$K_{PO} = \frac{100}{slope\,[\%]} = \frac{\Delta Q}{\Delta V} \tag{2.2}$$

Besides PI with line drop compensation (II.B) the slope control is the most common AVR strategy in power system applications and moreover matches the UK grid code requirements which define a voltage slope characteristic at the PCC of a WPP. [14]

The output of all AVR schemes in Fig. 2.3 provides a reactive power reference Q_{ref}^{WPP} for the WPP. Then, there are internal reactive power losses within the WPP, which are caused by transformers, array cables and for offshore WPP in particular the export cable. Hence, the voltage control has to take them into account. In [2, p. 23], various candidate configurations regarding the WPP main controller are presented and their schemes depicted

in Fig. 2.5:

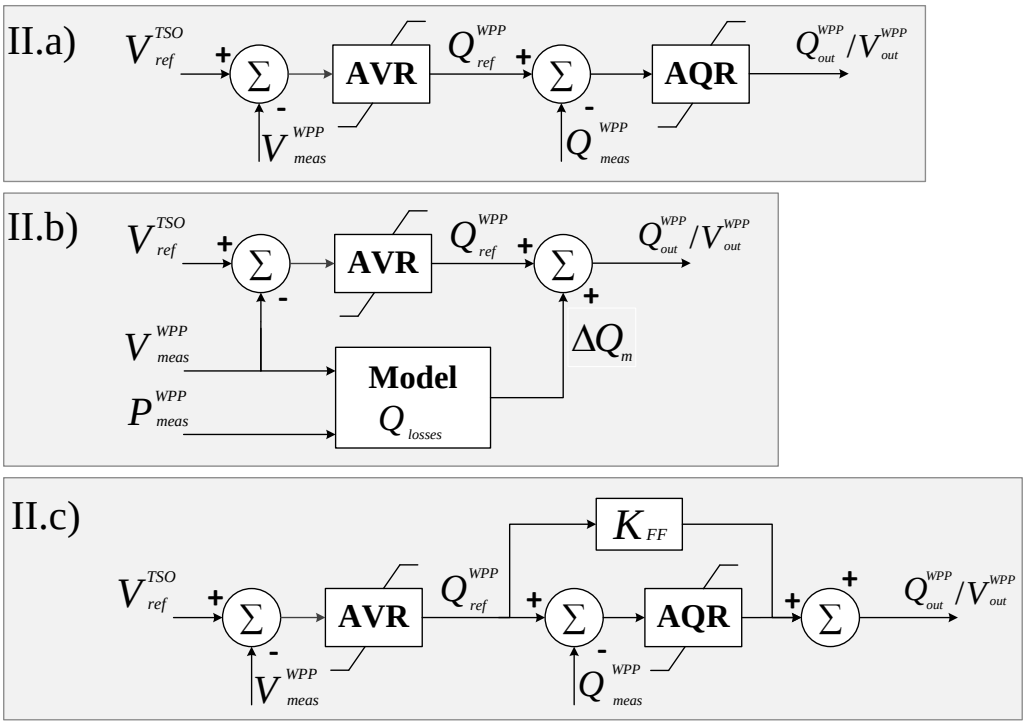

Fig. 2.5: Three strategies for voltage main controller regarding compensation for internal reactive power losses of WPP: (II.a) AQR, (II.b) Wind power plant model, (II.c) AQR with feed-forward

II.a) One approach is by simply taking into account the actual reactive power of the WPP (Q_{meas}^{WPP}) and using a PI controlled AQR to initiate the reference signals (Q_{out}^{WPP}/ V_{out}^{WPP}) for the whole WPP (Fig. 2.5 II.a). The closed loop control ensures accurate compensation of reactive power losses, but has the disadvantage of adding a delay in the response due to the additional controller.

II.b) The second control scheme is realized by adding a reactive power correction ΔQ_m to the reference signal, which is based on a WPP model (Fig. 2.5 II.b). It uses voltage and active power measurements of the WPP and calculates the reactive power losses. The author of [2, p. 39] claims that „the use of a mathematical model of the park internal network [...] does not provide the advantage of removing one lag from the plant control (the integral part of the AQR)“. Hence, it seems pointless to replace the AQR by using this strategy.

II.c) In order to reduce the response time of voltage control at WPP level, the first approach of II.a) can be modified by adding a feed-forward loop with a gain K_{FF} (Fig. 2.5 II.c). This can provide fast initiation of Q_{out}^{WPP}/ V_{out}^{WPP} by bypassing the AQR. On the other hand, the control response may overshoot to an undesired extent.

However, all presented strategies for the WPP voltage main controller cannot be evaluated for themselves, since their performance depends on various aspects such as sensitivity to grid stiffness (SCR) and interaction with the chosen control strategy at WTG level. Thus, WPP control coordination is elaborated in section 2.5. [2, p. 23]

2.3 Wind Power Plant Dispatch Function

The dispatch function of the WPP controller can be realized in various ways, depending on their reference input signals Q_{out}^{WPP} (1.) or V_{out}^{WPP} (2.) and their level of sophistication.

1.a) For reactive power setpoints received from the WPP main controller the simplest method is to send the same reactive power reference signals to all WTGs of the WPP, so that $Q_{ref}^{WTG} = Q_{out}^{WPP}$ applying per-unit values (cp. Fig. 2.1). The disadvantage of this distribution function is that equal setpoint values to each WTG would cause voltage variations within collector feeders, since the voltage levels are affected by the following two factors: the reactive power differences along the array cables and the actual active power production of the WTGs, which may differ from each other due to wake effects particularly in offshore WPPs. In a worst case WTGs may be tripped due to voltage instability and equipment voltage ratings. Moreover, the active power losses may increase due to unequal loading of components. [1]

1.b) The second factor of having different active power levels can be compensated by regarding the actual active power production of the ith WTG. Eq. 2.3 expresses the proportional distribution of reactive power setpoints $Q_{ref}^{WTG,i}$ by using the ratio of available reactive power $Q_{av}^{WTG,i}$ of the ith WTG and the total available reactive power of all n WTGs together. [18]

$$Q_{ref}^{WTG,i} = \frac{Q_{av}^{WTG,i}}{\sum_{i=1}^{n} Q_{av}^{WTG,i}} \cdot Q_{out}^{WPP} \tag{2.3}$$

The available reactive power is determined by the WTG's apparent power rating $S_r^{WTG,i}$ and the available active power $P_{av}^{WTG,i}$ according to Eq. 2.4, so that none of the WTGs will be overloaded. [18]

$$Q_{av}^{WTG,i} = \sqrt{(S_r^{WTG,i})^2 - (P_{av}^{WTG,i})^2} \tag{2.4}$$

1.c) Moreover, there exist some optimized dispatch control strategies that define the reactive power setpoints by regarding the active power losses in the collector system. One optimization algorithm formulates several sub-objective functions to be minimized in order to decrease both the deviation between WPP active and reactive power outputs

and TSO reference values as well as the active power losses in the WPP [19]. Another similar approach is presented in [20] and distinguishes between no-load losses, caused by transformers, and load losses in the system. However, these methodologies of the dispatch function are not further elaborated, since the focus of this project is not laid on active power optimization.

The previous dispatch strategies of (1.a - 1.c) take into consideration a reactive power input signal Q_{out}^{WPP}. When a voltage reference V_{out}^{WPP} is provided by the main controller, the following dispatch strategies are found in present research studies:

2.a) One way is to distribute the signals equally to the WTGs, so that $V_{ref}^{WTG} = V_{out}^{WPP}$ when applying per-unit values (cp. Fig. 2.1). In this way, the voltage levels within the collector system are ensured and the WTGs would provide reactive power according to their mismatch of V_{ref}^{WTG} and V_{meas}^{WTG} respectively. Hence, it does not require to consider the actual active power production (cp. dispatch strategy 1.b) for distributing the signals to the WTGs.

2.b) However, for the case when the injected reactive power of the WTGs is not sufficient to fulfill the grid code requirements, a dispatch strategy is presented in [2, p. 44], which includes the application of a STATCOM as a reactive power back-up for the WPP. It is depicted in Fig. 2.6. It uses active power measurements at the PCC to calculate a

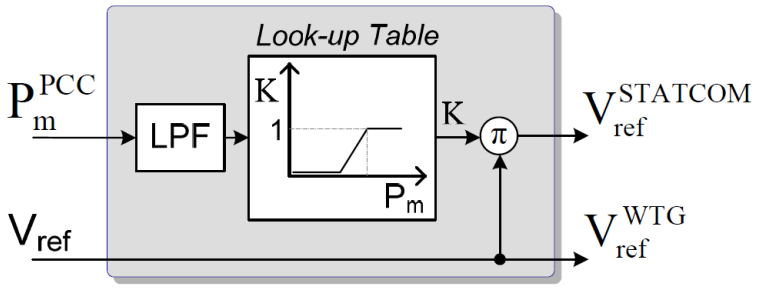

Fig. 2.6: Dispatcher module with STATCOM application acc. to [2, p. 44]

K factor according to a look-up table. If $K = 0$, only the WTGs contribute to voltage control. If $K > 0$, the STATCOM supports voltage control. The look-up table is defined according to a load flow analysis, so that the K factor varies between 0 and 1 depending on the operation conditions where the WTGs cannot fulfill the grid code requirements. It has to be emphasized that this dispatch strategy is designed for using the STATCOM in steady-state operation and not for dynamic voltage control.

2.4 Wind Turbine Control Level

The WTG control level regards only the grid side converter of a WTG with full-scale converter (type IV), since reactive power exchange with the grid is decoupled from the generator side by the DC link (Fig. 2.7).

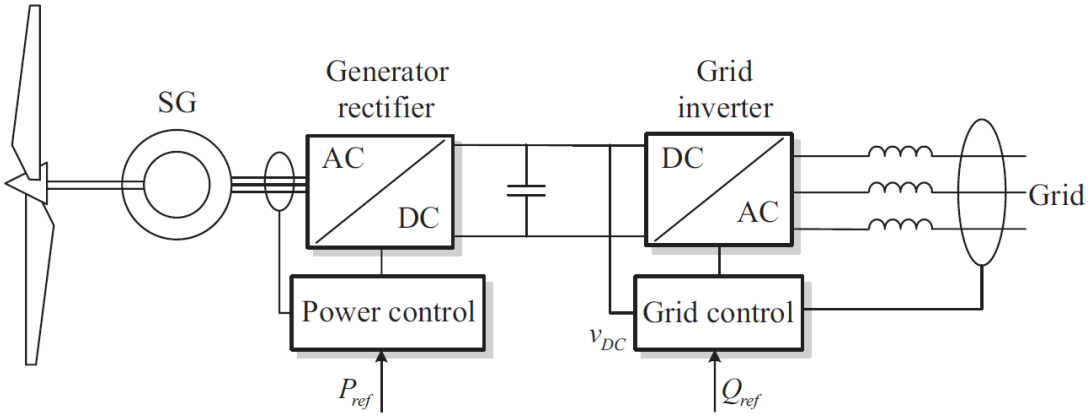

Fig. 2.7: Synchronous generator with back-to-back converter (Type-IV WTG) [3, p. 137]

WTG reactive power control is comprised of an inner loop and an outer loop or a combination of several outer loops. The inner loop is commonly a current controller (CC), which is designed to achieve short settling times (Fig. 2.8 and 2.9). Regarding reactive power control it requires a q-axis current reference $I_{q,ref}$ in order to set the converter voltage, together with the d-axis current reference $I_{d,ref}$ coming from the active power or DC voltage control. The details of grid converter control of WTGs are further elaborated in chapter 5.1. [3, p. 213][21, p. 56]

However, the focus of this section is laid on various strategies of the outer control loop. The authors of [14] distinguish between two methods of calculating the actuator reference (Q_{ref}^{WTG} or V_{ref}^{WTG}) and define them as *centralized* (1.) and *distributed* (2.) voltage control system respectively.

1. *Centralized* voltage control

In a *centralized* voltage control system the voltage control is managed only on WPP level. Then the WPP main controller sends reactive power references and the WTGs should have implemented an AQR as an outer control. [14]

1.a) One option is to place an AVR subsequent to the AQR as depicted in Fig. 2.8 1.a), where the AQR regards the voltage limits and the AVR the current limits of the WTG converter. However, in [14] it is claimed that „it is not needed to have so many nested

controls, when the WPP has already a Q compensator“. The additional AVR introduces another time delay and thereby slows down the whole voltage control of the WPP.

1.b) Hence, an alternative would be to only use an AQR, which is a common method for the outer control loop of a grid connected converter (Fig. 2.8 1.b) [3, p. 205 ff.]. The absence of an AVR can be compensated by a subordinate fast voltage control loop as presented in [16]. It adds an input value for $I_{q,ref}$ that affects the reactive power output of the WTG in case of a grid fault due to its fast response time. The operation mode at the WTG level is basically switched from reactive power control during normal operation to voltage control during a fault. However, since fault conditions are not considered in this project, this possible add-on of fast voltage control is of minor importance.

The disadvantage of *centralized* voltage control is that, during sudden voltage changes at WTG level, the AQR would require commands from the WPP controller to react and compensate for those voltage changes. Furthermore and in particular for large offshore WPPs with long feeders, the steady-state voltage would increase along the line with each WTG, when using identical reactive power setpoints for every WTG. [16]

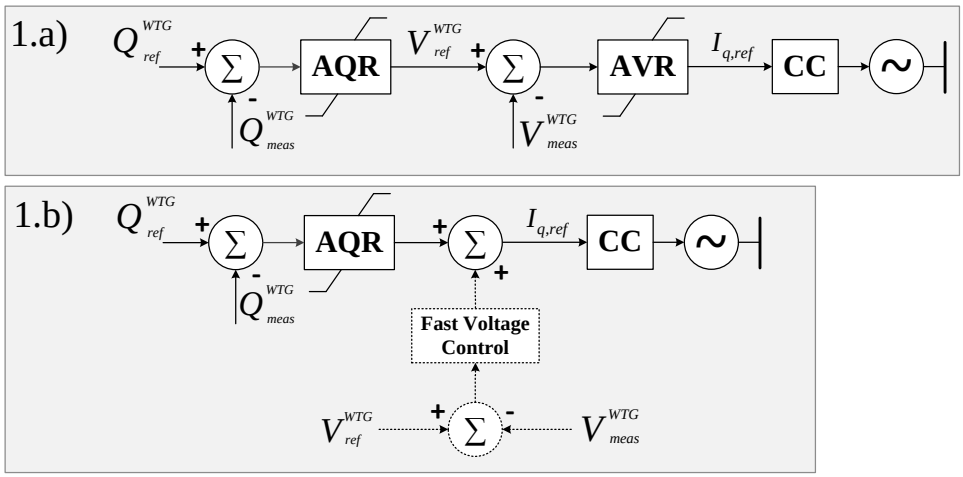

Fig. 2.8: Various strategies for outer loop of q-axis WTG control with reactive power references: (1.a) cascaded AQR and AVR, (1.b) only AQR

2. *Distributed* voltage control

To overcome this problem, a voltage controller (AVR) can be placed as outer control of the WTG. It follows the voltage references set by the WPP controller. In this way, a secondary voltage control can adjust the terminal voltages at WTG level and thereby take countermeasures for reactive power flow changes in the system.

2.a) Likewise for the *centralized* voltage control, one strategy is to cascade an AVR and AQR, now in opposing order (Fig. 2.9 2.a). On the one hand, it is again alleged that such

a control sequence is overdesigned leading to additional undesired time delays [14]. On the other hand, this control strategy is applied in [16], where a fast continuous voltage control is active both during normal operation and faults. The fast response of the AVR enables this control strategy to reduce undesired voltage changes during normal operation, as for instance caused by wind fluctuations. However, in this particular study the communication delay of the investigated WPP has been relatively low, so that a cascaded AVR and AQR would not be an disadvantage in terms of response times.

2.b) According to [14], the preferred *distributed* voltage control strategy is by only using an AVR as outer control loop (Fig. 2.9 2.b), likewise to method 1.b) being a common control strategy of grid connected converters [22].

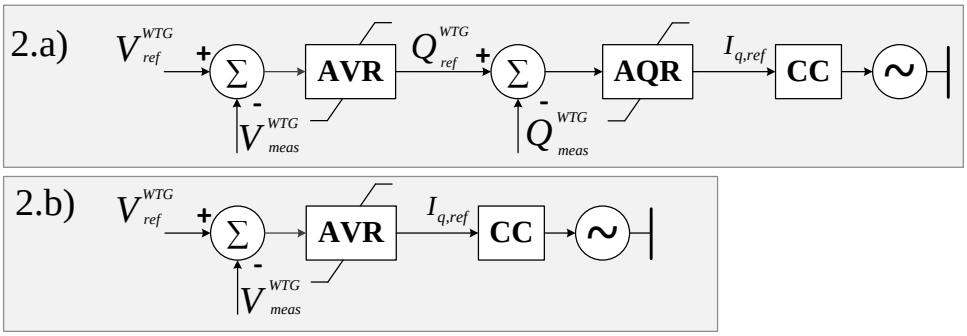

Fig. 2.9: Various strategies for outer loop of q-axis WTG control with voltage references: (2.a) cascaded AVR and AQR, (2.b) only AVR

2.5 Wind Power Plant Control Coordination

As already mentioned, various strategies for the relevant control functions *Main Controller*, *Dispatch function* and *Wind Turbine Control Level* can be assessed individually to a certain extent, but need further elaboration regarding the overall control coordination of the WPP. In order to evaluate combinations of various approaches, certain criteria regarding WPP control performance are required. Those can be identified mainly in [2] and are enumerated subsequently.

1. Grid code requirements defining the overall control strategy (reactive power, power factor or voltage control) as well as the demanded control response times
2. Grid stiffness expressed by the SCR
3. Signal time delays affected by the communication technology and number of WTGs
4. Control capabilities of individual WTGs and possible demand of FACTS (e.g. STATCOM)

In [14] several combinations of WPP control concepts are analyzed with respect to sensitivity to SCR changes. The main focus is laid on assessing different performances of *centralized* voltage control (1.b) and *distributed* voltage control (2.b) on WTG level (cp. section 2.4). It is concluded that the *distributed* voltage control reacts faster to grid voltage changes than the *centralized* voltage control and is moreover less sensitive to changes of SCR. While for a range of $5 < SCR < 25$ the *centralized* control strategy would require three different control settings, a single tuning process is sufficient for the *distributed* control approach in order to fulfill the grid code requirements regarding dynamic voltage control. It is claimed that not only changes in SCR, but also the parametrization of the voltage controller's slope gain K_{PO} affects the design constraints. Hence, it is of importance how the TSOs demand the settings of the slope control.

When having relatively large communication delays between WPP and WTG controller, the *centralized* voltage control might not fulfill the demanded time delay. For communication technologies exhibiting relatively low time delays, the impact of SCR on the design constraints is reduced, so that similar responses can be obtained for both *centralized* and *distributed* voltage control. [14]

Furthermore it is ascertained that by adding a feed-forward loop for the Q compensator of the WPP main controller (cp. Fig. 2.5 c), both WTG *centralized* and *distributed* voltage control systems tend to overshoot for grid voltage changes. However, this WPP control approach can be of advantage, when direct reference signals to the WTGs bypassing the Q compensator reduce the time response of the whole voltage control. [14]

It can be stated that WPP control coordination depends on many factors and not all of them have been reflected in present research studies, so that the optimal voltage control strategy cannot directly be ascertained. Much more importantly, none of the studies provide generic guidelines how to approach the tuning process of any of the presented coordinated voltage control strategies. Cascading of controllers (AVR and AQR) on WPP level and their distinct purpose within the overall control architecture is not captured by any standards or public recommendations.

However, one of the project objectives is to provide first guidances by analyzing basically the above listed criteria (1. - 4.). Therefore, as a starting point it seems reasonable to perform assessment studies for one base case control architecture, which is selected from the observations of this chapter as follows:

- *Main Controller:* As it is commonly used in today's WPPs, scheme II.a) with cascaded AVR and AQR serves as a base control strategy. For the AVR a slope control (II.C) is required by UK grid code.

- *Dispatch function:* The simplest dispatch method by sending equal reference points to all individual units is applied (1.a).
- *Wind Turbine Control Level:* As the *centralized* control stategy is typically used in today's WPP, scheme I.b) with reactive power references serves as a base case control strategy for WTGs.

2.6 Modelling of Wind Power Plants for Voltage Control Analysis

As one of the project objectives covers the model representation of WPPs for voltage control analysis, it is worth investigating the state-of-the-art regarding this topic.

It is ascertained that when dealing with WPP control issues, the majority of present research studies reveals their findings by time-domain simulations, which indicate the usage of numerical models. In [18] different scenarios are simulated to show how an already developed controller performs in a WPP with doubly-fed induction generators. Similar objective is observed in [23], where the performance of coordinated control of fixed and variable speed WPPs should be validated by numerical simulations. However, those studies provide quantitative measures regarding the control behaviour, but they lack qualitative observations with respect to the design and tuning process.

Such analyses can be conducted in frequency domain, which is achieved in [24], where the authors develop a complete small-signal model of the WTG with direct-drive PMSG connected to a power system. By means of Eigenvalue analysis, the dynamic modes of the WTG are assessed, which helps to design the controller parameters. However, this study does not regard the model implementation of a number of WTGs into an overall WPP.

The small-signal approach is also selected in [21] and [25], where the entire WPP is modelled as one single WTG instead of a multi-turbine WPP representation.

The former study presents such an aggregated model of the WPP to perform studies of low frequency inter-area oscillations in power systems. Here, the focus is laid on implementing a central damping controller for mitigating system oscillations. Thus, the internal location of individual WTGs within the WPP is irrelevant for this type of study.

In [25] the aim is to investigate and design a WPP voltage controller, which resembles also the objectives of this project. However, it is found to be unnecessary by the author to introduce a complex model of the WPP, but rather to summarize the dynamics of the WTGs to one aggregated time constant. It has the advantage of reducing the complexity

of the WPP and hence the computation time required for control design. On the other hand, it lacks the actual dynamics occuring within the WPP, which might lead to reduced accuracy of the performed studies. Moreover, the *Dispatch function* (cp. section 2.3) is not investigatable, hence the individual contribution of WTGs to voltage control cannot be provided.

In this study, a complex small-signal model of the whole WPP introducing all individual units is developed in order to enable the highest degree of assessing control design and tuning with respect to all control functions according to Fig. 2.1 of section 2.1.

2.7 Static Synchronous Compensator - STATCOM

As this project investigates the embedded application of STATCOMs for voltage control in WPPs, this additional section briefly outlines its operation principle and control modes.

The STATCOM is a member of the FACTS family of devices and can be used to enhance a WPP with the ability to deliver or absorb reactive power from the grid. It is a fairly new breed of reactive power compensators which is based on Voltage Source Converter (VSC) technology. By controlling the output current of the STATCOM it is possible to control either the nodal voltage magnitude or reactive power injected at the connected bus. This reactive power compensation provides some benefits to this study as reducing the losses from the remote location of the WTGs to the grid and a faster dynamic response. Compared to other reactive power compensation units, the STATCOM has one major advantage: it is capable of providing full reactive power support independent from the actual voltage at the connection point, which is desired during faults. [26]

The configuration of the STATCOM circuit is illustrated in Fig. 2.10. The STATCOM consists of one VSC with a capacitor on the DC side of the converter and is commonly grid connected by a step-up transformer. The VSC is equipped with Insulated Gate Bipolar Transistors (IGBTs) [26].

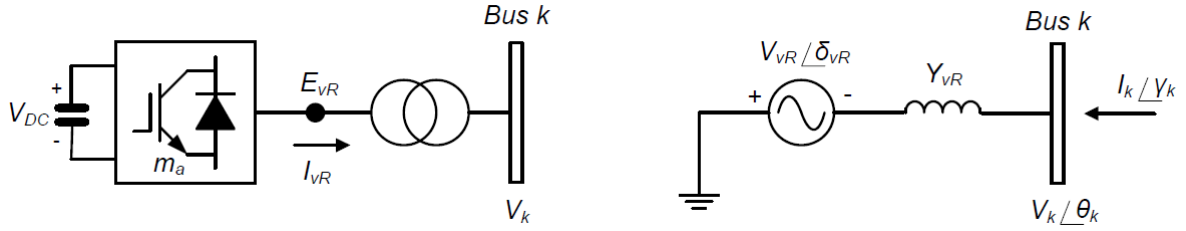

Fig. 2.10: STATCOM scheme with equivalent circuit representation [4].

2.7.1 Operation principle

The operational principle of a STATCOM is illustrated by Fig. 2.11. As aforementioned, the STATCOM can be treated as a synchronous voltage source, due to the fact that its output voltage is controllable. By neglecting active power losses within the STATCOM circuit, the compensator voltage (V_{Comp}) is in phase with the grid voltage (V_{Grid}). If $V_{comp} < V_{grid}$, current will flow from the grid to the STATCOM, resulting in reactive power absorption. In this case the system will be under-excited. For the opposed scenario ($V_{comp} > V_{grid}$), reactive power will be delivered to the grid, indicating an over-excited system. In Fig. 2.11 this working principle is illustrated by phasor diagrams. [26]

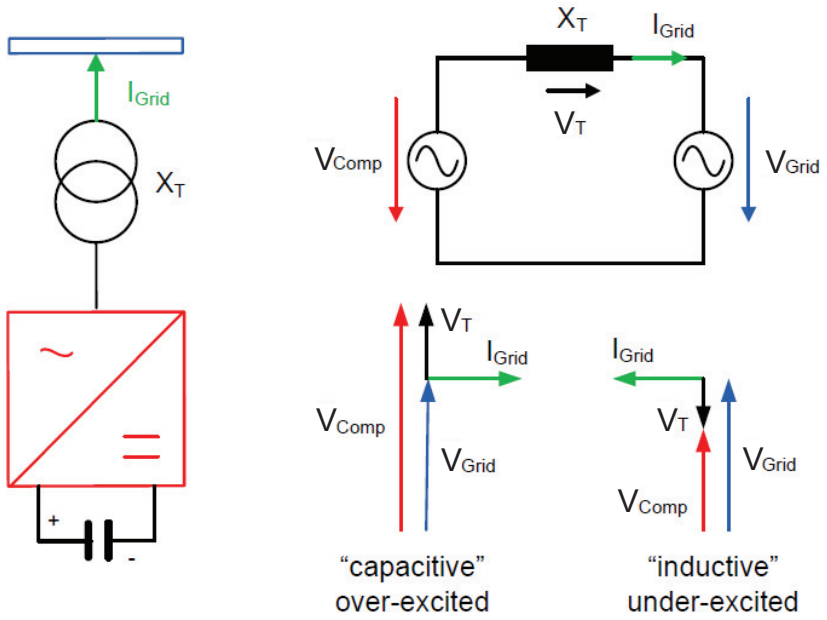

Fig. 2.11: Schematic representation of working principle of STATCOM [4].

2.7.2 Control modes

The control of reactive power flow provided by a STATCOM can be realized in one of the following control modes.

Normally, if the STATCOM is a standalone unit, it has the same control characteristic (slope control) as the main WPP controller explained in section 2.2.

However, since the STATCOM is an integrated part of the main WPP controller, the control mode of STATCOMs used in this study is reactive power control. This type of control strategy regulates the reactive power injection to the local bus, to which the STATCOM is connected, according to a reference received from the WPP controller.

2.8 Summary

In this chapter it has been presented the status quo strategies regarding reactive power and voltage control associated with WPPs. Different control functions such as the WPP *Main Controller* and *Dispatch function* as well as *Wind Turbine Control Level* have been detected and their various possible characteristics described. Certain factors influencing the overall WPP control coordination such as grid stiffness and system delays have been obtained and a control architecture has been selected to be applied in this project. Moreover, this chapter has covered a state-of-the-art regarding modelling of WPPs for control analysis. It has been ascertained that the small-signal approach enables most qualitative analyses, hence its methodology is introduced in the following chapter.

3 Small-Signal Analysis Methodology

In this chapter the methodology for small-signal analysis is given. At first, an introduction to this topic is given, where the state-of-the-art regarding small-signal analysis is explained (section 3.1). Subsequently, the general approach for modelling and analysis of state-space systems is discussed (section 3.2). Finally, some performance criteria of small-signal analysis applied in this study are explained (section 3.3).

3.1 Introduction to Small-Signal Analysis

AC power systems imply a non-linear behaviour, even in steady-state condition, due to their periodially time-varying variables. As the application of non-linear control theories to such complex systems is not very practical, they are often simulated numerically in order to understand the system behaviour and interactions (cp. chapter 2.6). However, numerical simulations do not generate the qualitative information and insight in control aspects that analytical models can provide. In order to analyze power system control during normal operation, the occurrence of small-signal changes may be assumed. Then, the models are able to be linearized around an operation point for the purpose of this analysis. However, it requires a fixed operating point to directly apply small-signal linearization techniques, which is not given by periodically time-varying variables. It can be achieved by phasor-based models. Here, sinusoidal voltages and currents are represented as RMS phasors, averaged over one fundamental period, that in steady-state become DC variables. In this way, the models can be used for small-signal linearization. Another method being typically used in power electronic converters is to transform the three-phase variables into DC variables by using the synchronous dq-reference frame. In addition to permitting small-signal analysis this approach enables decoupled control of active and reactive power.

There are mainly two ways to perform small-signal analysis; by state-space models or by impedance-based models. The state-space model is developed in time domain. However, the analysis of state-space models can be performed in frequency domain by using transfer functions. Meanwhile, the impedance-based model is developed and analyzed in frequency domain.

The impedance-based approach works by defining the in- and output impedances of each main component of the power system. The main advantages and disadvantages of impedance-based model are as follows:

- It is straightforward to obtain a model in a linear form;
- Adding or removing system components or changing their operation mode is achieved by only modifying one new element of the system impedance;
- If the impedance of the system cannot be obtained analytically, there is the possibility to obtain it experimentally;
- The main disadvantage of this method is that it cannot be used to perform phasor-based modelling.

The state-space model uses state variables to describe a system by a set of first-order differential equations, rather than by one or more nth-order differential equations. The main advantages and disadvantages of state-space model are as follows:

- It enables to model each component separately and then merge them together to form an overall system;
- It is possible to separate plant components and controller components in order to perform small-signal analysis individually;
- A disadvantage of this method is that every time there are significant changes in the structure of the power system, the state-space expressions have to be reformulated.

However, as one may not expect many changes in the structure of one single WPP system, it allows the application of state-space models. Furthermore, the possibility of separating plant- and controller components makes this method suitable for this study. In this project a state-space model is developed, which represents the overall system network by phasor variables, while the individual components such as WTG and STATCOM are modelled based on the dq-reference frame. In the next section an introduction to this approach is given. [27]

3.2 State-Space Method for Small-Signal Analysis

The aim of this section is to discuss how the state-space approach is used to derive a model for small-signal analysis of a dynamic system. All the mathematical expressions of this sections are obtained according to [8].

The input and output dynamics of the system can be described by a set of state-space equations. Thus, not only the dynamic behaviour of the in- and output variables, but also

of the internal state variables of the considered system are regarded. Eq. 3.1 represents the state-space in a classical form and is written in the matrix form, where the dynamics of the state variables $\mathring{\mathbf{x}}$ are obtained by linking the system state matrix $\mathbf{A}$ with the state vector $\mathbf{x}$ and the input matrix $\mathbf{B}$ with the input vector $\mathbf{u}$. The output vector $\mathbf{y}$ is calculated likewise by the output matrix $\mathbf{C}$ and feedforward matrix $\mathbf{D}$.

$$\begin{aligned} \mathring{\mathbf{x}} &= \mathbf{A}\mathbf{x} + \mathbf{B}\mathbf{u} \\ \mathbf{y} &= \mathbf{C}\mathbf{x} + \mathbf{D}\mathbf{u} \end{aligned} \tag{3.1}$$

The analysis is usually related to a non-linear set of system equations, dynamic relations as well as network equations. In order to use the state-space method, a linearization of the non-linear system has to be performed around one operating point. In many cases the starting point for the scope of analysis is a non-linear model. Eq. 3.2 illustrates a way to linearize the state-space expressions, where $\triangle\mathbf{x}$ is used to illustrate small deviations, $\mathbf{x}_0$ is the initial state vector and $\mathbf{u}_0$ is the initial input vector corresponding to the operating point.

$$\begin{aligned} \mathbf{x} &= \mathbf{x_0} + \triangle\mathbf{x} \\ \mathbf{u} &= \mathbf{u_0} + \triangle\mathbf{u} \end{aligned} \tag{3.2}$$

However, an introduction to linearization techniques is not given in this study, since it can be found in the standard literature [8, 28, 29]. The technique used in this project is by means of Taylor series, where the state equations are approximated by neglecting the high-order terms. The linearized form of Eq. 3.1 is given by Eq. 3.3, where only the change of the corresponding variables is regarded at a certain operating point.

$$\begin{aligned} \triangle\mathring{\mathbf{x}} &= \mathbf{A}\triangle\mathbf{x} + \mathbf{B}\triangle\mathbf{u} \\ \triangle\mathbf{y} &= \mathbf{C}\triangle\mathbf{x} + \mathbf{D}\triangle\mathbf{u} \end{aligned} \tag{3.3}$$

When having an expression of the system in state-space, it is straightforward to achieve an overall transfer function of the system. The transfer function is a mathematical representation used to describe the in- and output behaviour of the system. It can be derived from Eq. 3.3, which finally leads to the overall transfer function of the system described by Eq. 3.4.

$$G(s) = \frac{\triangle y(s)}{\triangle u(s)} = \mathbf{C}(s\mathbf{I} - \mathbf{A})^{-1}\mathbf{B} + \mathbf{D} \tag{3.4}$$

Transfer functions are important in order to design controllers and are relevant for the performance criteria of small-signal analysis, which are outlined subsequently.

3.3 Performance Criteria for Control and Small-Signal Analysis

Small-signal performance criteria are normally used to evaluate the stability and performance of closed-loop control systems. In the following, it is outlined the methods applied for regarding small-signal performance criteria, which are specified by both generic guidelines and the UK grid code.

Absolute Stability: Pole-Zero-Map and Eigenvalues

The absolute stability of a system is determined by the placement of the poles of a transfer function. The pole-zero map can be used to determine if all the poles of the open-loop system are located in the left-half plane of the complex s-plane, which is a measure of a stable system.

Another approach used to assess the small-signal performance of a closed-loop control system is by calculating the Eigenvalues of the state-space function, which has been derived in Eq. 3.3. There is a closely relationship between the poles of the transfer function and the Eigenvalues of the system matrix $\mathbf{A}$. In fact, the poles of transfer function correspond to the Eigenvalues of the state-space system matrix [30].

The Eigenvalues are generally an indication of system stability for the particular linearized system. Furthermore, the Eigenvalues are capable of identifying poorly damped or unstable modes in dynamic models.

Eigenvalues may be real or complex. A real Eigenvalue corresponds to a non-oscillatory mode, whereas a complex Eigenvalue describes an oscillatory mode. In order to associate the state variables of a system to the existing modes, the participation matrix $\mathbf{P_i}$ is evaluated. Its participation factors $\mathbf{p_{ki}}$ are obtained by Eq. 3.5, where the right (Φ) and left (Ψ) eigenvectors of the system matrix $\boldsymbol{A}$ are used. The magnitudes of $\mathbf{p_{ki}}$ provide a measure of the relative participation of the kth state variable in the ith mode and vice versa. [8, p. 707 ff.]

$$\mathbf{P_i} = \begin{bmatrix} \mathbf{p_{1i}} \\ \mathbf{p_{2i}} \\ \vdots \\ \mathbf{p_{ni}} \end{bmatrix} = \begin{bmatrix} \mathbf{\Phi_{1i}\Psi_{i1}} \\ \mathbf{\Phi_{2i}\Psi_{i2}} \\ \vdots \\ \mathbf{\Phi_{ni}\Psi_{in}} \end{bmatrix} \tag{3.5}$$

Relative Stability: Root Locus and Gain & Phase Margin

The root locus is used to plot the roots of the characteristic equation of the closed loop system, and can be used to gather information regarding movement of the poles when certain parameters are changed in the system. The parameters resulting in variation of the pole placment are mainly the gain and the time constant of the controller. The root locus provides information about the stability of the system, meaning it is possible to evaluate how much the gain can be modified before the system becomes unstable, which is observed by the movement of closed-loop poles along the root locus. Moreover, a root locus plot can be used to evaluate certain design requirements for the closed-loop system. Criteria such as overshoot, rise and settling time can be concluded by the natural frequency and damping of the closed-loop poles, which are observable by certain equipotential lines within the complex plane. [28]

Even though the poles of the open-loop system are located at the left-hand-side of the complex s-plane, certain gain values of the controller can force the closed-loop system to become unstable. The open-loop frequency response is used to determine the gain and phase margin, both of which are measures of relative stability and can be determined from the Bode plot. The system is considered as stable, if it has a positive gain and phase margin. Those margins indicate how much the gain and phase can be changed, before the closed-loop system becomes unstable [11]. In order to have a stable closed-loop system, certain recommended values of the gain and a phase margin are given the table 3.1.

Tab. 3.1: Generally accepted values of gain and phase margin for feedback control systems acc. to [11]

Gain margin	> 6 dB
Phase margin	> 40 deg

Bandwidth of Closed-Loop System

Another parameter of interest is the bandwidth ω_b of a closed-loop system. It is a measure of the dynamic response of the system as well as its rise time, meaning how fast the system will response to input changes [11]. The bandwidth is determined by the bode plot of the closed-loop system and obtained at the frequency, where the magnitude decreases by 3 dB related to its DC gain. According to [6, p, 214], it is required that the overall voltage control system needs to include elements which can provide a limited bandwidth output, so it cannot excite the higher frequency oscillations on other plants being connected to the network.

3.4 Summary

This chapter has given a brief description of the methodology of small-signal analysis. An introduction has been provided of how to represent a small-signal model in state-space form and perform its linearization, before finally to obtain a transfer function of the state-space expression. In the last step, it has been presented a list of performance criteria and related tools, which will be used in this project to assess control and small-signal behaviour. Their scope of application is stated in the system characterization, which is outlined in subsequent chapter.

4 System Characterization

This chapter describes the overall study approach. At first, a description of the WPP used in this study is given (section 4.1). Subsequently, the relevant grid code requirements are specified (section 4.2). Finally, a definition of scenarios and their success criteria is given (section 4.3).

4.1 System Description of the Wind Power Plant Network

In this section the benchmark WPP used in this study is described. The WPP layout is provided by *DONG Energy* and represents a WPP being located in UK. Therefore, the WPP takes into account the requirements for transmission systems in UK and general engineering rules for WPP topologies. The single line diagram of the WPP can be seen in Fig. 4.1. The WPP is composed of 35 WTGs of variable speed, full-scale power conversion and a rated power of 6 MW, which are connected radially to a MV busbar of 34 kV. The WTGs are divided into six arrays, where one is composed of 5 WTGs and the remaining five arrays are composed of 6 WTGs. Two offshore transformers (GT) located at one offshore substation convert the voltage level to 150 kV. They are required according to [31, p. 35] in order to ensure stable operation in case of planned or fault outages of a single offshore transformer. Three arrays are connected to each transformer. The power generation of the WTGs is transferred to the external grid through two export cables connected in series, an offshore cable (ECS offshore) of 10 km length and an onshore cable (ECS onshore) of 19 km length. Two C-type harmonic filters are connected to respectively 150 kV and to 275 kV, where the PCC is defined. They are used for harmonic mitigation and provide reactive power due to their capacitances. Furthermore, a mechanically switched reactor (MSR) is connected to 34 kV level. The MSR is implemented to compensate for the reactive power supplied by the long export cables and to compensate permanent disturbances, hence improving the steady-state operation [2, p. 45]. Moreover, two STATCOMs with an MVA rating of ± 25 Mvar respectively are connected to the same busbar for the purpose of dynamic reactive power compensation (cp. chapter 2.7). Two supergrid transformers

(STGs) boost the voltage to 275 kV, where the network representation is completed by connection to the external grid.

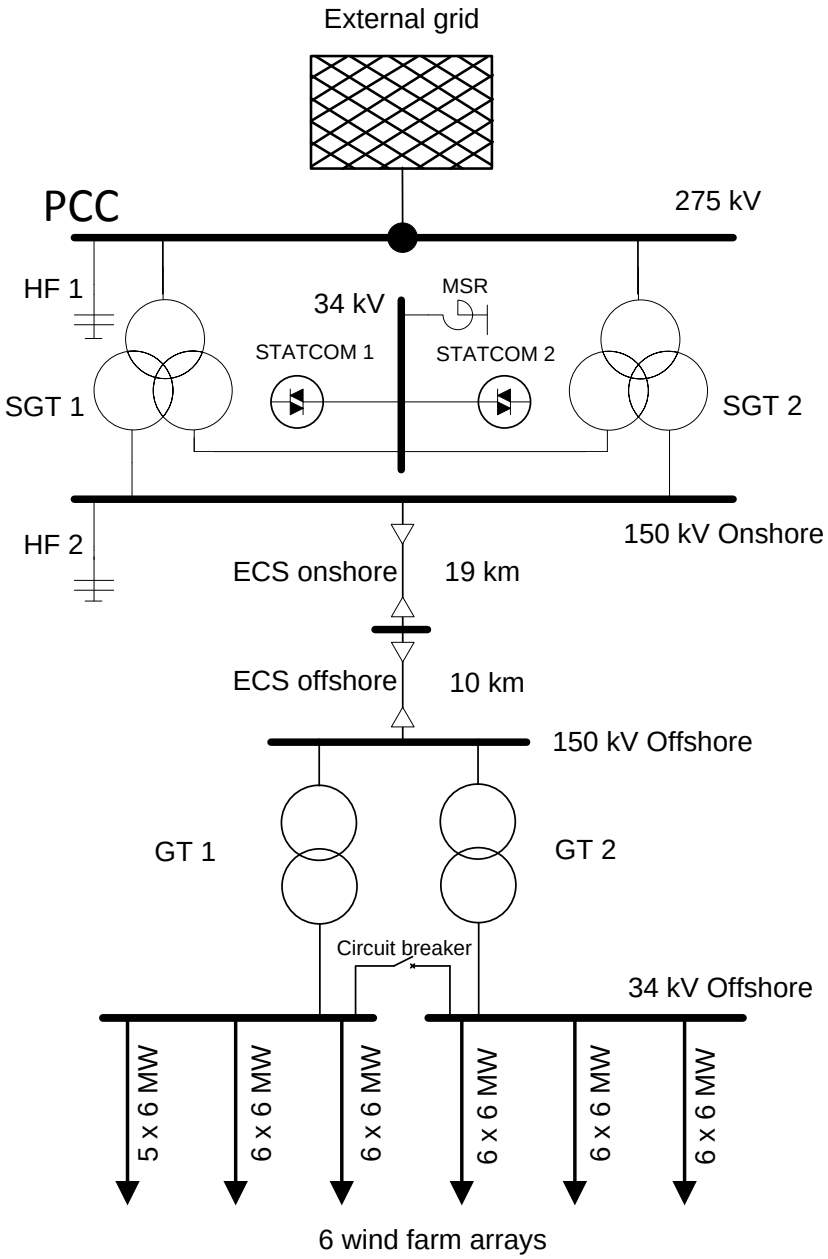

Fig. 4.1: Single line diagram of benchmark offshore wind power plant, investigated in this study

4.2 Grid Code Requirements

In the beginning of the era of wind power most of the individual WTGs or even the first small WPPs have been directly connected to the distribution grid, due to relatively small levels of integration. But as larger WTGs have been incorporated into WPPs with

sizes starting to reach same levels as for conventional power plants, it has resulted in an increasing concern for TSOs regarding power quality and network stability issues. As a result of that, TSOs have formulated grid codes regarding different parameters such as grid stiffness, transmission voltage levels and WTG topology. This requirements made by TSOs need to be fulfilled in order for the WPP to become grid code compliant. Grid codes are country specific and since the WPP used in this project is located in UK, the associated grid code is taken into account.

The UK grid code [6] sets out the operating procedures and principles of a power plants and also determines the relationship between the *National Grid Electricity Transmission* (NGET) and the users of the *National Electricity Transmission System* (NETS). This grid code covers different subjects dealing with connection of a WPP to the NETS, but only the chapter *Connection Conditions* is relevant for this study, since it specifies the technical and operational conditions that have to be met by users seeking connection with the NETS, i.e. offshore WPPs. The *Connection Conditions* criteria are specified for different aspects of the whole system operation to be met at the PCC. There are a number of issues specified by grid codes, i.e. frequency and active power control, voltage control, FRT behaviour, power quality characteristics and protective devices. Only the voltage control will be relevant for this study.

4.2.1 Voltage Control Requirements

According to the UK grid code a WPP controller has to be able to perform a continuously automatic voltage control of the WPP without introducing any instability over the entire operation range. Reactive power or power factor control shall not be regarded. However, the WPPs must be capable of supplying certain reactive power at certain active power outputs. The required steady-state reactive power capability is shown by a PQ chart in App. A.4.

Lately NGET has prepared a guidance note with some specific requirements regarding voltage control requirements of a WPP [5]. The design requirements for voltage control are illustrated in Fig. 4.2.

The relevant parameters are given by rise time (t_r), settling time (t_s) and delay time (t_d). From Fig. 4.2 it can be seen that the controller shall response within 0.2 seconds and reach 90 % of the set point in a linear way within 1 seconds. The settling time shall not exceed 2 seconds, where the peak-to-peak amplitude of any oscillations shall be less than 5 % of the steady-state value.

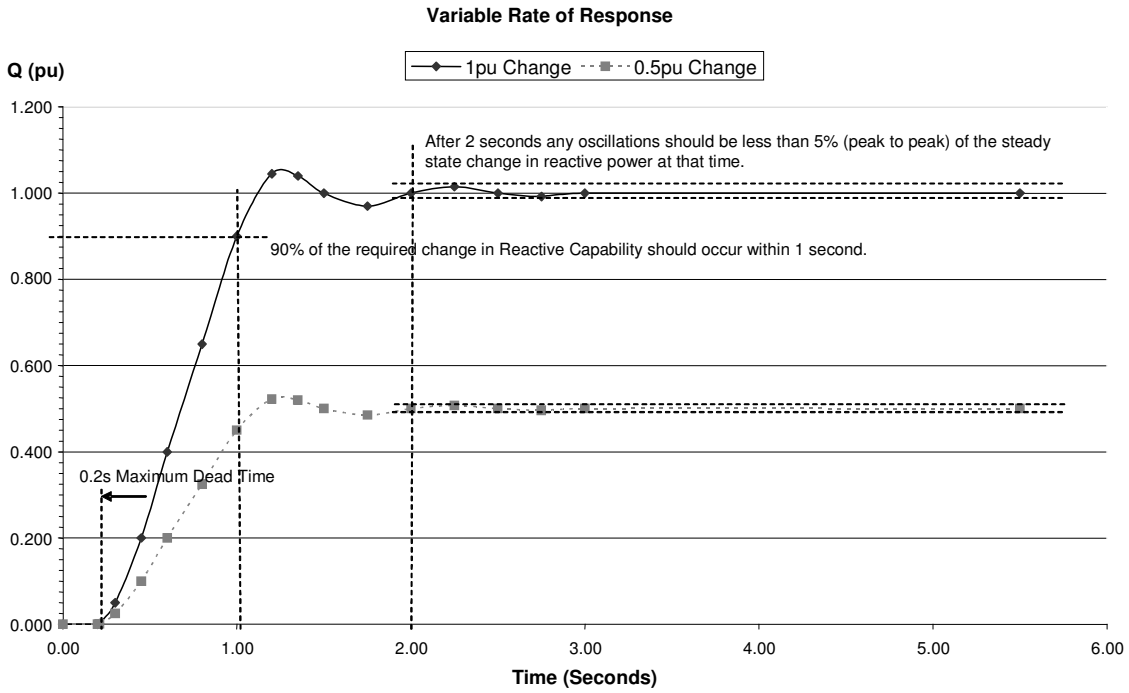

Fig. 4.2: Rate of reactive power response proportional to the size of the step change specified in UK grid code [5]

In the UK grid codes there is no requirement specifying the maximum overshoot of the system response. However, according to the *IEEE Guide for Evaluation of the Dynamic Performance of a Control System* [11] an overshoot of $OS < 15\,\%$ is recommended and used as performance criteria in this study.

Moreover, it is stipulated by the UK grid code to „include elements that limit the bandwidth of the output signal“. A bandwidth of 0 - 5 Hz is assumed to be acceptable.

Even with present voltage controllers there will occur steady-state voltage variations deviating from 1 pu. The UK grid code states that the normal operating range of voltages at the PCC and the HV transmission network of the WPP must remain within $\pm$ 10 % of the rated voltage. At MV levels of the WPP arrays, the voltage range is specified by the standard *EN 50160* [32], which recommends the same operating range of $\pm$ 10 %.

This voltage band is to be maintained by a slope control (cp. chapter 2.2), whose characteristic shall be adjustable over the range from 2 % to 7 %. It is depicted in Fig. 4.3, where a percentage change in voltage based on nominal results in a change of reactive power from 0 to Q_{min} or 0 to Q_{max}.

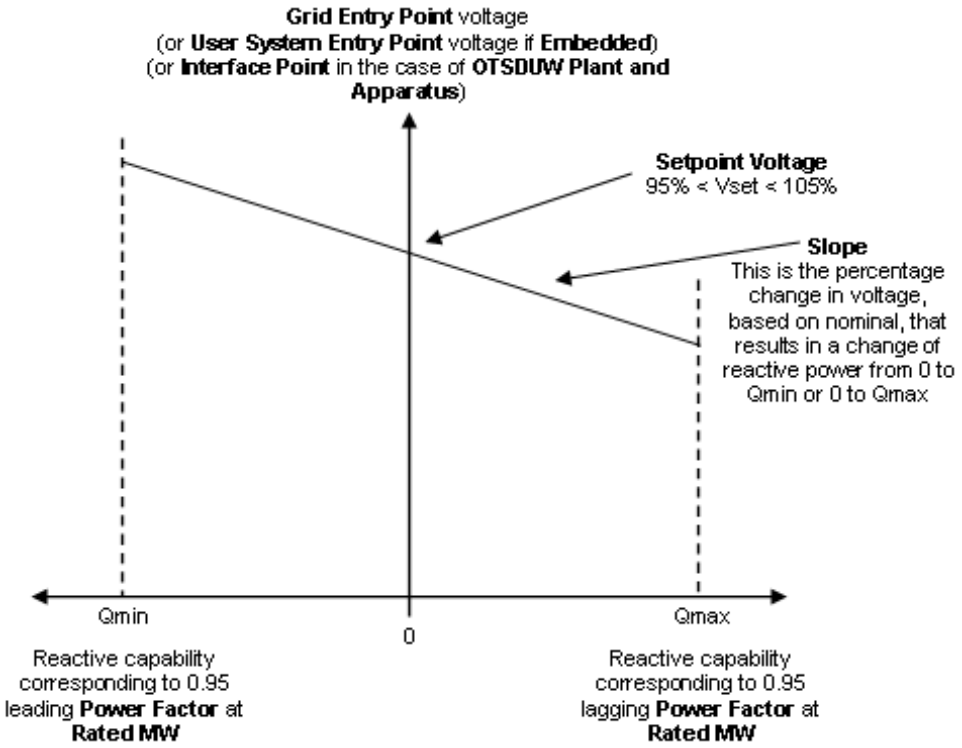

Fig. 4.3: Slope characteristic of the voltage control acc. to UK grid code [6]

4.3 Definition of Scenarios and Evaluation

In this section the definition and sequence of assessment scenarios and their evaluation is outlined, regarding the small-signal performance criteria of chapter 3.3 and the grid code requirements of previous section. First, the developed small-signal models have to be verified and validated. Subsequently, the design and tuning process of the WPP voltage control is conducted.

4.3.1 Model Verification

The small-signal models of the WTG and the whole WPP are developed in chapter 5. Their functionality needs to be verified by applying Pole-Zero-Map and Eigenvalue analysis. The verification process is succeeded, if all poles or else Eigenvalues take on values < 0.

4.3.2 Model Validation

In order to validate the performance of the linearized models against results of existing and already approved simulation tools, following steps are applied:

I. The WTG small-signal model is validated against a numerical EMT model. The performance is assessed by considering the dynamic modes being captured within the relevant system bandwidth of 5 Hz.

II. The overall WPP model is validated against power flow simulations in order to assess the change of network states obtained by step responses of the linearized model. Following scenarios are taken into consideration:
a.) Different number of active WPP arrays and thereby connected WTGs
b.) Different grid stiffnesses of the WPP connection

The validation process is assumed to be succeeded, if for all simulations an error of $< 5\,\%$ is obtained.

4.3.3 Control Design and Tuning

In order to investigate the WPP voltage control performance, the following stages and their respective success criteria are taken into account:

I. As outlined in chapter 2.5, the control architecture includes an AQR being used for compensating reactive power losses of the WPP network. Its design target is formulated by following criteria for the closed-loop system response:
A.) Due to the constraints of present ramp-rate limiters for reactive power change, the AQR response should avoid overshoot to limit the rate of change to a minimum value. The permitted overshoot is specified as $OS < 5\,\%$.
B.) Besides fulfilling criterion A.), the system response should be as fast as possible with regard to rise time and settling time to obtain a decent speed for reactive power output.

II. The design of the voltage slope control (AVR) is achieved by following criteria:
A.) In order match the speed of AVR and AQR to not decelerate the overall control behaviour, the bandwidth ω_b of the upstream system, namely namely the closed-loop system of AQR, should be regarded for determining the time response of the AVR.
B.) To ensure sufficient relative stability of the system, a gain margin of $G_m > 6\,\mathrm{dB}$ and a phase margin of $P_m > 40\,\mathrm{deg}$ should be ensured for the closed-loop system.

III. The final tuning process of voltage control is conducted by applying root locus analysis. The requirements summarized in Tab. 4.1 are used as target criteria in order to examine the control performance.

Tab. 4.1: Design requirements for voltage control

Parameter	Value	Unit
t_d	0.2	[s]
t_r	1.0	[s]
t_s	2.0	[s]
OS	15	[%]

For all three stages there are various test scenarios to be considered in order to analyze WPP voltage control for the whole operating range:

1. The WPP operates with different active power production levels, which are represented by following operating conditions:
   a.) WTGs around cut-in wind speed: $P_{WTG} = 0.1\,\text{pu}$
   b.) WTGs at average wind-speed: $P_{WTG} = 0.5\,\text{pu}$
   c.) WTGs at rated wind speed: $P_{WTG} = 1\,\text{pu}$
2. As this study regards the incorporation of dynamic compensation units for voltage control, following test cases are investigated:
   a.) Reactive power contribution by only WTGs
   b.) Reactive power contribution by both WTGs and STATCOMs

As voltage control is highly affected by the grid connection of WPPs, a large focus is laid on analyzing the dynamic behaviour of the system for different grid stiffnesses. In particular, step III. of the control design and tuning process requires some guidelines how to approach voltage control for different grid conditions. Thus, a realistic range of SCR ($SCR_{min}...SCR_{max}$) for UK grid is applied.

4.4 Summary

This chapter has given a brief description of the WPP used in this study, containing the WPP layout and its relevant system components. Furthermore, the relevant grid code requirements regarding voltage control in WPP have been explained by means of the UK grid code, where basically the demands for slope control as well as the reactive power output are specified. Based on that and on the performance criteria for control analysis (cp. chapter 3.3), a definition of the test scenarios and their evaluation measures have been outlined. The most important aspects of the evaluation process throughout this project are the model verification and validation as well as the control design and tuning, since they are required to assess the functionality and performance of the models developed in subsequent chapter.

5 System Design

This chapter describes the approach for the modelling of WPP components used for this study. The focus is to capture mainly the power system dynamics which are relevant with respect to the overall WPP voltage control, where the specified maximum bandwidth frequency is stated to be $f_b = 5\,\mathrm{Hz}$.

First, a small-signal model of the WTG is derived, where the focus is laid on the grid side converter and its relevant controllers affecting reactive power supply. Subsequent Eigenvalue analysis of the state-space representation provides the dominant system dynamics and verifies the modelling process (section 5.1).

The modelling approach of a STATCOM can be associated to the WTG, as its characteristics are describable analogously (section 5.2).

Then, the characterization of WPP components such as transformers, cables and external grid is elaborated. Due to the low frequency area to be regarded, for these components similar model considerations as for power flow studies are applied and discussed (section 5.3).

However, the best practice of linking all those WPP elements in state-space has not been established yet. Therefore, the following section provides a comprehensive WPP model in terms of a Multiple-Input-Multiple-Output (MIMO) system, whose functionality is verified by pole-zero-evaluation (section 5.4).

It is applicable for the overall WPP control level, whose various elements are outlined by transfer functions (section 5.5).

Finally, the benefits of the proposed model for this study and its adequacy for other types of studies is discussed.

5.1 Modelling of Wind Turbine Generators

As aforementioned, the WPP studied here consists of variable speed WTGs with full-scale power conversion, i.e. type-4 WTGs. This WTG type is chosen, as nowadays it is widely

used in wind power applications due to its higher efficiency and less complexity to deal with grid-related problems [33]. The WTG characteristics are modelled to a level of detail that captures its dynamics being relevant for the voltage control analysis of this study. Therefore a reduced electrical model of type-4 WTGs is developed for the purpose of this studies. It allows to finally set up the small-signal equations which can be linearized in order to study the system stability after suffering small disturbances.

Fig. 5.1 provides an overview of a type-4 WTG with a synchronous generator (SG). It is composed of two AC circuits which are decoupled by the DC-link of the full-scale converter. The machine side converter (MSC), in Fig. 5.1 labeled as generator rectifier, acts as a voltage source for the SG and controls the active power ouput of the WTG, whereas the grid side converter (GSC), in Fig. 5.1 labeled as grid inverter, controls the DC-link voltage and the reactive power output. The intermediate DC-link of the back-to-back converter system functions as buffer between the generator- and grid-side dynamics. Consequently, as this project focuses on reactive power and voltage control on the grid side of the WTG, there is no need to investigate the generator side.

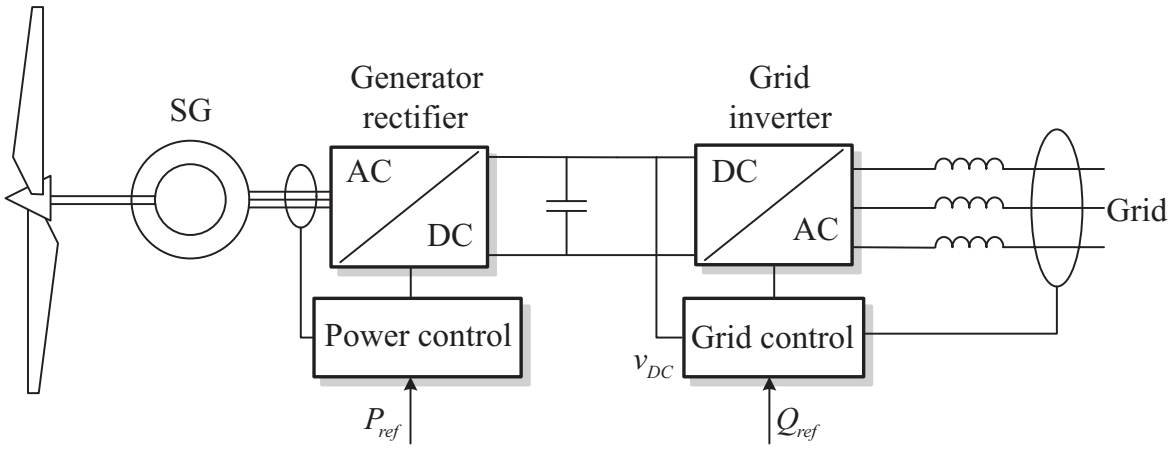

Fig. 5.1: Schematic of type-4 WTG with PMSG and back-to-back converter [3, p. 137]

5.1.1 Reduced Electrical Model

A reduced electrical model of a type-4 WTG in dq-reference frame is depicted in Fig. 5.2. It regards only the GSC and its controllers. Moreover, the schematics in Fig. 5.2 imply the WTG to be connected to a constant voltage source. However, when being grid-connected a GSC is affected by changes of voltage magnitude and angle at the connection point. Then a phase-locked loop (PLL) block is required in order to estimate changes in voltage angle. According to [34] a half-cycle from the fundamental grid frequency can be assumed

as the time constant of the angle tracking process, leading to a PLL bandwidth of 100 Hz. However, since it is outside the considered bandwidth of 5 Hz, it can be stated that the PLL will not affect the overall WPP voltage control dynamics. Hence, it is neglected for the reduced model of the WTG. The mathematical description of the system is derived

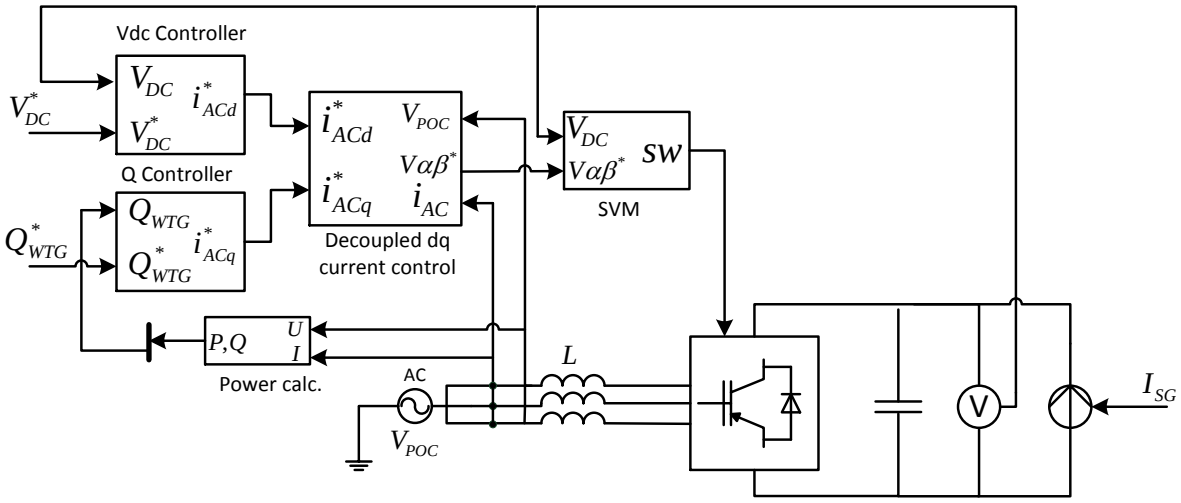

Fig. 5.2: Schematic diagram of grid-side converter and its controller for a type-4 WTG

subsequently. It originates from a small-signal model of type-4 WTG in [24], though adapted for a GSC including reactive power control. The GSC control consists of outer loops and inner CC loops, as already outlined in chapter 2.4. The input power P_{SG} coming from the SG is simply represented by a constant DC current source feeding the DC-link, so that Eq. 5.1 applies.

$$P_{SG} = I_{SG} V_{DC} \tag{5.1}$$

The expressions for the voltages v_{ACdq} at the AC terminal of the GSC are given by Eq. 5.2, where ω is the electrical angular velocity of the power grid voltage. It has to be stated that the WTG is connected to the point of connection (POC) via an LC filter used for eliminating low frequency harmonics as well as a step-up transformer. However, as the impedance of the shunt capacitance branch will be high for the investigated frequency range, it can be neglected. Moreover, a high X/R ratio of output filter and transformer can be assumed ($R \approx 0$), so that the circuit can be reduced to one series inductance L. [21, p. 51 ff.]

$$\begin{cases} v_{ACd} = L\frac{di_{ACd}}{dt} - \omega L i_{ACq} + v_{POCd} \\ v_{ACq} = L\frac{di_{ACq}}{dt} + \omega L i_{ACd} + v_{POCq} \end{cases} \tag{5.2}$$

In order to achieve a decoupled control of DC-link voltage and reactive power, the dq-reference frame of the WTG is normally aligned with the POC voltage, so that Eq. 5.3 applies.

$$\begin{cases} v_{POCd} = V_{POC} \\ v_{POCq} = 0 \end{cases} \tag{5.3}$$

Only during angle changes of the POC voltage, the q-axis voltage shows values unequal to zero. By neglecting the PLL dynamics as stated previously, the expressions in Eq. 5.3 are assumed to be valid also during small disturbances. Then, the active and reactive power output of the WTG can be described by Eq. 5.4.

$$\begin{cases} P_{WTG} = \frac{3}{2} i_{ACd} v_{POCd} \\ Q_{WTG} = -\frac{3}{2} i_{ACq} v_{POCd} \end{cases} \tag{5.4}$$

The d-axis current i_{ACd} is controlled to maintain a stable DC-link voltage V^*_{DC}, whereas the q-axis current i_{ACq} is regulated to obtain the reference reactive power Q^*_{WTG}. The schematic of the controller circuit is illustrated in Fig. 5.3 and the control equations are given by Eq. 5.5. 4 intermediate state variables φ_1, φ_2, φ_3 and φ_4 are introduced in order to express the dynamics of each PI controller presented in Fig. 5.3 a - d. The derivatives of each intermediate state variable $\frac{d\varphi}{dt}$ is defined prior to the respective PI controller, so that φ is obtained subsequent to the respective integral part.

$$\begin{cases} \frac{d\varphi_1}{dt} = V_{DC} - V^*_{DC} \\ i^*_{ACd} = K_{P,DC}(V_{DC} - V^*_{DC}) + K_{I,DC}\varphi_1 \\ \frac{d\varphi_2}{dt} = i^*_{ACd} - i_{ACd} \\ v^*_{ACd} = K_{P,id}(i^*_{ACd} - i_{ACd}) + K_{I,id}\varphi_2 - \omega L i_{ACq} + v_{POCd} \\ \frac{d\varphi_3}{dt} = Q_{WTG} - Q^*_{WTG} \\ i^*_{ACq} = K_{P,Q}(Q_{WTG} - Q^*_{WTG}) + K_{I,Q}\varphi_3 \\ \frac{d\varphi_4}{dt} = i^*_{ACq} - i_{ACq} \\ v^*_{ACq} = K_{P,iq}(i^*_{ACq} - i_{ACq}) + K_{I,iq}\varphi_4 + \omega L i_{ACd} + v_{POCq} \end{cases} \tag{5.5}$$

As the dynamic process of the space vector modulation (SVM) is determined by the switching frequency in the kHz range, the voltages at the AC terminal are assumed to be reached infitinitely fast, so that $v_{ACd} = v^*_{ACd}$ and $v_{ACq} = v^*_{ACq}$. According to Eq. 5.5 the

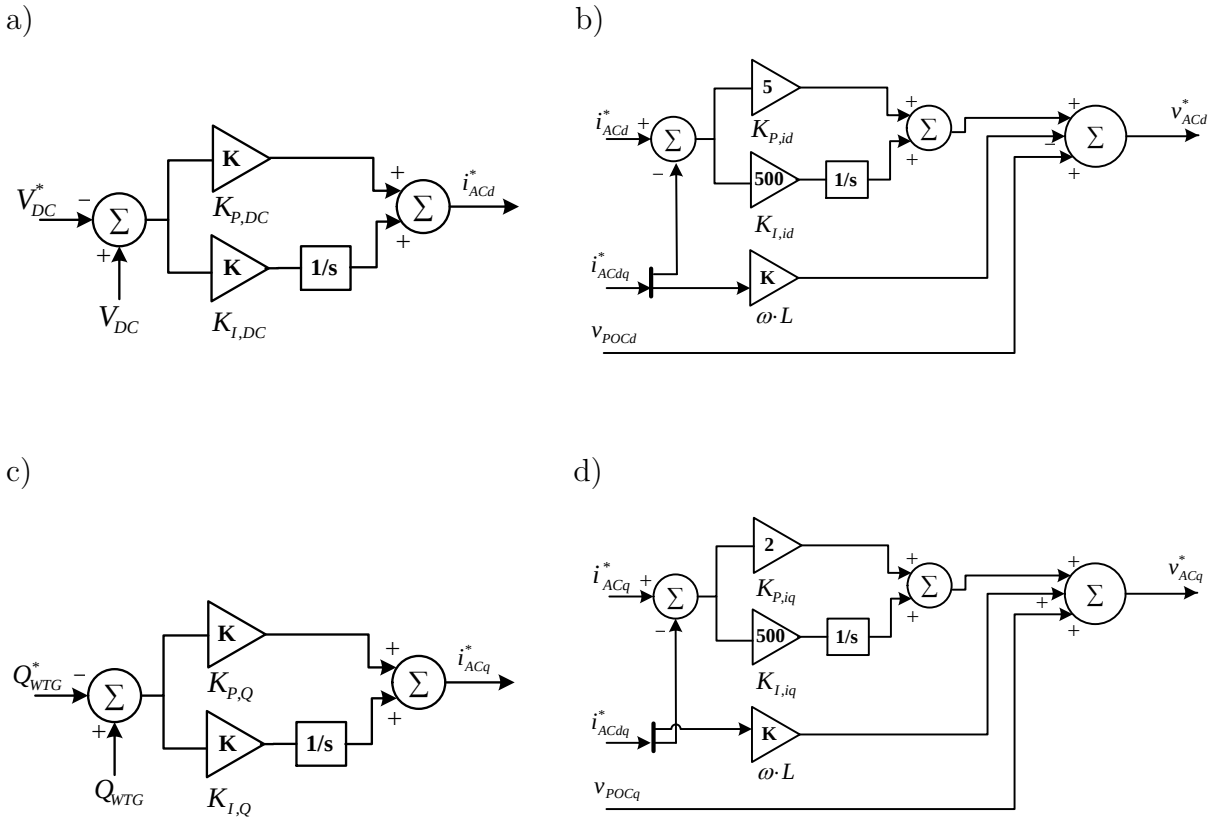

Fig. 5.3: Schematic diagram of GSC controllers: a) DC-link voltage controller, b) d-axis current controller, c) reactive power controller, d) q-axis current controller

dynamics of the current flowing across the inductance can be captured by Eq. 5.6.

$$\begin{cases} L\frac{di_{ACd}}{dt} = K_{P,id}(i^*_{ACd} - i_{ACd}) + K_{I,id}\varphi_2 \\ L\frac{di_{ACq}}{dt} = K_{P,iq}(i^*_{ACq} - i_{ACq}) + K_{I,iq}\varphi_4 \end{cases} \tag{5.6}$$

The power balance of the DC-link is described by the charging behaviour of the capacitor C (Eq. 5.7), where due to the negligence of resistances the WTG active power output equals the active power at the AC terminal of the GSC ($P_{WTG} = P_{AC}$).

$$C \cdot V_{DC}\frac{dV_{DC}}{dt} = P_{SG} - P_{AC} = P_{SG} - P_{WTG} \tag{5.7}$$

Finally, the voltage angle δ_{POC} at the POC needs to be taken into account in order to link the WTG model to the overall WPP model. Since the WTG is expressed by its own dq-reference frame, the output currents being linked to the WPP model have to be transformed to a common reference frame [8, p. 793]. By using the voltage angle at the POC of each WTG, the individual dq-variables can be connected to the phasor variables of the WPP model, which will be presented in section 5.3.

Fig. 5.4 shows the relationship of the current space vector in the stationary two-axis reference frame and the rotating dq-reference frame.

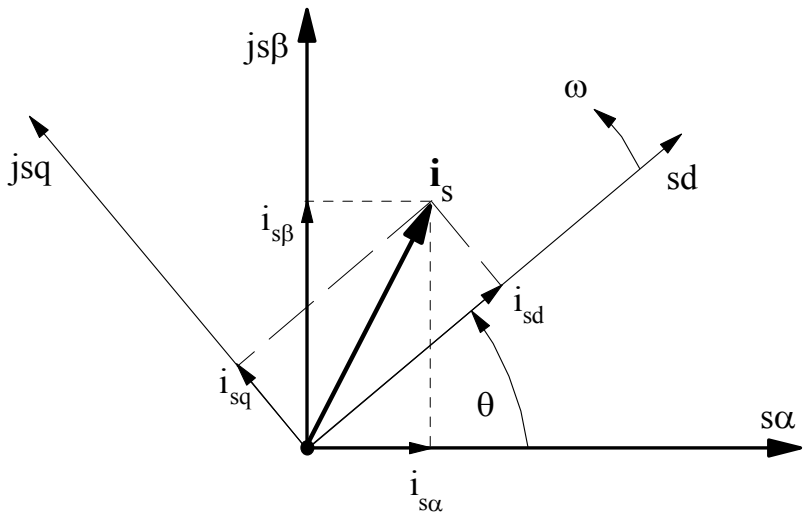

Fig. 5.4: Relationship of current space vector components in stationary and rotating reference frames [7]

The former is referred to be the common reference frame represented by real and imaginary components of the phasor variables, whereas the latter defines the individual dq-variables. Eq. 5.8 describes the Forward Park Transformation by Fig. 5.4, which can be applied to the real and imaginary currents of the WTG as expressed in Eq. 5.9.

$$\begin{bmatrix} i_{s\alpha} \\ i_{s\beta} \end{bmatrix} = \begin{bmatrix} \cos\theta & -\sin\theta \\ \sin\theta & \cos\theta \end{bmatrix} \begin{bmatrix} i_{sd} \\ i_{sq} \end{bmatrix} \tag{5.8}$$

$$\begin{cases} i_{AC,Re} = i_{ACd} \cdot \cos\delta_{POC} - i_{ACq} \cdot \sin\delta_{POC} \\ i_{AC,Im} = i_{ACd} \cdot \sin\delta_{POC} + i_{ACq} \cdot \cos\delta_{POC} \end{cases} \tag{5.9}$$

5.1.2 Small-Signal Model

Eq. 5.1 to 5.9 describing the electrical behaviour of the WTG are used to develop a state-space model. As previously mentioned in chapter 3 it enables to study the system stability after being subjected to small disturbances at a certain operating point.

The state-variables of the system are directly obtained by the dynamic equations (cp. Eq. 5.5 to 5.7), so that the following state vector applies.

$$\mathbf{x} = \begin{bmatrix} \varphi_1 & \varphi_2 & \varphi_3 & \varphi_4 & i_{ACd} & i_{ACq} & V_{DC} \end{bmatrix}^T \tag{5.10}$$

The input vector is defined as follows, where the reactive power reference Q^*_{WTG}, the voltage magnitude V_{POC} and angle δ_{POC} at the POC, the DC-link voltage reference V^*_{DC} and the DC current I_{SG}, representing the power input from the SG to the GSC, act as input variables to the system.

$$\mathbf{u} = \begin{bmatrix} Q^*_{WTG} & V_{POC} & V^*_{DC} & I_{SG} & \delta_{POC} \end{bmatrix}^T \tag{5.11}$$

As mentioned previously, the output of the system provides the real and imaginary components $i_{AC,Re}$ and $i_{AC,Im}$ of the WTG. Moreover, the reactive power output Q_{WTG} is defined as an output variable being used later on for the model validation (cp. chapter 6.1).

$$\mathbf{y} = \begin{bmatrix} i_{AC,Re} & i_{AC,Im} & Q_{WTG} \end{bmatrix}^T \tag{5.12}$$

By linearizing around steady-state values the linearized differential equations of the whole WTG model are developed with the resulting matrices $\boldsymbol{A}$, $\boldsymbol{B}$, $\boldsymbol{C}$ and $\boldsymbol{D}$ linking $\mathbf{x}$, $\mathbf{u}$ and $\mathbf{y}$ (cp. Eq. 3.3 of chapter 3.2). For a detailed presentation of the linearized model please refer to App. A.1.

5.1.3 Model Verification

In order to verify the obtained small-signal model of the WTG, the Eigenproperties of the system state matrix $\boldsymbol{A}$ are characterized. By computing the Eigenvalues, one can determine whether the system is stable and moreover analyze the oscillation and evanescent modes of the system and their origin (cp. chapter 3.3). Tab. 5.1 shows the Eigenvalues and their associated frequencies, damping ratios and time constants. It can be seen that the system will be stable after being subjected to a small disturbance, since all the Eigenvalues have negative real parts. All modes are evanescent and not oscillating, as none of the Eigenvalues is imaginary and all damping ratios are $\zeta = 1$. Tab. 5.2 depicts the associated participation matrix being used to analyze which state variables have a high participation in the mode corresponding to a certain Eigenvalue.

Tab. 5.1: Eigenvalues, frequency, damping ratio and time constant of the system matrix **A** of WTG state-space model

No.	Eigenvalues λ	Frequency f [Hz]	Damping ratio ζ	Time constant τ [s]
1	-9856	1568.68	1	0.0001
2	-801	127.53	1	0.0013
3	-101	16.03	1	0.0099
4	-14	2.16	1	0.0737
5	-5872	934.57	1	0.0002
6	-13	2.12	1	0.0750
7	-262	41.66	1	0.0038

Tab. 5.2: Participation matrix obtained for the system matrix **A**

(0.000∠0.00)	(0.019∠180.00)	(0.001∠0.00)	(**1.017∠0.00**)	φ_1
(0.011∠180.00)	(0.005∠0.00)	(**1.005∠0.00**)	(0.000∠0.00)	φ_2
(0.000∠0.00)	(0.000∠0.00)	(0.000∠0.00)	(0.000∠180.00)	φ_3
(0.000∠180.00)	(0.000∠180.00)	(0.000∠180.00)	(0.000∠180.00)	φ_4
(**1.042∠0.00**)	(0.035∠180.00)	(0.007∠180.00)	(0.000∠0.00)	i_{ACd}
(0.000∠180.00)	(0.000∠180.00)	(0.000∠0.00)	(0.000∠180.00)	i_{ACq}
(0.032∠180.00)	(**1.049∠0.00**)	(0.000∠0.00)	(0.018∠180.00)	V_{DC}
λ_1	λ_2	λ_3	λ_4	

(0.000∠0.00)	(0.000∠180.00)	(0.000∠0.00)	φ_1
(0.000∠0.00)	(0.000∠180.00)	(0.000∠180.00)	φ_2
(0.002∠180.00)	(**1.000∠0.00**)	(0.003∠0.00)	φ_3
(0.047∠180.00)	(0.000∠0.00)	(**1.047∠0.00**)	φ_4
(0.000∠180.00)	(0.000∠180.00)	(0.000∠0.00)	i_{ACd}
(**1.049∠0.00**)	(0.000∠0.00)	(0.049∠180.00)	i_{ACq}
(0.000∠180.00)	(0.000∠0.00)	(0.000∠180.00)	V_{DC}
λ_5	λ_6	λ_7	

By analyzing the results of Tab. 5.1 and 5.2, the following can be observed:

- λ_1 is highly sensitive to i_{ACd} and λ_5 to i_{ACq}. Their associated time constants are below $\tau_{1,5} < 1\,\text{ms}$. Both are mainly affected by the converter inductance in the way that the larger L, the larger the time constant.
- λ_2 is highly sensitive to V_{DC} and thereby influenced by the DC-link capacitance, whose sizing affects the time response in a proportional relation.
- λ_3 is highly sensitive to φ_2 and is mainly affected by the d-axis CC parameters $K_{P,id}$ and $K_{I,id}$, whereas λ_7 is highly sensitive to φ_4 and is mainly affected by the q-axis

CC parameters $K_{P,iq}$ and $K_{I,iq}$. Their time constants of $\tau_3 = 10\,\text{ms}$ and $\tau_7 = 4\,\text{ms}$ are in the range of miliseconds, which is typical for CCs of GSCs [21, p. 56]. By looking at the frequencies associated with those Eigenvalues ($f_3 = 16\,\text{Hz}$, $f_7 = 42\,\text{Hz}$), it can be stated that they will not affect the relevant WPP control dynamics, as they are outside the considered bandwidth of 5 Hz.

- λ_4 is highly sensitive to φ_1 and is mainly affected by the DC-link controller parameters $K_{P,DC}$ and $K_{I,DC}$, whereas λ_6 is highly sensitive to φ_3 and is mainly affected by the reactive power controller parameters $K_{P,Q}$ and $K_{I,Q}$. Their time constants of $\tau_4 = 74\,\text{ms}$ and $\tau_6 = 75\,\text{ms}$ imply that those control loops reach their reference target within a few hundreds of miliseconds, being typical for multi-megawatt WTGs [21, p. 56]. Those Eigenvalues exhibit frequencies around $f_{4,6} \approx 2\,\text{Hz}$, hence being highly relevant for the overall voltage control of the WPP.

In order to assess the WTG response with regard to reactive power supply, the Single-Input-Single-Output (SISO) transfer function with $Q_{WTG}*$ as input and Q_{WTG} as output is computed by applying the theories outlined in chapter 3.2. The transfer function is characterized by a third-order system of type 2 being shown in Eq. 5.13 for exemplary initial values of $P_{WTG,0} = 1\,\text{pu}$, $Q_{WTG,0} = 0\,\text{pu}$, $V_{POC,0} = 1\,\text{pu}$ and $\delta_{POC,0} = 0\,\text{deg}$.

$$G_{Q^*_{WTG}Q_{WTG}}(s) = \frac{\triangle Q_{WTG}(s)}{\triangle Q^*_{WTG}(s)} = \frac{2049s^2 + 5.94 \cdot 10^5 s + 2.05 \cdot 10^7}{s^3 + 6147s^2 + 1.62 \cdot 10^6 s + 2.05 \cdot 10^7} \tag{5.13}$$

The frequency response obtained in MATLAB is shown as bode plot in Fig. 5.5.

It can be seen that the system has an infinite gain margin and a phase margin of 180 deg, hence indicating a relatively stable system with abundant margins. Moreover, in Fig. 5.5 the three poles (x) and two zeros (o) of the transfer function are indicated along the frequency spectrum. The system poles of the transfer function correspond to the Eigenvalues of the system in state-space domain. As outlined previously, Eigenvalues λ_5, λ_6 and λ_7 are associated with the reactive power controller and hence appear as poles of the transfer function $G_{Q^*_{WTG}Q_{WTG}}(s)$. Pole λ_6 at $\omega_6 = 2\pi \cdot 2.12\,\text{Hz} = 13.32\,\frac{\text{rad}}{\text{s}}$ causes the decline in magnitude, until the first zero counteracts. As the second zero and pole λ_7 at $\omega_7 = 2\pi \cdot 41.66\,\text{Hz} = 261.76\,\frac{\text{rad}}{\text{s}}$ are located closed to each other the magnitude remains constant, until pole λ_5 at $\omega_5 = 2\pi \cdot 934.57\,\text{Hz} = 5872.1\,\frac{\text{rad}}{\text{s}}$ forces the magnitude to decrease further.

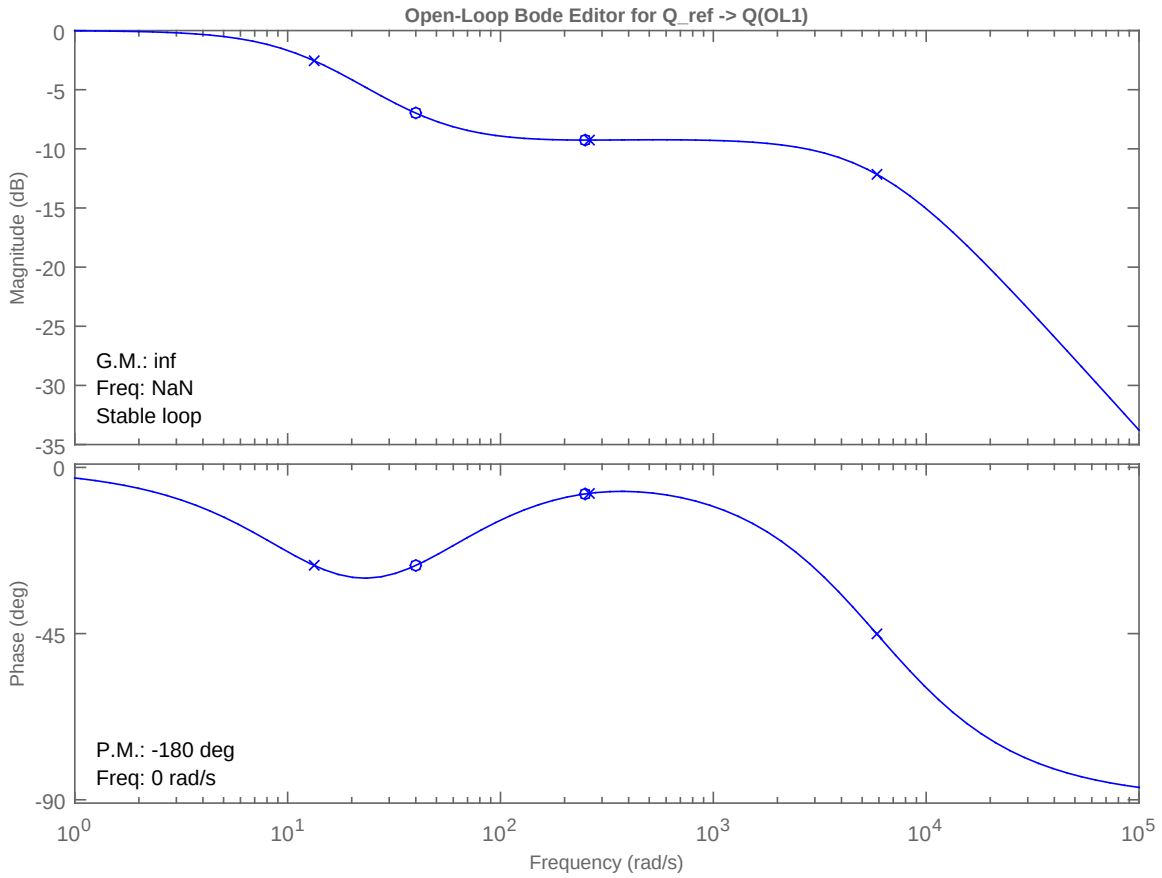

Fig. 5.5: Frequency response of $G_{Q^*_{WTG}Q_{WTG}}(s)$ of WTG state-space model

5.2 Modelling of STATCOM

As outlined in chapter 2.7, two STATCOMs are embedded in the WPP network for the purpose of dynamic reactive power contribution. Likewise for the WTGs, the control mode of the STATCOM aims for reactive power reference. Hence, the same schematics of the GSC for a type-4 WTG and its controllers according to Fig. 5.2 can be applied. However, as the STATCOM does not produce active power, the DC-link capacitor is not charged by a DC current source as for the WTG. On the other hand, a real STATCOM requires active power from the grid in order to compensate for resistive losses. This is achieved by controlling the DC-link voltage. However, as for the WTG the resistive losses are disregarded due to the dominant impact of the line reactance.

The complete state-space model of the STATCOM is developed according to the considerations and derivations for the WTG model described in section 5.1.

5.3 Modelling of Wind Power Plant Network Components

The WPP network, namely an interconnected set of electrical lines and transformers both onshore and offshore, transfers the power generated by the WTGs to the PCC, where the interface of WPP network and external grid is defined. Hence, all network components need to be modelled with respect to the purpose of voltage control analysis.

5.3.1 Cables

According to [8, p. 208], underground cables with line lengths of less than 60 km can be represented by the classical RLC π-model with lumped parameters for the purpose of power system stability analysis. Hence, both export and array cables are modelled by their respective line resistance R, line reactance X and shunt admittance Y as shown in Fig. 5.6, whose values are provided in per unit length.

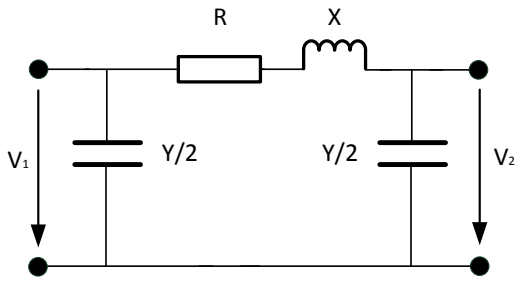

Fig. 5.6: Cable π-model with lumped parameters acc. to [8, p. 207]

5.3.2 Transformers

According to [8, p. 231 ff.], transformers can be represented by an equivalent series RL impedance corresponding to the circuit depicted in Fig. 5.7.

Due to the large impedance in big power transformers the exciting current is very small. Hence, the shunt branch core loss resistance R_c and magnetizing reactance X_m can be neglected [9, p.79].

The transformer is characterized by the rated power S_{rT}, the short-circuit voltage u_k and the copper losses P_{copper}. The equivalent impedance is calculated according to Eq. 5.14 -

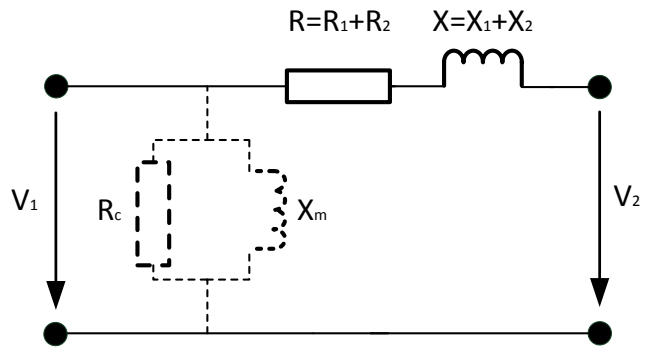

Fig. 5.7: Approximate equivalent circuit of the transformers acc. to [9, p.79]

5.16 , where Z_T, R_T and X_T describe the short-circuit impedance, resistance and reactance based on the rated voltage V_{rT} of either the HV or LV side of the transformer [35].

$$Z_T = \frac{V_{rT}^2}{S_{rT}} \cdot \frac{u_k}{100} \tag{5.14}$$

$$R_T = \frac{V_{rT}^2}{S_{rT}} \cdot \frac{P_{copper}}{S_{rT}} \tag{5.15}$$

$$X_T = \sqrt{Z_T^2 - R_T^2} \tag{5.16}$$

For a three-winding transformer as for the SGTs (cp. Fig. 4.1), those parameters are determined equally by using the rated power specified for each winding, the short-circuit impedance defined between the respective windings and the rated voltage of either HV, MV or LV side of the transformer [36].

Apart from voltage transformation, transformers are often used for control of voltage and reactive power flow, which is realized by taps in one or more windings for changing the turns ratio. In particular OLTCs are applied, when the changes need to be frequent [8, p. 231]. However, it has been stated by [2, p. 48 f.] by analyzing the controller time responses that OLTC are deployed for steady-state voltage control, while WTGs and STATCOM are used for dynamic voltage control. Hence, tap dependent impedances are disregarded for the transformer modelling.

5.3.3 Mechanically Switched Reactor and Harmonic Filters

Both mechanically switched reactor (MSR) and C-type harmonic filters (HFs) are modelled by shunt admittances connected to their corresponding busses. Both components feature active power losses, in particular the harmonic filter including, which includes resistances for damping purposes. However, for the sake of simplicity and due to the fact that this

study does not focus on active power losses, they are disregarded. Then Eq. 5.17 describes the shunt susceptance B_{shunt}, where positive Q_{shunt} expresses Mvar injection (capacitor) and negative Q_{shunt} Mvar absorption (reactor). [8, p. 627 ff.]

$$B_{shunt} = \frac{Q_{shunt}}{V^2} \tag{5.17}$$

MSRs are capable of switching several reactor banks with certain step sizing [2, p.45]. However, the power flow studies of the WPP network (cp. App. A.4) show that a MSR rating of 100 % enables the WTGs to use the largest part of their Q capability for dynamic responses and hence is applied for this studies.

5.3.4 External Grid

The external grid is represented by the Thevenin equivalent circuit depicted in Fig. 5.8, where V_{grid} is the line-to-line voltage of an infinite stiff grid and Z_{grid} the grid impedance. Z_{grid} is determined by the short-circuit power, which is present in case of a system fault.

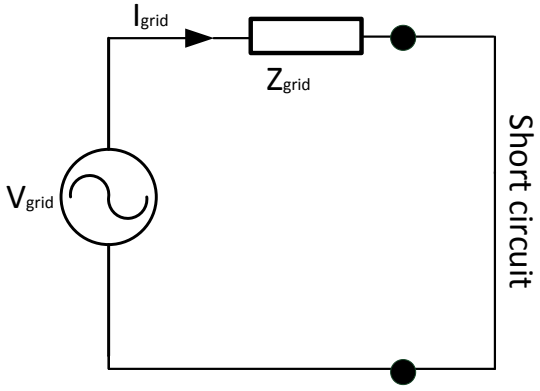

Fig. 5.8: Definition of short-circuit power and impedance of the external grid by Thevenin equivalent circuit acc. to [10, p. 33]

This fault level is described by the current I_{grid} that will flow into a network in case of a short-circuit. The corresponding short-circuit power S_{grid} is calculated according to eq. 5.18.

$$S_{grid} = \sqrt{3} I_{grid} V_{grid} = \frac{V_{grid}^2}{Z_{grid}} \tag{5.18}$$

If the short-circuit power is large, then the grid impedance is small. This leads to the fact that voltage variations between the ideal voltage source of the infinite stiff grid and the connected network are likely to be less substantial, indicating a stiff grid. Vice versa,

a low short-circuit power and high grid impedance cause significant voltage variations and thereby characterize a relatively weak grid [10, p. 32 ff.]. The grid stiffness can be measured by the ratio of short-circuit power and rated power of the connected power plant according to Eq. 5.19. In [37] it is stated that a grid is stiff for short-circuit ratios of $SCR > 20$.

$$SCR = \frac{S_{grid}}{P_{WPP,r}} \tag{5.19}$$

In the *Electricity Ten Year Statement* provided by *National Grid* there are presented the fault levels for various locations in the UK grid [38]. The short-circuit power levels at grid voltages of $V_{grid} = 275\,\text{kV}$ vary between $S_{grid,min} = 735\,\text{MVA}$ and $S_{grid,max} = 21050\,\text{MVA}$ for all the listed locations, corresponding to short-circuit ratios of $SCR_{min} = 3.5$ and $SCR_{max} = 100$. However, by performing power flow studies it has been observed that the PQ-chart specified in the grid code requirements cannot be fulfilled by a weak grid connection with $SCR_{min} = 3.5$. A minimum short-circuit ratio of $SCR_{min} = 11$ has been obtained for the external grid that allows the considered WPP to be connected without violating steady-state grid code requirements. Hence, the assessment of dynamic voltage control is performed for the range of $SCR = 11...100$. For a description of the power flow studies please refer to App. A.4.

In order to obtain the resistive and reactive parts of the grid impedance, R_{grid} and X_{grid}, the XR-ratio is usually applied. A common value for the XR-ratio recommended in grid codes and used in studies (cp. [39] and [40]) is 10 and is also applied in this investigation. According to equations 5.20 to 5.22 the necessary design parameters for the external grid depending on S_{grid} and XR-ratio are summarized.

$$Z_{grid} = \frac{U_{grid}^2}{S_{grid}} \tag{5.20}$$

$$R_{grid} = \sqrt{Z_{grid}^2 - X_{grid}^2} = \frac{Z_{grid}}{\sqrt{1 + XR^2}} \tag{5.21}$$

$$X_{grid} = XR \cdot R_{grid} \tag{5.22}$$

5.4 Constructing of Wind Power Plant Model

All network components and the individual state-space models of WTG and STATCOM described in previous sections needs to be connected. This is achieved by a set of algebraic, complex equations according to Kirchhoff's law in a common synchronous reference frame. The functional diagram of the WPP network model is depicted in Fig. 5.9. Both STATCOM

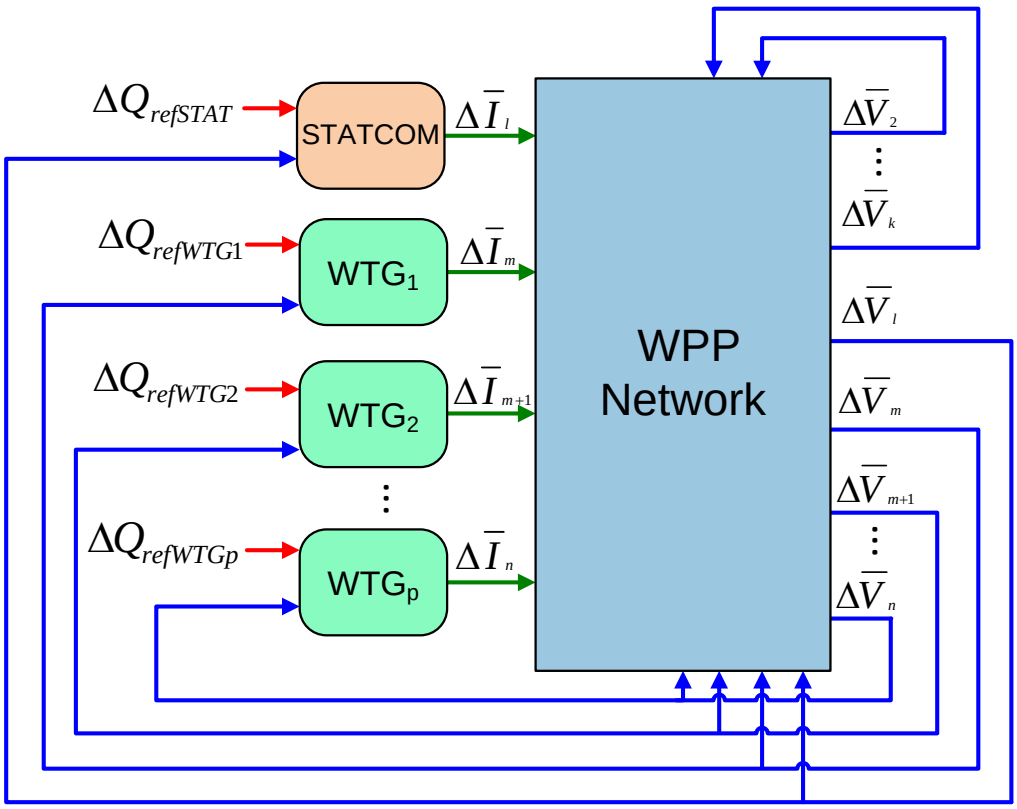

Fig. 5.9: Functional diagram of wind power plant model used for the state-space representation

and WTGs, numbered from 1 to p, receive reactive power reference signals from the WPP controller. Then, by knowing the current injections from those interconnected dynamic devices, the network voltage at each bus can be resolved (in Fig. 5.9 voltages and currents indexed by $l, m...n$). In [41] the state-space representation of the network is achieved by directly linking current injections to bus voltages by the impedance matrix of the network. However, this approach is not applicable for networks that also contain busses without current injections, meaning busses without connected WTGs (in Fig. 5.9 voltages indexed by $2...k$). One has to notice that not only current injections influence the bus voltages, but also voltage changes of adjacent busses. In order to reflect this aspect, Eq. 5.23 originating from the power flow theory can be applied [42].

$$\bar{V}_i = \frac{1}{Y_{ii}}(\bar{I}_i - \sum_{j=1 \neq i}^{n} Y_{ij}\bar{V}_j) \tag{5.23}$$

The i-th voltage is affected by both the i-th current injection and the sum of all adjacent current flows resulting from the j-th voltage. The feedback loop of the adjacent bus voltages is realized by using the non-diagonal elements Y_{ij} of the network admittance matrix, while the current injections are linked by the diagonal elements Y_{ii}.

Finally, for setting up the state-space model of the WPP network, the complex phasors are treated separately by real and imaginary components. It is worth mentioning that real and imaginary components of voltages and currents are mutually coupled according to Eq. 5.24 and 5.25, where G represents the conductance and B the susceptance.

$$[\mathrm{I}] = [\mathrm{Y}]\,[\mathrm{V}] \tag{5.24}$$

$$I_{Re} + jI_{Im} = (G + jB) \cdot (V_{Re} + jV_{Im}) \tag{5.25}$$

The respective voltage magnitudes and angles used as input variables for the WTG model are obtained by Eq. 5.26.

$$\begin{cases} V = \sqrt{V_{Re}^2 + V_{Im}^2} \\ \delta = \tan \frac{V_{Im}}{V_{Re}} \end{cases} \tag{5.26}$$

In this way, the state-space model is capable of calculating the voltage magnitudes and angles at every single bus of the network. Moreover, for performing WPP control the reactive power Q_{PCC}, exchanged with the external grid and measured at the PCC, is calculated according to Eq. 5.27.

$$Q_{PCC} = \frac{V_{PCC}(V_{PCC} - V_{grid}\cos\delta_{PCC})}{X_{grid}} \tag{5.27}$$

Using the already linear Eq. 5.23 and linearizing Eq. 5.26 and 5.27 around steady-state values yields to a state-space representation of the WPP network model. For a complete presentation of the linearized model please refer to App. A.3, where the linking of individual state-space functions to an overall MIMO state-space system is outlined.

5.4.1 Model Verification

The overall WPP state-space model is verified by assessing the MIMO system with $\mathbf{\Delta Q_{ref}}$ as input signals and $\mathbf{\Delta V}$ as output signals (cp. Fig. 5.9). It represents the *Plant* of a typical feedback control system not having regarded the *Controller* yet. However, in order to verify the model linking process of this section, it seems reasonable to investigate the incomplete open-loop system illustrated in Fig. 5.9.

The pole-zero plot shows the location in the complex plane of both poles and zeros of the

MIMO system. It is depicted in Fig. 5.10. It can be seen that all poles are located in the

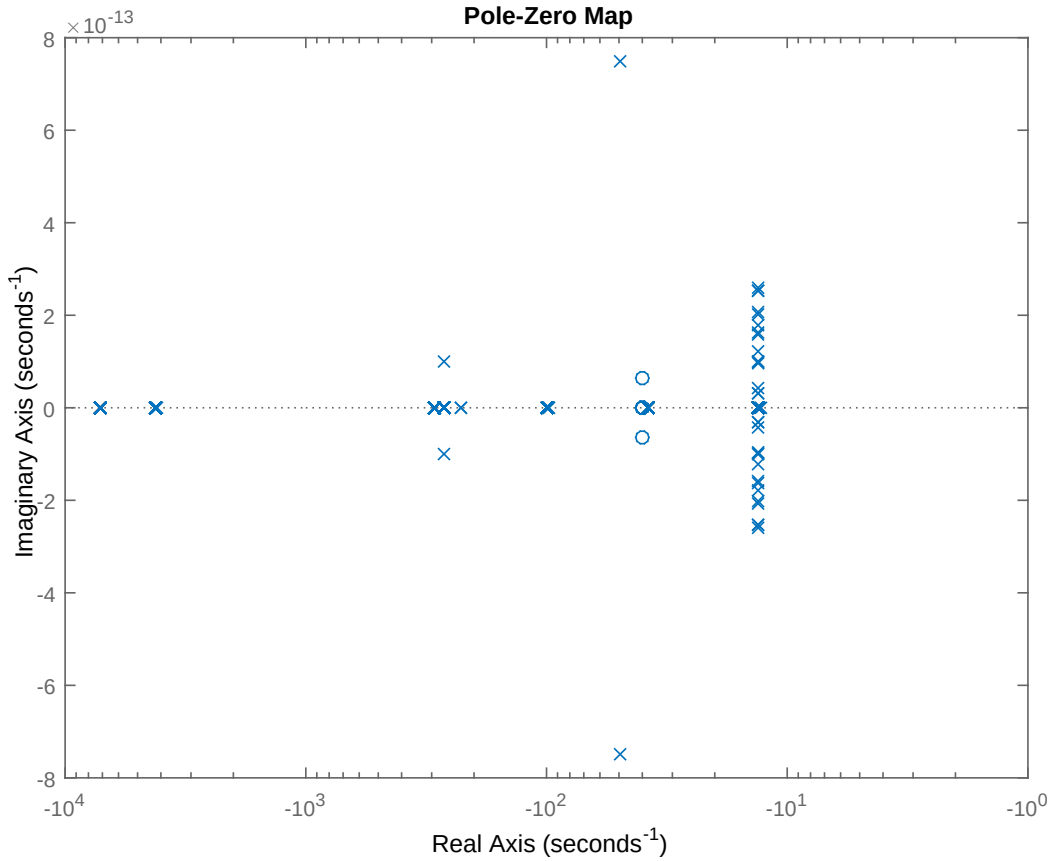

Fig. 5.10: Pole-zero map of MIMO system of WPP with $\mathbf{\Delta Q_{ref}}$ as input signals and $\mathbf{\Delta V}$ as output signals acc. to Fig. 5.9

left hand side of the complex plane, indicating that the overall model is stable.

5.5 Modelling of Wind Power Plant Control

As it was already outlined in the state-of-the-art studies of chapter 2, the WPP control receives reference and measured feedback signals and provides set-points to the individual WTGs and STATCOM. For this study the WPP main controller is selected to feature an outer voltage control loop (AVR) and an inner reactive power control loop (AQR) according to control scheme II.a) of chapter 2.2. The system representation is illustrated in Fig. 5.11.

The feedback loops of both voltage V_{PCC} and reactive power Q_{PCC} include meters, which sense the voltages and currents. The measurement devices sample the physical output signal of the current transformers (CTs) and voltage transformers (VTs) by first calculating

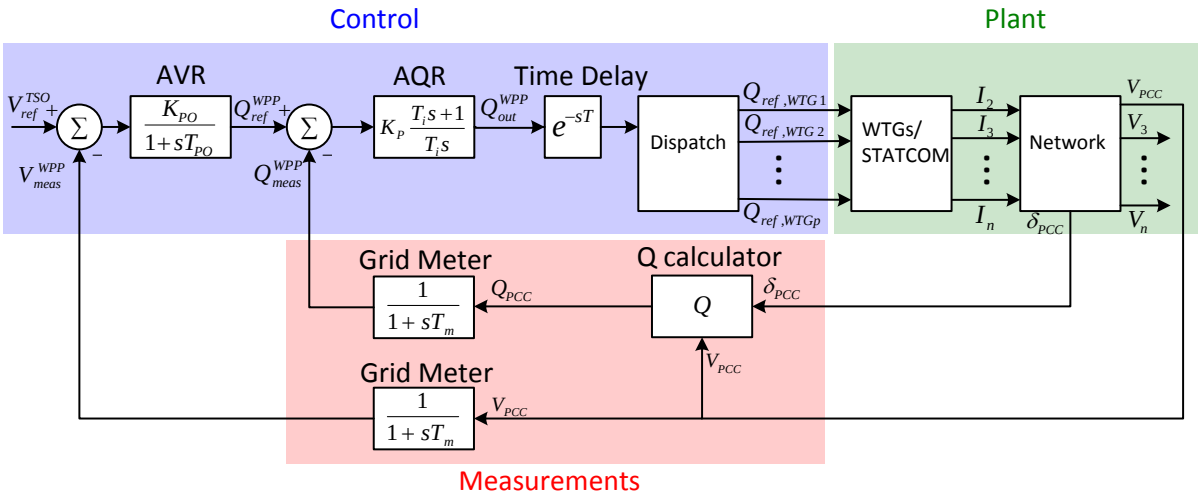

Fig. 5.11: System representation for the overall wind power plant voltage control

cycle RMS values and then filtering for anti-aliasing. This process can be described by a first-order time response according to Eq. 5.28.

$$F_m(s) = \frac{1}{1 + sT_m} \tag{5.28}$$

A time constant of $T_m = 15\,\text{ms}$ may be assumed for the grid meters [2, p. 28].

The s-domain transfer functions of the AVR and AQR are given according to Eq. 5.29 and 5.30.

$$F_{AVR}(s) = \frac{K_{PO}}{1 + sT_{PO}} \tag{5.29}$$

$$F_{AQR}(s) = K_p \frac{T_i s + 1}{T_i s} \tag{5.30}$$

However, in real life discretized control is implemented which exhibits a sampling time T_s. It can be considered as a pure delay using half of the sampling time [25].

Moreover, the WPP control also contains a processor, that computes the control and dispatcher algorithms, as well as a communication hub. According to [2, p. 21] „this communication hub collects all the feedbacks, packs and sends all the necessary references for the correct operation of the WTGs, STATCOM [...], using for that purpose the communication WPP Ethernet network and specific protocols.“ This whole process introduces a time delay T_{com}, which is grouped together with the sampling delay leading to a total system delay T according to Eq. 5.31.

$$T = 0.5T_s + T_{com} \tag{5.31}$$

Its transfer function is described by Eq. 5.32, where the non-linear expression for the delay

e^{-sT} is replaced by a linearized approximation, namely the first-order Pade function [2, p. 28].

$$F_{del}(s) = e^{-sT} \approx \frac{1 - \frac{1}{2}sT}{1 + \frac{1}{2}sT} \tag{5.32}$$

The dispatch function can be described by Eq. 5.33, where the individual WTGs and the STATCOMs participate in reactive power control depending on their contribution factor K.

$$\begin{bmatrix} Q_{ref,STAT} \\ Q_{ref,WTG1} \\ Q_{ref,WTG2} \\ ... \\ Q_{refWTGp} \end{bmatrix} = \begin{bmatrix} K_{STAT} \\ K_{WTG1} \\ K_{WTG2} \\ ... \\ K_{WTGp} \end{bmatrix} \begin{bmatrix} Q_{out}^{WPP} \end{bmatrix} \tag{5.33}$$

It needs to be regarded that the WTGs' contribution is limited due to their reactive power capability limit. A typical Q range of a type-4 WTG is $\Delta Q_{WTG,max} = \pm 0.6\,\text{pu}$, based on its designed power rating [43]. Moreover, it is worth mentioning that dependent on the dispatching method (cp. chapter 2.3) the individual WTGs may send their actual active power production to the WPP controller in order to evaluate how much reactive power they can contribute. Therefore, another communication delay is introduced, which however can be captured by the previously mentioned value T_{com}. [2, p. 21 ff.]

5.6 Model Adequacy

The proposed model has been developed for the purpose of analyzing voltage control aspects on WPP level.

- The separated modelling steps of first realizing the *Plant* in sections 5.1 - 5.4 and subsequent implementation of the *Control* part enable the user to apply generic tools for analyzing typical feedback control systems (cp. chapter 3.3). In this way, various control strategies may be evaluated for the same plant system in order to optimize the performance of WPP voltage control.

As model aggregation techniques have not been considered, the model includes every single component of the WPP. This can be disadvantageous, as its execution leads to longer computation times. Moreover, such a high-order system seems to be challenging when designing the WPP control, which is outlined later in chapter 7. However, adequate model order reduction can be applied for control tuning, so that only the dominant poles and zeros of the overall WPP transfer function are regarded.

- On the other hand, such an extensive model enables the user not only to evaluate the WPP voltage control performance at the PCC, but also to investigate the behaviour within the WPP. In this way, the voltage magnitudes of the array network are accessible during time-domain simulations of the state-space model, enabling to check the voltage limits of the MV network.

- In this context, the greatest benefit is the capability of performing analyses for the WPP dispatch function, which has not been established yet in recent WPP control studies. Various techniques of integrating the WTGs and STATCOMs into voltage control can be analyzed, as the reactive power supply of the individual devices is accessible and in this way comparable to their capability limits respectively.

- Moreover, a comprehensive state-space representation of the whole WPP allows for analyzing the Eigenvalues of the system. In this way, possibly occurring power system oscillations and their origin can be investigated.

The model features some limitations, which can be summarized as follows:

- Representing the overall system by phasor variables prevents the model from being subjected to any asymmetric disturbances. The overall modelling philosophy relies on voltage and current symmetry assumption.

- Moreover, using phasor variables forestalls the possibility of observing voltage and current waveforms, hence disabling the user to investigate the characteristics in EMT domain. Thus, all stability problems observable in high frequency range are not representable by this model. Obviously, harmonic emission studies also can also not be performed.

- Sub-synchronous interactions in the typical frequency region of 10 - 50 Hz are not considered, as the dynamics occurring at frequencies higher than the specified bandwidth of 5 Hz are not sufficiently described for every single network component.

- Small-signal linearization implies that for decent accuracy the model can only be used for the application of small-signal disturbances. Hence, it disqualifies the model from being used for FRT studies, characterized by large disturbances.

- As only the GSC of the WTG is considered in the state-space model, it disallows the investigation of any dynamics occurring on the generator side of the full-scale converter.

5.7 Summary

This chapter has focussed on the modelling of the system components of the WPP. A large focus is laid on the state-space representation of WTGs and STATCOMs, since they determine the most significant dynamics of the plant. Regarding the WTG model, only the grid side converter has been captured to respect reactive power contribution. Its functionality has been successfully validated by Eigenvalue analysis. Building the WPP model has been achieved by creating a MIMO state-space system, embedding all individual components such as WTGs, STATCOMs, cables, transformers, filters, reactor and the external grid. Connecting small-signal changes of voltages and currents has been realized by considerations taken from the power flow theory, as it can be applied for a phasor based model with small time constants involved in the network dynamics. Moreover, the transfer functions being relevant for the overall WPP control have been specified, embracing both AVR and AQR as well as the dispatch function and possible system delays. Finally, the adequacy of the complete model has been evaluated. A comprehensive system analysis with respect to voltage control is enabled by the small-signal model, which prior to application requires a thorough validation process, which is presented in subsequent chapter.

6 Model Validation

This chapter describes the validation of the WTG model and the overall WPP model. Firstly, the validation of the WTG controller is performed, where the Q controller and DC-link voltage controller are validated against an EMT model, which is developed in the simulation platform *PLECS* (section 6.1). Finally, the overall WPP model is validated against load flow simulation performed in *MATLAB* (section 6.2). The results obtained of these validations are evaluated according to the evaluation criteria stated in chapter 4.3.

6.1 Validation of WTG Model

The purpose of this section is to present the most representative simulation results in order to validate the performance of the state-space model of a WTG, which has been developed in chapter 5.1. The state-space model of the WTG is validated according to an EMT model which is developed in the simulation platform *PLECS*. The model verification of chapter 5.1.3 has shown that both outer control loops exhibit frequencies within the considered bandwidth of these studies. Hence, two different tests are performed in order to validate the performance of the outer controller of the WTG state-space model. Firstly, a step-response for reactive power is performed in order to validate the performance of the Q controller. Finally, a disturbance in active power is injected in order validate the performance of the DC-link voltage controller.

6.1.1 Validation of Q controller

Following test cases are performed in order to validate the response performance of the Q-controller.

1. $\triangle Q_{ref}^{WTG} = 0.1\,\text{pu}$ starting at $Q_0^{WTG} = 0\,\text{pu}$
2. $\triangle Q_{ref}^{WTG} = 1\,\text{pu}$ starting at $Q_0^{WTG} = 0\,\text{pu}$
3. $\triangle Q_{ref}^{WTG} = -0.5\,\text{pu}$ starting at $Q_0^{WTG} = 1\,\text{pu}$

Test case (1.) is performed to analyze the performance of the state-space model for a relatively small disturbance of $\triangle Q_{ref}^{WTG} = 0.1\,\text{pu}$, whereas test case (2.) considers a larger disturbance of 1 pu. Meanwhile, test case (3.) aims for validating a negative step response of $\triangle Q_{ref}^{WTG} = 1\,\text{pu}$.

The results for test case (1.) are depicted in Fig. 6.1, where the step responses of both models are shown on the upper side and their relative error on the lower side. The step is triggered at $t = 0.3\,s$ and the simulation lasts for 1 s.

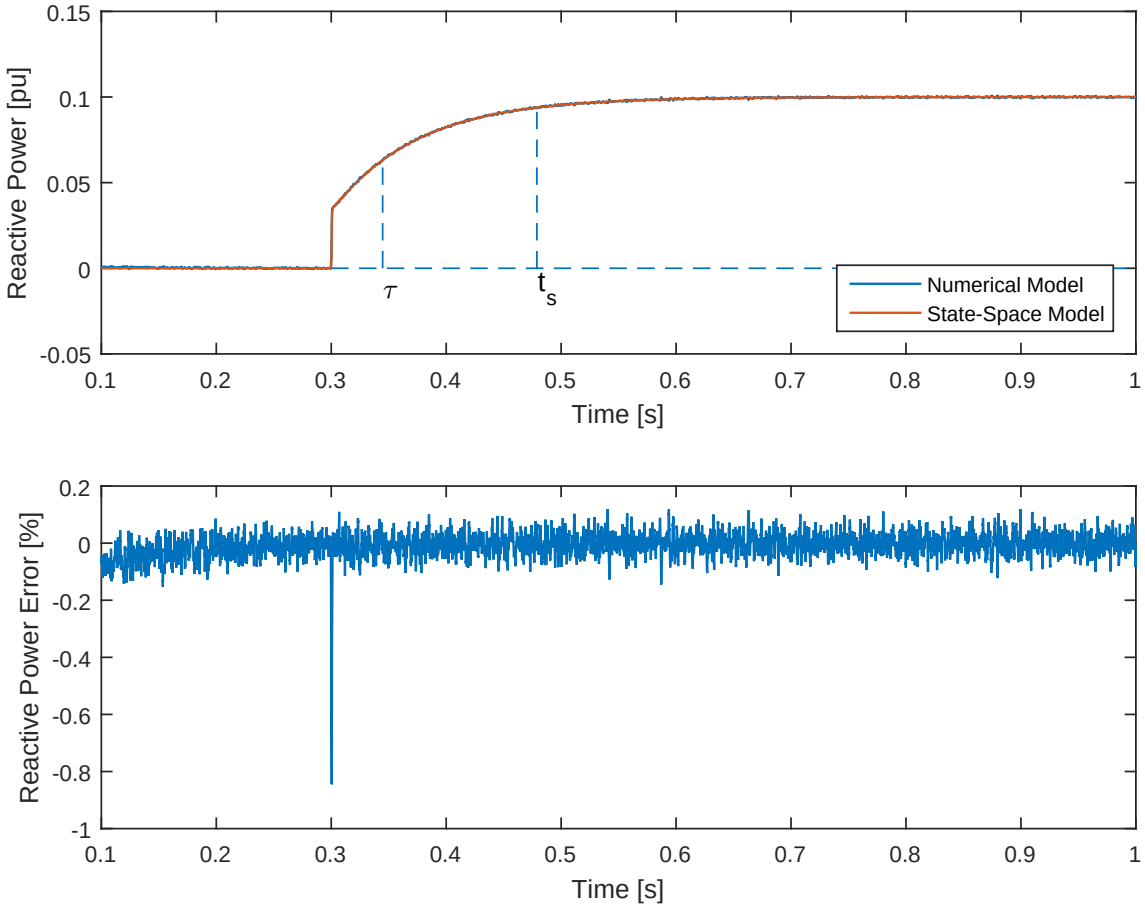

Fig. 6.1: Reactive power step response for state-space model and EMT model ($\triangle Q_{ref}^{WTG} = 0.1\,\text{pu}$ starting at $Q_0^{WTG} = 0\,\text{pu}$)

When considering step responses, there are certain parameters of interest being used for performance validation. As mentioned in chapter 5.1.3, the Q controller is described by a third-order system. By looking at the response in Fig. 6.1, a steep rise of reactive power in the very first instant can be observed. However, in real life this does not occur due to the presence of ramp-rate limiters. They prevent fast transients in the system by limiting the rate of reactive power per time. An exemplary value found for the maximum reactive power ramp-rate of the *Vestas V112* WTG amounts to 20 pu/sec [44].

By disregarding the fast transient in the beginning of the step response, one might approximately assume the system to be of first-order. Then one significant parameter will be the time constant τ, which is defined as the response of a controller to a step input and represents the time it takes the system's step response to reach 63.2 % of the final steady-state output. On the other hand the settling time t_s is a measure of the time required for the output to settle within a certain value of its final value. For a 2 % criterion the settling time amounts to $t_s = 4\tau$. In order to validate the state-space model by the EMT model, it is reasonable to analyze the error for these significant numbers.

As it can be seen in Fig. 6.1, the Q step response in the state-space model is similar to the simulated one in the EMT model. The calculated relative errors of $err_\tau = 0.112\,\%$ and $err_{ts} = 0.038\,\%$ are within an acceptable range (cp. chapter 4.3).

The results for test case (2.) are depicted in Fig. 6.2.

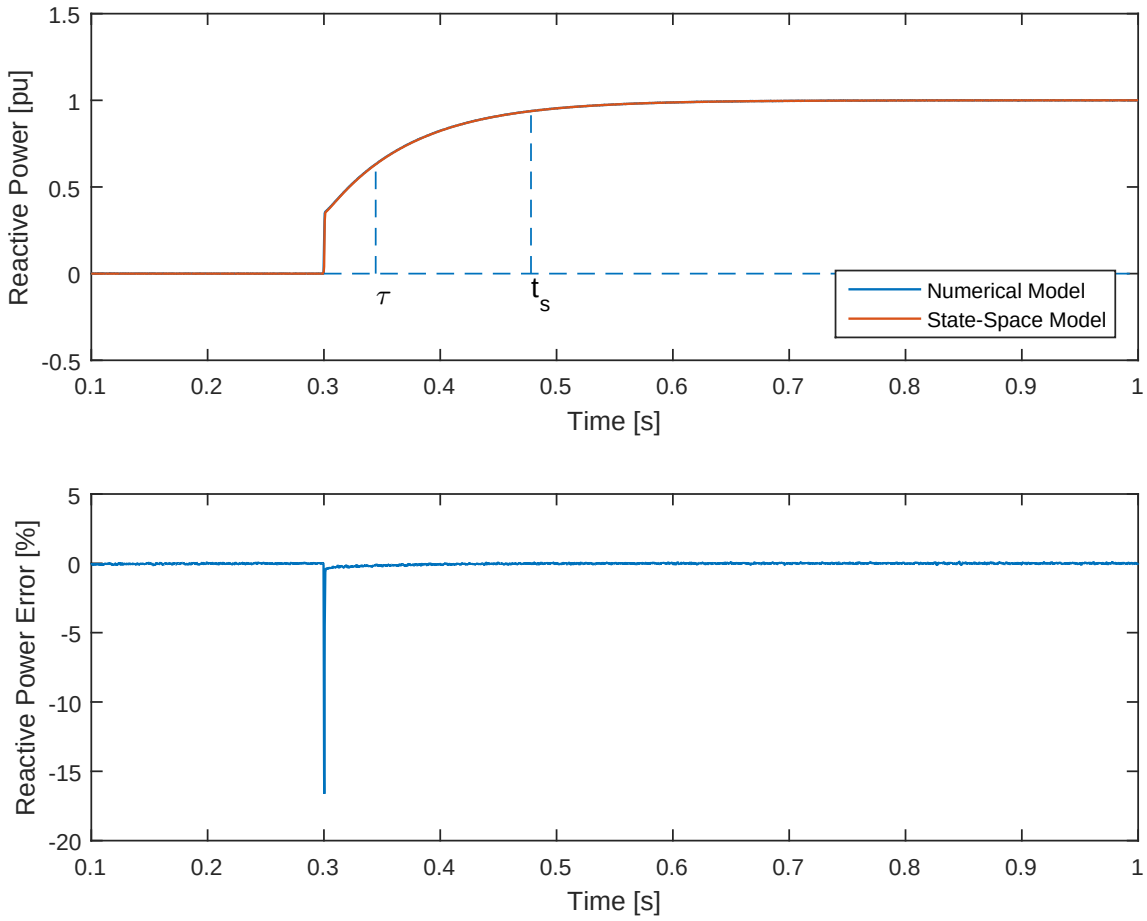

Fig. 6.2: Reactive power step response for state-space model and EMT model ($\triangle Q_{ref}^{WTG} = 1\,\text{pu}$ starting at $Q_0^{WTG} = 0\,\text{pu}$)

Likewise for the first test case the relative errors of $err_\tau = 1.010\,\%$ and $err_{ts} = 0.167\,\%$ at the significant instants of time are within an acceptable range. However, the largest relative error throughout the whole simulation amounts to approximately 17 % and is observed at the instant of triggering the step ($t = 0.3\,s$). As this large error is only present for a single time step of the system response, it may arise due to a slight step offset in the mathematical computation of both simulation models.

The results of test case (3.) are depicted in Fig. 6.3. The relative errors of $err_\tau = 0.597\,\%$ and $err_{ts} = 0.070\,\%$ are within an acceptable range. Hence, a negative step response performs results as accurate as positive step responses.

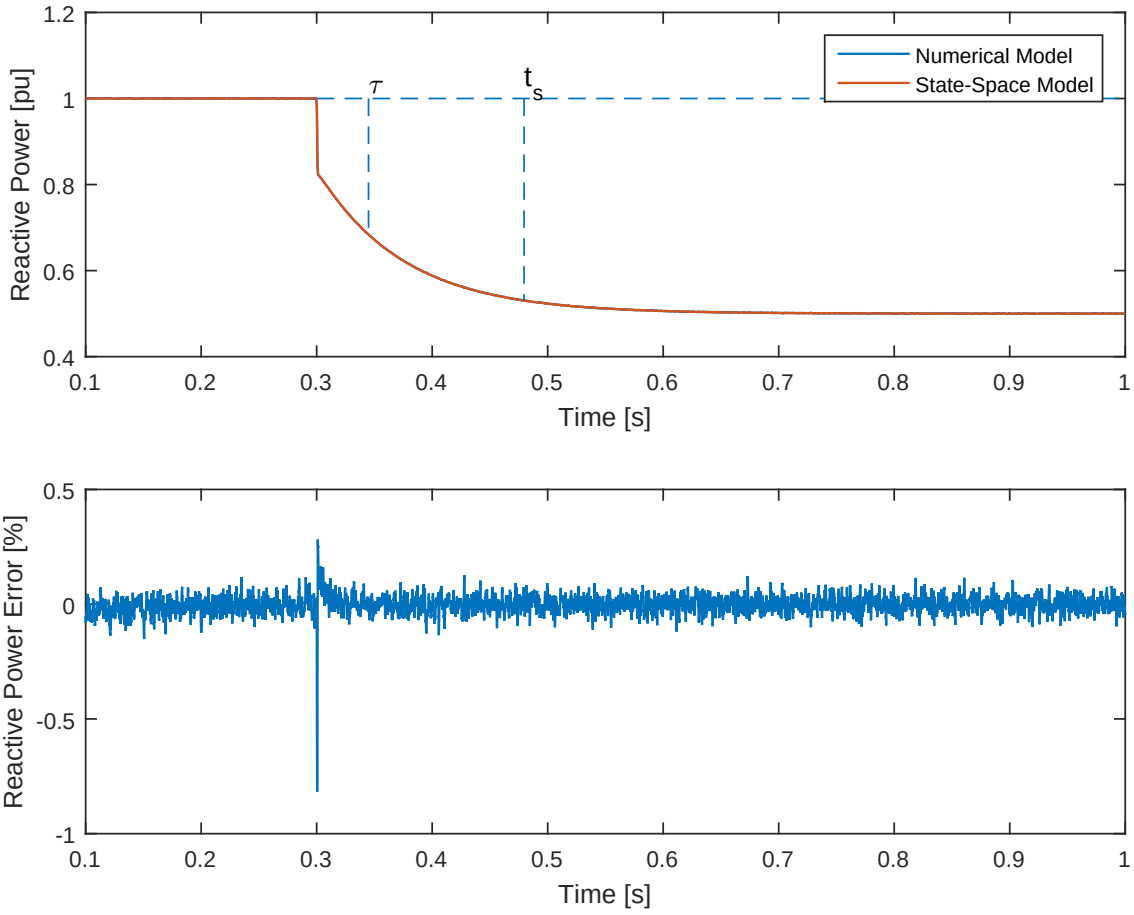

Fig. 6.3: Reactive power step response for state-space model and EMT model ($\triangle Q_{ref}^{WTG} = -0.5\,\text{pu}$ starting at $Q_0^{WTG} = 1\,\text{pu}$)

It is worth mentioning that the time constant $\tau = 0.045\,s$ and the settling time $t_s = 0.180\,s$ are the same for all three test cases. However, it is expected that the response time of a system is only affected by its internal behaviour and not by the input to the system.

The calculated relative errors of the previous mentioned simulations test cases are depicted in Tab. 6.1, where the largest error is less than 1.010 % . That leads to the conclusion

that the Q controller of the state-space model is performing in accordance to the EMT model with an acceptable error.

Tab. 6.1: Calculated relative errors err_τ and err_{t_s} for all three test cases of Q controller validation

Test case	err_τ [%]	err_{t_s} [%]	Validation
1.	< 0.112	< 0.0382	Passed
2.	< 1.010	< 0.1670	Passed
3.	< 0.597	< 0.070	Passed

It is observable for all three test cases (Fig. 6.1 - 6.3) that high frequency fluctuations occur in the calculated relative error depicted on the lower side of the figures respectively. However, this is due to the fact that the EMT model regards the space vector modulation of the GSC, acting with a switching frequeny in the kHz range, whereas the state-space model treats this process to be infinitely fast.

The most important observation of this section is that even for large Q steps of $\triangle Q_{ref}^{WTG} = 1\,\text{pu}$ (test case 2) the linearized state space model is performing with an acceptable error compared to the EMT model. Noticing that for the case of large voltage deviations full reactive power supply may be required from the STATCOM, this model is capable of simulating such extreme changes in reactive power. However, in order to fully evaluate the state-space model a validation of the other outer controller is required, namely the DC-link voltage controller, which is outlined subsequently.

6.1.2 Validation of DC-link voltage controller

Following test cases are performed in order to validate the response performance of the DC-link voltage controller, where a step of the DC current ΔI_{SG} represents an active power change of the WTG.

1. $\triangle I_{SG} = 0.01\,\text{pu}$ starting at $I_{SG,0} = 0\,\text{pu}$
2. $\triangle I_{SG} = 0.1\,\text{pu}$ starting at $I_{SG,0} = 0\,\text{pu}$
3. $\triangle I_{SG} = -0.1\,\text{pu}$ starting at $I_{SG,0} = 0.5\,\text{pu}$

All three test cases are selected to reflect the same step patterns as for validating the Q controller, meaning that both a relatively small disturbance (1.), a larger disturbance (2.) and finally a negative step change (3.) are considered for the sake of validation. However, since one might naturally not expect active power surges or drops of the WTG, the magnitudes of the step changes are reduced accordingly.

The results of test case (1.) are depicted in Fig. 6.4, where the step responses of both models are shown on the upper side and their relative error on the lower side.

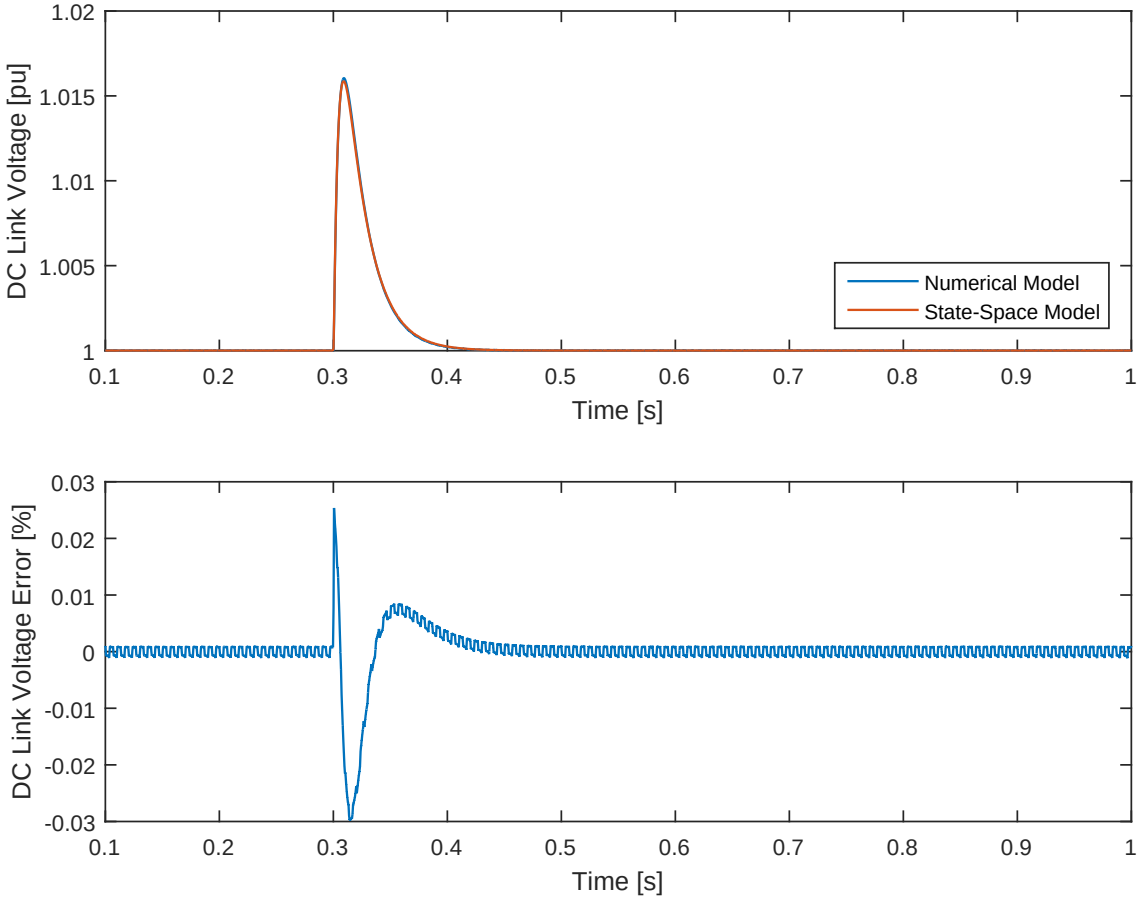

Fig. 6.4: Active power disturbance for state-space model and EMT model ($\triangle I_{SG} = 0.01\,\text{pu}$ starting at $I_{SG,0} = 0\,\text{pu}$)

The step is triggered at $t = 0.3\,s$ and the simulation lasts for 1 s. The dynamics of the DC-link voltage shown on the upper side of Fig. 6.4 are affected by both the capacitor and the DC-link voltage controller. For a positive $\triangle I_{SG} = 0.01\,\text{pu}$, the DC current will charge the capacitor in the very first instant, resulting in an increasing DC-link voltage. Subsequently, the controller will counteract, so that the mismatch between measured and reference value will disappear resulting in a final steady-state value of 1 pu.

As it can be seen in Fig. 6.4, the step response of the state-space model is similar to the simulated one of the EMT model. Furthermore, the disturbance in DC-link voltage is eliminated after approximately the same time in both models. However, it can be seen on the lower side of Fig. 6.4 that the largest error appears during the dynamic period of $t \approx 0.3 - 0.4\,s$. This deviation in the simulation results may occur due to the fact that the capacitor in the EMT model is not represented as an ideal capacitor. The capacitor circuit

naturally includes a parasitic resistance either in series or parallel, which will introduce some damping during dynamic processes. On the other hand, the state-space model does only regard the capacitance C. The relative error is obtained to be less than 0.03 % throughout the whole simulation of 1 s.

The results of test case (2.) are depicted in Fig. 6.5.

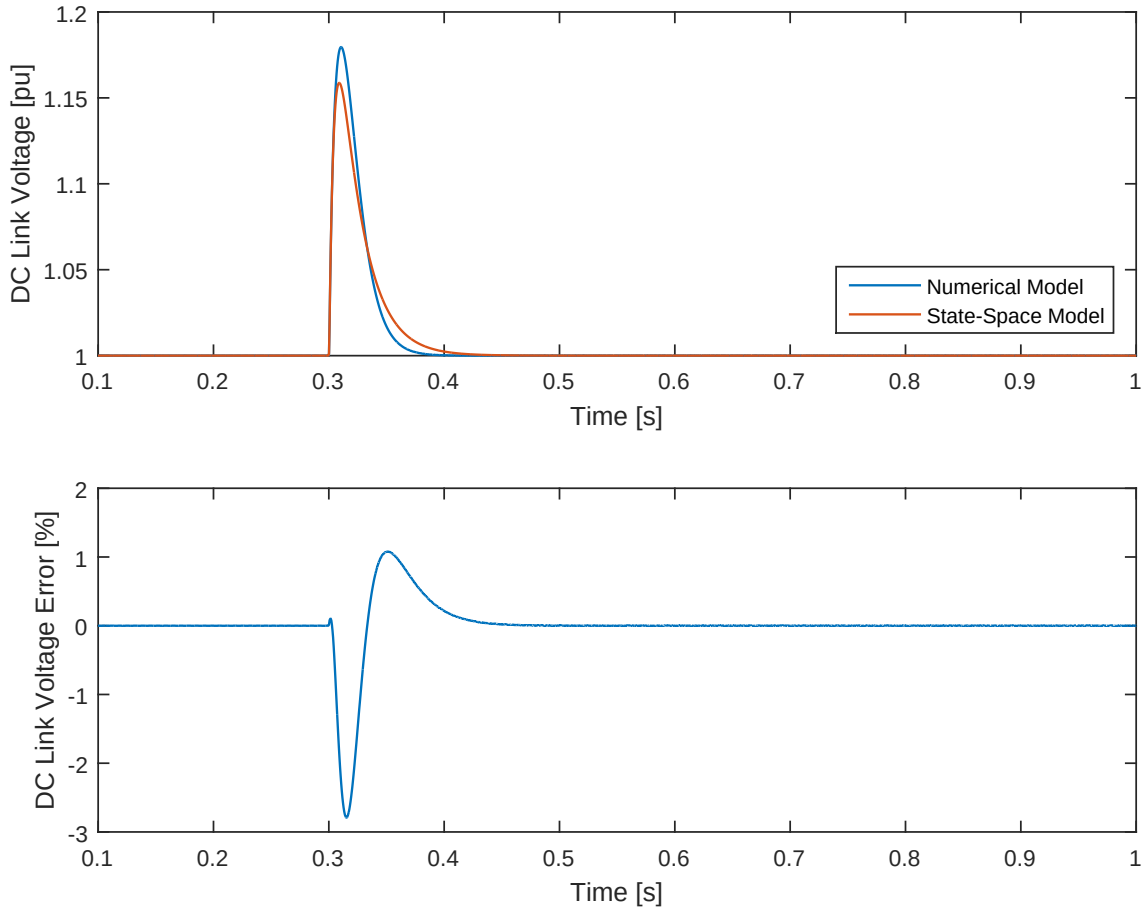

Fig. 6.5: Active power disturbance for state-space model and EMT model ($\triangle I_{SG} = 0.1\,\text{pu}$ starting at $I_{SG,0} = 0\,\text{pu}$)

A mismatch is observed in the step response of the state-space model compared to the simulated one in the EMT model. The EMT model exhibits a larger overshoot compared to the state-space model. It is likely to be caused by the different representation of the capacitive circuit as aforementioned. Since the step input is 10 times larger than for test case (1.), the error pattern during the dynamic period of $t \approx 0.3 - 0.4\,s$ is accordingly. This is assumed to be caused by the capacitor issues as aforementioned. However, a relative error of less than 3 % throughout the simulation can still be considered as acceptable.

The results of test case (3.) are depicted in Fig. 6.6. The relative error is calculated to be less than 1 % throughout the whole simulation. Hence, a negative step response performs

results as accurate as positive step responses.

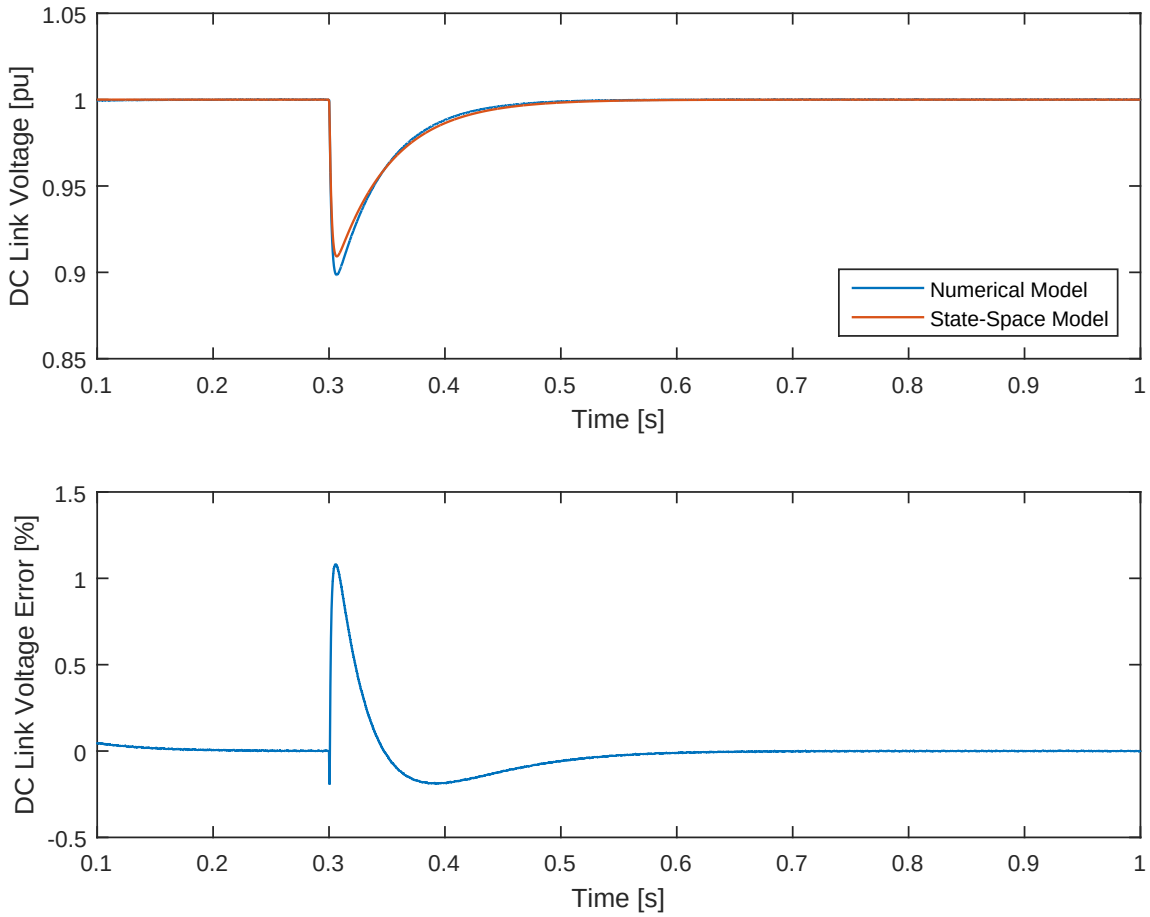

Fig. 6.6: Active power disturbance for state-space model and EMT model ($\triangle I_{SG} = -0.1\,\text{pu}$ starting at $I_{SG,0} = 0.5\,\text{pu}$)

The calculated relative error of the aforementioned simulations test cases are depicted in Tab. 6.2, where the largest error is less than 3 %.

Tab. 6.2: Calculated relative errors err_{max} for all three test cases of DC-link controller validation

Test case	$\lvert err_{max} \rvert$ [%]	Validation
1.	< 0.03	Passed
2.	< 3.00	Passed
3.	< 1.00	Passed

This leads to the conclusion that the DC-link voltage controller of the state-space model is performing in accordance to the EMT model with an acceptable error. Furthermore, it can be seen that the mismatch of both models increases significantly for increasing active power step changes. However, the dynamics of active power changes do not effect the

usage of the state-space model, since the purpose of this project is to investigate voltage control. It is worth emphasizing that an accurate representation of reactive power changes as proved in section 6.1.1 is crucial for the scope of this study.

6.2 Validation of WPP Model

6.2.1 Steady-State Performance

After successfully validating the state-space model of a single WTG, the purpose of this section is to show whether the network constructing for the WPP model, developed in chapter 5.4, provides reasonable results. Since a numerical model of the WPP is not available, the overall dynamic performance cannot be validated against a benchmark model. However, the WPP dyamics are imposed by the individual behaviour of the WTGs, which has been proved. It is of higher relevance to show, whether the change of network states are consistent with the actual power flow changes. Thus, following approach is applied for validating the WPP model:

a) Perform load flow calculation with $Q_0^{WTG1...p} = 0$ for initialization of state-space model and save the initial values of bus voltages;

b) Apply step change $\triangle Q_{ref}^{WTG1...p}$ to the state-space model and obtain deviation in bus voltages ΔV_{SS};

c) Perform load flow calculation with $Q_0^{WTG1...p} + \triangle Q_{ref}^{WTG1...p}$ and obtain deviation to initial bus voltages ΔV_{LF} ;

d) Compute error of ΔV_{SS} and ΔV_{LF} for all bus voltages of the network.

The validation of the WPP state-space model is performed for a stiff grid (SCR_{max}) step-by-step, meaning that the model is validated for an increasing number of connected arrays. Finally, the model is tested for a weak grid (SCR_{min}). Following test cases are performed:

1. $\triangle Q_{ref}^{WTG1...5} = 0.50\,\text{pu}$ for 1 array and external grid with SCR_{max}
2. $\triangle Q_{ref}^{WTG1...17} = 0.50\,\text{pu}$ for 3 arrays and external grid with SCR_{max}
3. $\triangle Q_{ref}^{WTG1...35} = 0.50\,\text{pu}$ for 6 arrays and external grid with SCR_{max}
4. $\triangle Q_{ref}^{WTG1...35} = 0.17\,\text{pu}$ for 6 arrays and external grid with SCR_{min}

The results for test case (1.) are depicted in Fig. 6.7 where the voltage deviation in per-unit of both models is shown on the upper side and their mismatch in percent on the lower side.

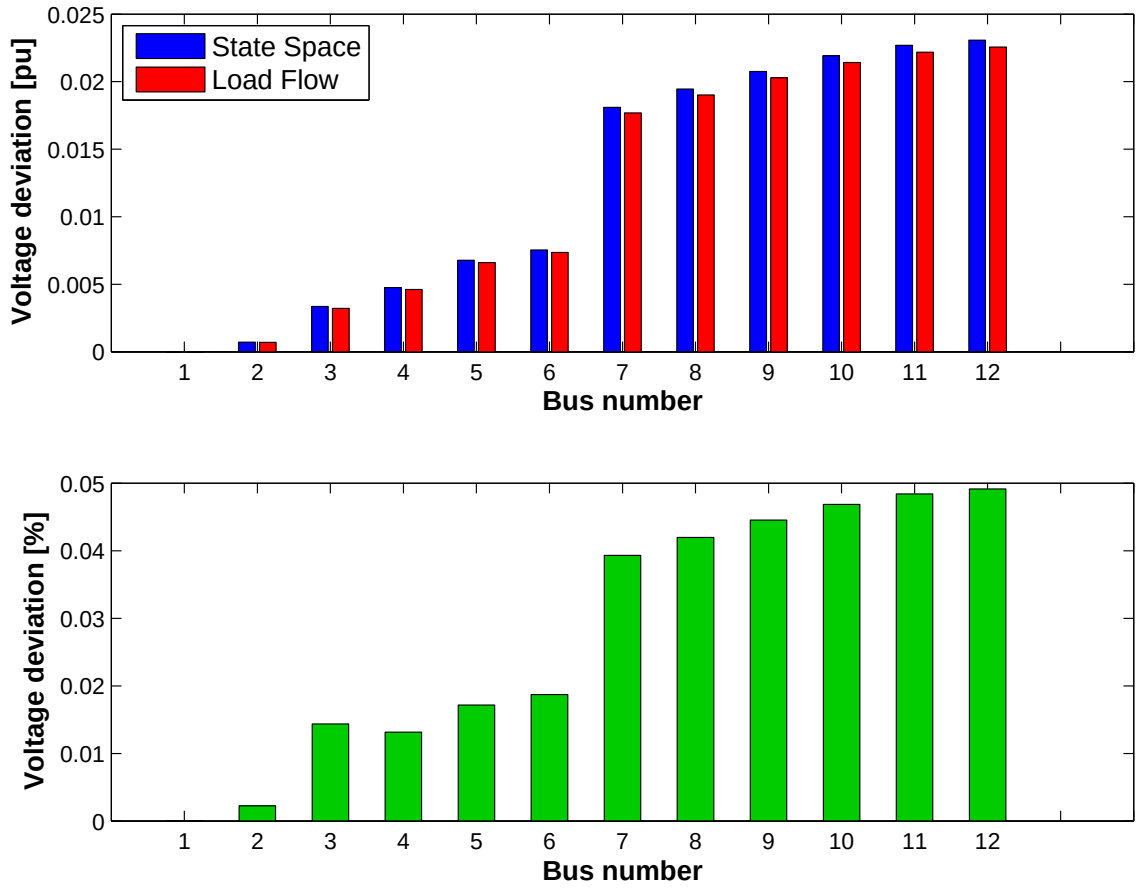

Fig. 6.7: Voltage deviations of network busses with 1 WPP array connected to a strong grid, for a Q step change of $\triangle Q_{ref}^{WTG1...5} = 0.5\,\mathrm{pu}$

As it can be seen, the results are fairly similar with a maximum error of $err_1 = 0.05\,\%$. It can be noted that the largest mismatch between both simulations is obtained for busses 7 to 12. Those busses are located in the array network, where the WTGs are connected and reactive power injected.

The results for test case (2.) are depicted in Fig. 6.8. Likewise for the first test case, the similarity between both simulations is observed with an maximum error of $err_2 = 0.40\,\%$. When looking at the lower part of Fig. 6.8, the error is increased by connecting two additional arrays compared to test case (1.). On one side, this could be explained by the fact that the individual load flow calculations a) and c) recalculate the network independent of each other, while the state-space model obtains its final values in b) by using the initial conditions of a), thus being a linearized model. Hence, an increasing number of busses, that actually receive additional reactive power injections, increases the mismatch between state-space and load flow simulations. On the other side, the errors obtained throughout all the test cases may as well be affected by the load flow method, since those calculations

are always subjected to convergence tolerances.

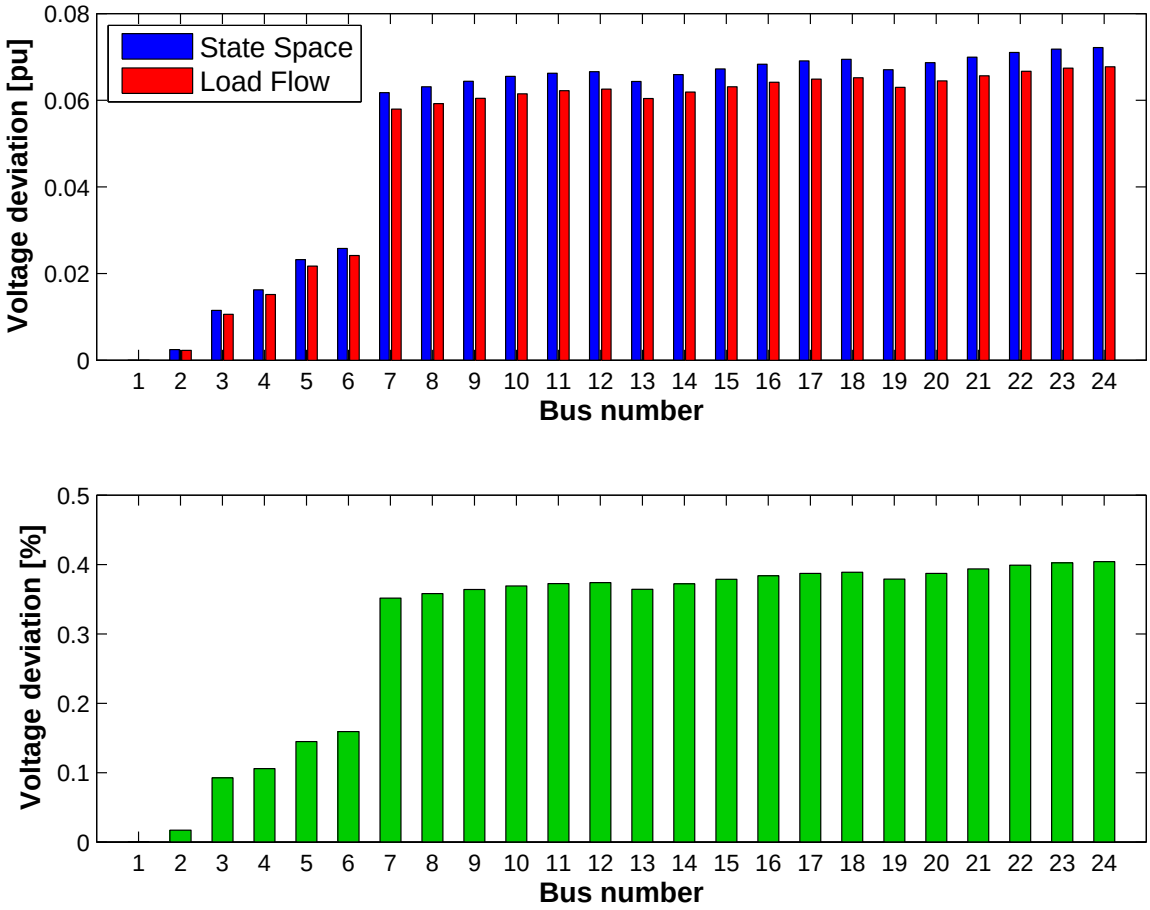

Fig. 6.8: Voltage deviations of network busses with 3 WPP arrays connected to a strong grid, for a Q step change of $\triangle Q_{ref}^{WTG1...17} = 0.5\,\mathrm{pu}$

The results for test case (3.) are depicted in Fig. 6.9. In this case the WPP network is fully represented by the connection of all 35 WTGs. According to the previous considerations the error rises slightly for an increasing number of connected busses, so that the maximum error amounts to $err_3 = 0.76\,\%$ which is still within an acceptable range. It must be emphasized that for the PCC voltage (bus 2), being the control target of this study, the smallest error is obtained, residing in the permille range.

Moreover, by considering the upper part of Fig. 6.9 it can be observed that the voltage deviation is largest between bus 6 and 7, which is due to the offshore cable located in this branch. The offshore cable consumes a significant amount of reactive power due to its capacitance, hence affecting their adjacent bus voltages.

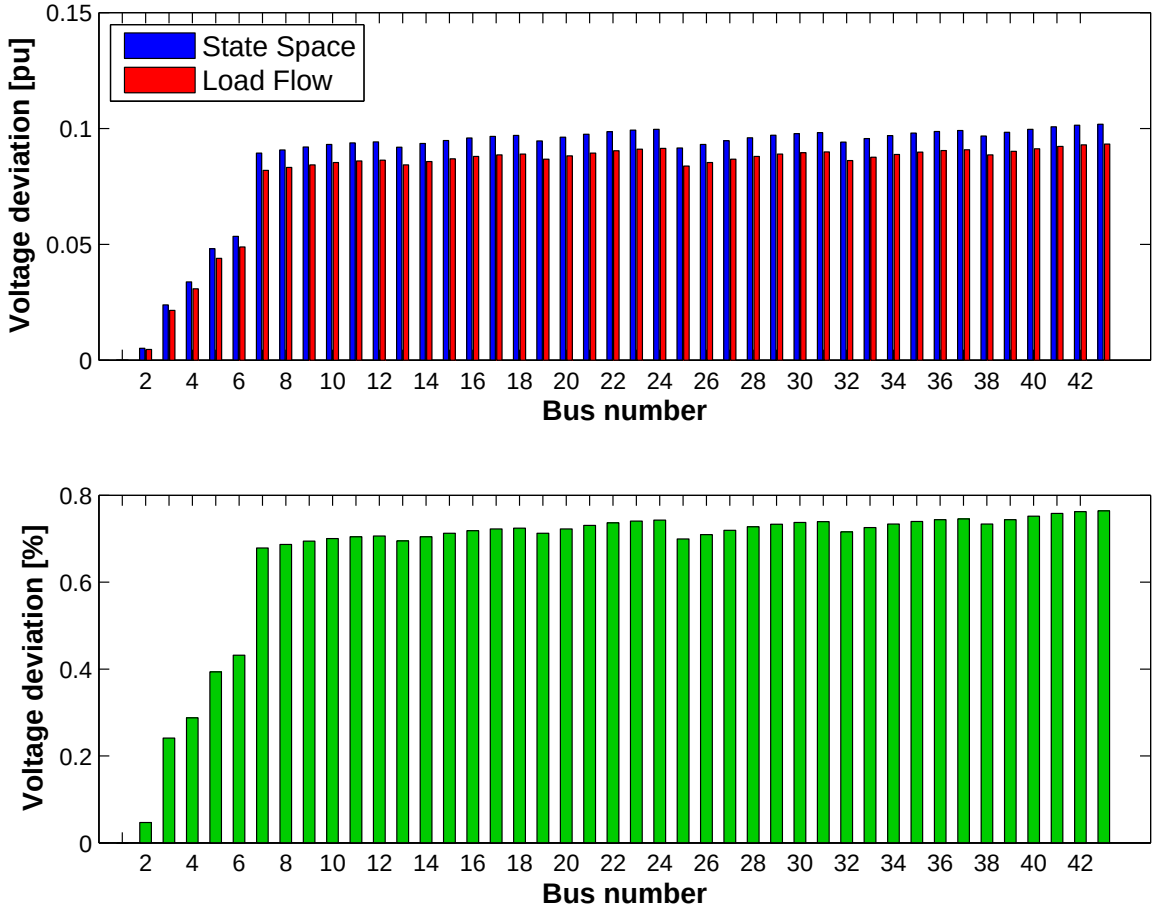

Fig. 6.9: Voltage deviations of network busses with all WPP arrays connected to a strong grid, for a Q step change of $\triangle Q_{ref}^{WTG1...35} = 0.5\,\text{pu}$

While the previous test cases are performed for a strong grid (SCR_{max}), test case (4.) is considers a weak grid connection (SCR_{min}) of the WPP. Under this condition, reactive power changes have a larger impact on the network voltages, which justifies one further test case for the purpose of model validation. It uses a lower step in reactive power ($\triangle Q_{ref}^{WTG1...35} = 0.17\,\text{pu} = 1\,\text{Mvar}$). The results are depicted in Fig. 6.10. The largest error amounts to $err_4 = 1.00\,\%$, which is still within an acceptable range. However, it can be observed that the error distribution along the busses is nearly balanced. The greater impact of reactive power injections in weak grids leads to a larger mismatch in voltages of the WPP transmission network (busses 2 to 6). The PCC voltage shows an error of $err_{4,PCC} = 0.79\,\%$, which however can be accepted for further usage of the state-space model.

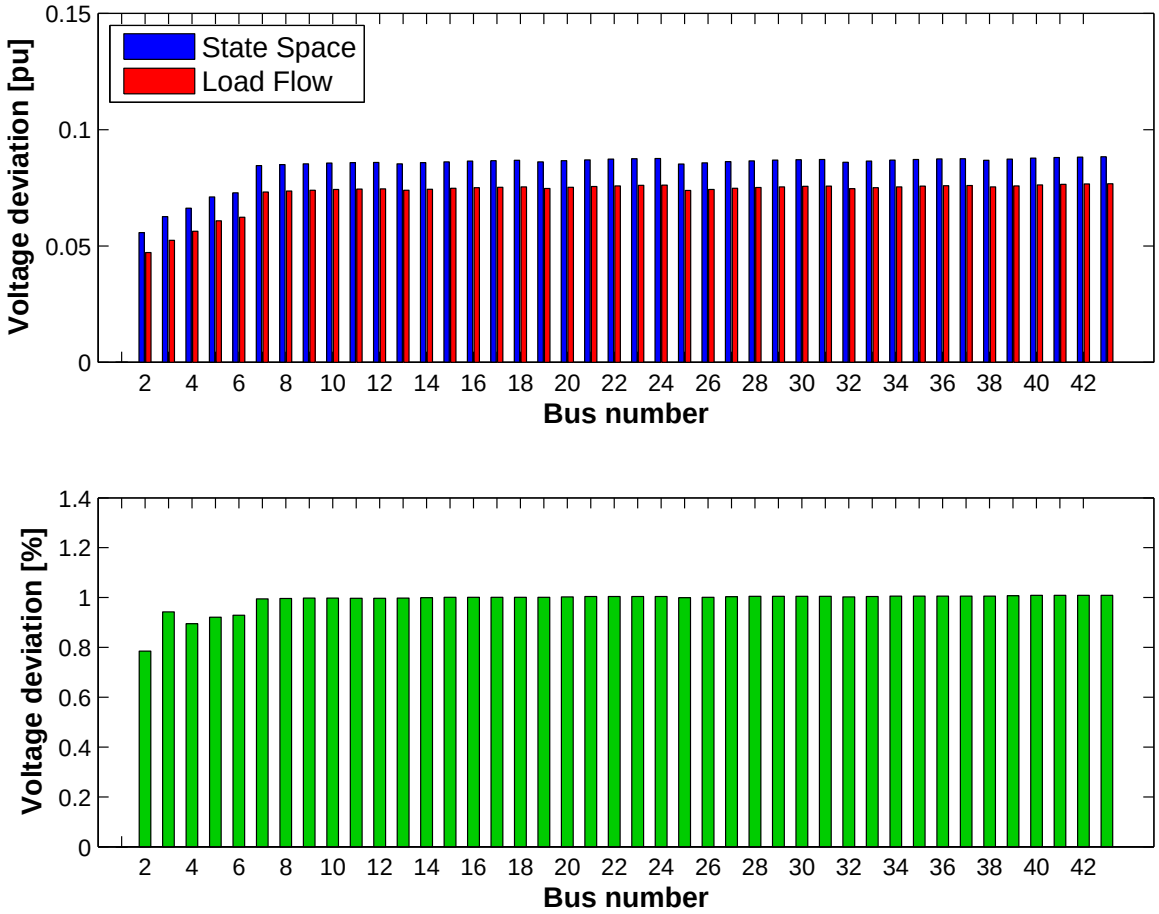

Fig. 6.10: Voltage deviations of network busses with all WPP arrays connected to a weak grid, for a Q step change of $\triangle Q_{ref}^{WTG1...35} = 0.17\,\text{pu}$

Summary

The calculated errors between the overall state-space model of WPP and the load flow model for all considered test cases are summarized in Tab. 6.3. The results lead to the conclusion that the overall state-space model of WPP is performing with an acceptable error.

Tab. 6.3: Calculated relative errors for all test cases of WPP model validation

Test case	Max. voltage error [%]	Error V_{PCC} [%]	Validation
1 array, SCR_{max}	0.05	0.00	Passed
2 arrays, SCR_{max}	0.40	0.02	Passed
6 arrays, SCR_{max}	0.76	0.05	Passed
6 arrays, SCR_{min}	1.00	0.79	Passed

6.2.2 Dynamic Performance

The validation target of this section has been to evaluate the steady-states of step responses performed by the state-space model. As a final step, the dynamic behaviour, leading from one state to another, is investigated. As the target of this study is to analyze voltage control at the PCC, bus 2 is chosen as an exemplary case. The step response is performed for test case (3.) with all WPP arrays connected and the result is depicted in Fig. 6.11, where a step of $\triangle Q_{ref}^{WTG1...35} = 0.50\,\text{pu} = 3\,\text{Mvar}$ is applied at $t = 0.1\,\text{s}$.

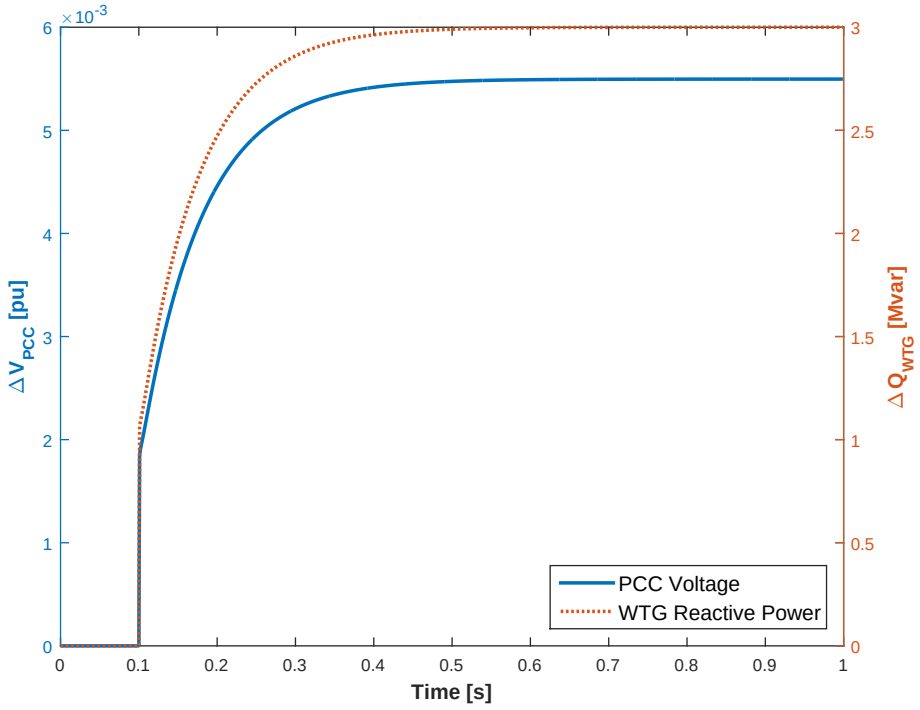

Fig. 6.11: PCC voltage (blue) and WTG reactive power output (red) for a reactive power step response ($\triangle Q_{ref}^{WTG1...35} = 0.5\,\text{pu}$ starting at $\triangle Q_0^{WTG1...35} = 0\,\text{pu}$)

It can be observed, that ΔV_{PCC} (blue) shows a steep rise in the beginning of the step response, whereupon it behaves like a first-order response. In this way, it features the same characteristic as a step response given to a single WTG, which has been analyzed in previous section for validating the Q controller of the WTG model. For illustration purposes, ΔQ_{WTG} is shown in Fig. 6.11 (red) as well. Both graphs have similar rise times ($t_r = 0.14...0.15\,\text{s}$) and settling times ($t_s = 0.25...0.26\,\text{s}$).

However, as aforementioned a ramp-rate limiter will prevent fast transients in the first instant of the response. Hence, to its simplest expression it can be treated as a first-order response in order to represent the most characteristic dynamics of the WPP model. This simplification is used for tuning the voltage controller in subsequent chapter.

6.3 Summary

This chapter has given a detailed explanation of the validations performed for the WTG model and the overall WPP model. The validation of the Q-controller and the DC-link voltage controller has shown that the obtained state-space model is performing in accordance with the numerical EMT model being used as a benchmark representation of a grid connected converter. The overall WPP model has been validated against load flow simulations, in different stages with various number of active WTGs. This has been done to evaluate whether the state changes of the network model coincide with actual power flow changes. Despite the fact that the mismatch between both models increases by implementing several WPP arrays, the overall validation error is still within an acceptable range. It allows to proceed with the WPP control design and tuning in subsequent chapter.

7 Design and Tuning of Voltage Control

This chapter deals with the design and subsequent tuning of the WPP voltage control. As presented in chapter 5.5, it contains a slope voltage controller (AVR) and a Q compensator (AQR), which compensates for internal reactive power losses of the WPP.

When considering linear control systems, it has to be ascertained that the overall stability criteria are fulfilled (cp. chapter 3.3). Generally, those criteria are not sufficient to prove satisfactory control behaviour. Moreover, there are various demands on stationary and dynamic behaviour of control circuits, which will subsequently be regarded for the design and tuning of both AQR and AVR individually [45, p. 46]. It leads to following stages that will be approached throughout this chapter:

First, the AQR is designed for a WPP system without time delays according to appropriate design methods being available for PI controllers. Then, the AQR performance is optimized for the presence of time delays (section 7.1).

As delays constitute a crucial variable for voltage control performance, the AVR is designed by regarding an extreme case value of time delay, which might be present in the WPP without violating the delay time requirement stipulated by the grid code (section 7.2).

Subsequently, a performance analysis of voltage control is conducted to evaluate the influence of the SCR on the system behaviour (section 7.3).

Based on those observations, some tuning steps are proposed in order to meet the performance criteria of reactive power output, which are specified in chapter 4.3 (section 7.4).

Finally, the tuning results are validated by performing voltage step responses to the system (section 7.5).

All steps take into account various test cases based on the scenarios defined in chapter 4.3 and are finally summarized by some guidelines regarding the control design and tuning process (section 7.6).

7.1 Design of AQR

In the standard literature regarding control design and optimization of PI controllers two basic methods are mentioned, namely *Modulus Optimum* (MO) and *Symmetrical Optimum* (SO) [45, p. 46].

The MO method is defined for control loops that require a fast response and for example is applied for inner current control loops of grid connected converters. It provides optimal responses for step inputs. However, as aforementioned in chapter 6.1, the reactive power control is limited by ramp-rates which lowers the demand of fast response times. In this case, the SO method is applicable. It moreover offers decent results for systems with time delays, in this way being a feasible solution for designing the AQR of the WPP controller. [46, 47]

7.1.1 Plant System without Time Delays

The SO method is applied to determine the gain K_p and time constant T_i of the PI controller with the transfer function $F_{AQR}(s)$ (cp. Eq. 5.30 in chapter 5.5). It can be applied, when the plant transfer function is described by a second-order system. With its time constants T_1 and T_2 and gain K_{plant}, the SO method is described by Eq. 7.1 - 7.4, which are only valid for systems, where $T_1 \gg T_2$ [45, p. 67 ff.].

$$T_i = 4k_1T_2 \tag{7.1}$$

$$K_p = k_2\frac{T_1}{2K_{plant}T_2} \tag{7.2}$$

$$k_1 = \frac{1+\left(\frac{T_2}{T_1}\right)^2}{\left(1+\frac{T_2}{T_1}\right)^3} \tag{7.3}$$

$$k_2 = 1+\left(\frac{T_2}{T_1}\right)^2 \tag{7.4}$$

For the AQR design the plant is described by a SISO system $G_{Q_{out}^{WPP}Q_{PCC}}(s)$ with Q_{out}^{WPP} as input and Q_{PCC} as output according to Fig. 5.11 of chapter 5.5. In this context the dispatch function is represented as a base case by equal reactive power contribution of all WTGs ($K_{WTG1...p} = 1$) without incorporation of the STATCOM ($K_{STAT} = 0$). The time delays are disregarded ($T = 0$), but will be considered later in this section. Since all individual WTGs are implemented in the overall state-space model, the plant transfer function is characterized by a high-order system (60^{th}) and hence needs to be reduced to a

second-order system, which is achieved by the MATLAB functions *balred(sys)* [48]. As illustrated by the Bode plots in Fig. 7.1, the reduced transfer function displays the same characteristics in the low frequency area compared to the original transfer function and hence can be used for the SO approach.

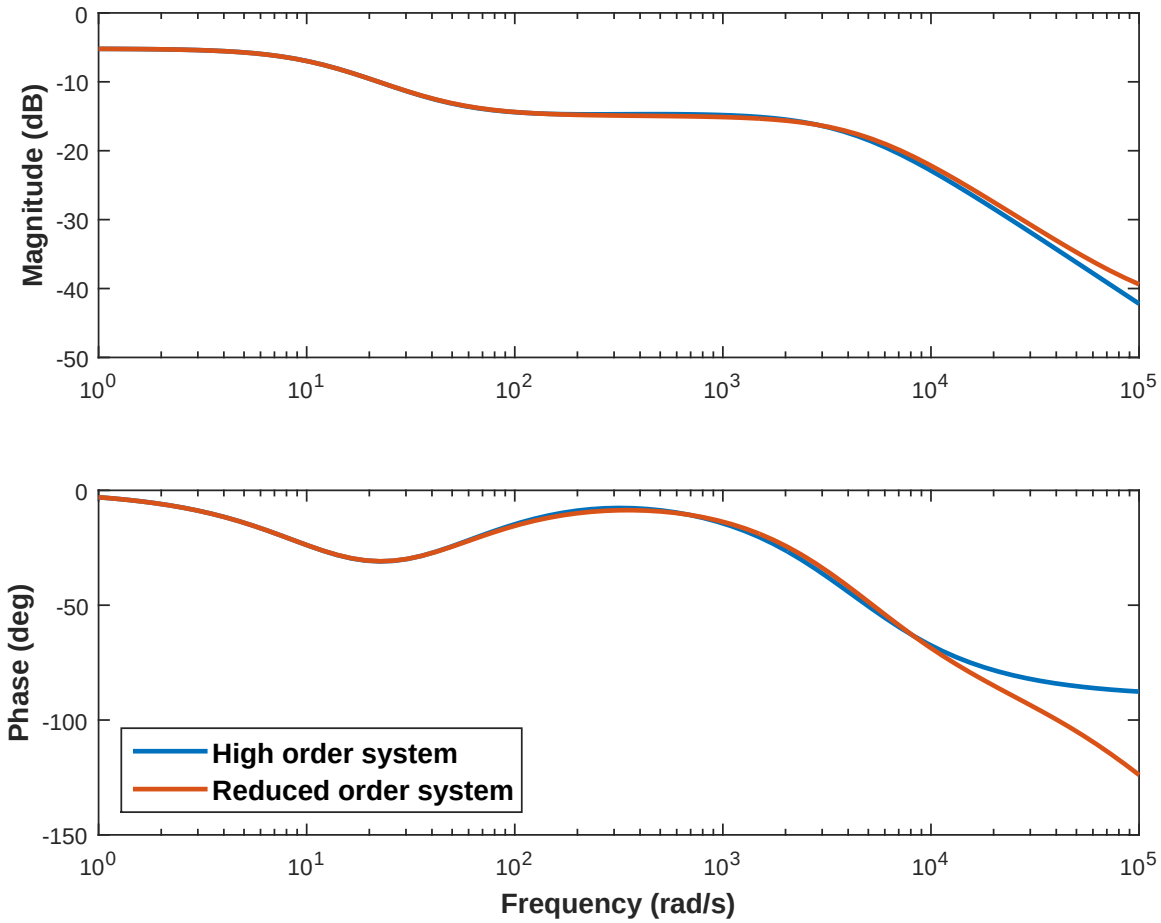

Fig. 7.1: Frequency response of $G_{Q_{out}^{WPP}Q_{PCC}}(s)$ for high-order system and reduced-order system

As a starting point, the AQR design is developed for a maximum grid stiffness SCR_{max} and with an initial active power production of $P_{WTG,0} = 0.5\,\text{pu}$. Moreover, the second-order plant function fulfills the condition $T_1 \gg T_2$, with values of $T_1 = 77.08\,\text{ms}$ and $T_2 = 0.21\,\text{ms}$. Thus, the the K_p and T_i of the AQR can be calculated using Eq. 7.1 and 7.2 and finally amount to:

$$K_p = 0.0055$$

$$T_i = 0.824\,\text{ms}$$

For the resulting closed-loop system several step responses are performed, taking into account various operating conditions of the WTGs as well as different grid stiffnesses. The

results are depicted in Fig. 7.2, where 6 test cases are applied to evaluate the system performance.

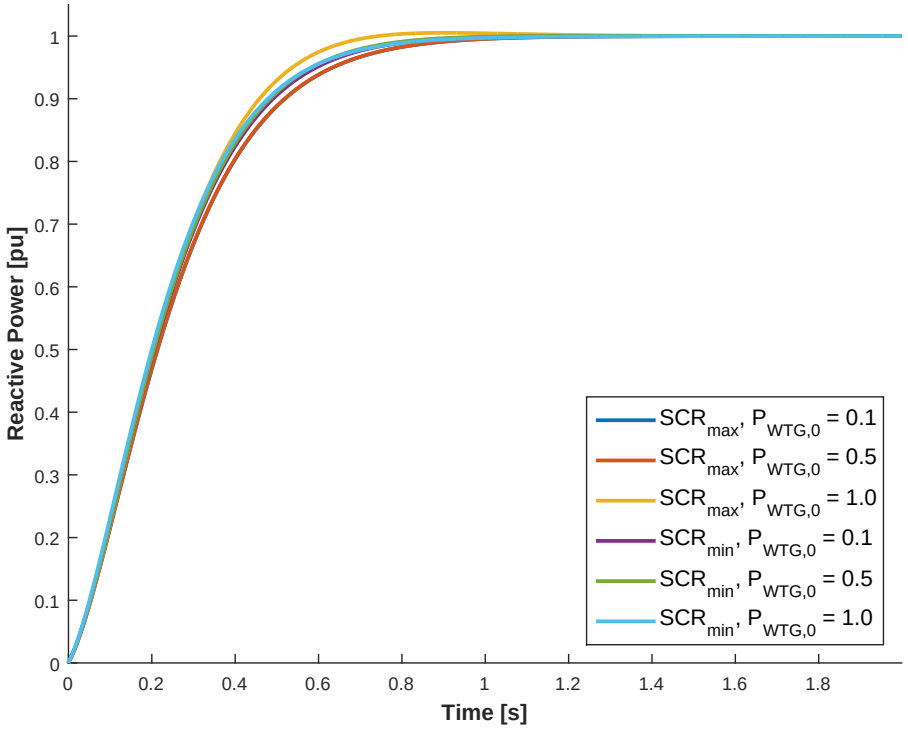

Fig. 7.2: Reactive power step response of closed-loop system with wind power plant AQR for various operating conditions and grid stiffnesses

The following observations can be made:

- Considering the test case with SCR_{max} and $P_{WTG,0} = 0.5\,\text{pu}$, for what the AQR design has been performed, a smooth system response is ascertained without overshoot and a settling time of $t_s = 0.74\,\text{s}$. The optimal parameters of the PI controller are obtained, since changing K_p or T_i would result in either overshoot or slower system response.
- The system response is not significantly affected by various operating conditions of the WTGs. The maximum overshoot of $OS = 0.51\,\%$ is observed for SCR_{max} and $P_{WTG,0} = 1\,\text{pu}$, which is below the specified limit of $OS < 5\,\%$. Hence, unique design of the AQR is sufficient for the WPP under various active power conditions.
- The system response does not deviate significantly for different grid stiffnesses. Hence, the control parameters of the AQR can be selected independent of the WPP location, in other words the SCR.

For all 6 test cases the rise time stays within the range of $t_r = 0.46...0.52\,\text{s}$ and the settling time within the range of $t_s = 0.60...0.74\,\text{s}$.

Another test case is performed to assess the behaviour of the AQR, when the STATCOMs are incorporated into reactive power supply. Fig. 7.3 shows the resulting Q step responses, where again the AQR design has been performed for SCR_{max} and $P_{WTG,0} = 0.5\,\text{pu}$.

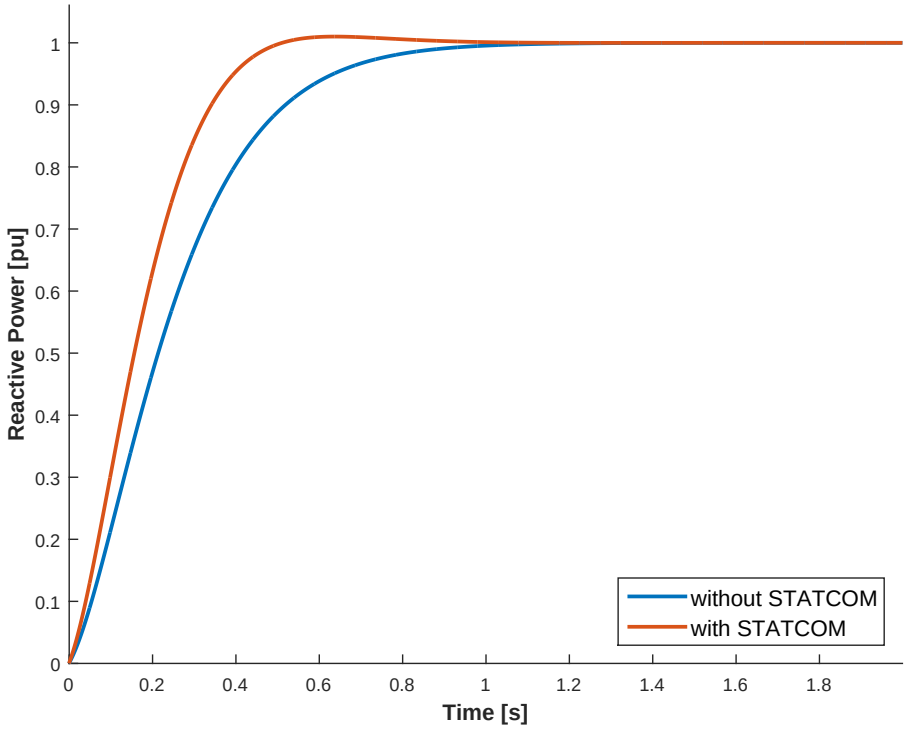

Fig. 7.3: Reactive power step response of closed-loop system with wind power plant AQR with and without implementation of STATCOM

The following observations can be made:

- The system response is accelerated by the integration of STATCOMs, as additional reactive power is initiated compared to the test case with only WTGs contributing. The rise time is reduced by $\Delta t_r = -0.18\,\text{s}$ and the settling time by $\Delta t_s = -0.3\,\text{s}$.
- The overshoot is increased by only $\Delta OS = 1.00\%$. It implies that unique design of the AQR is sufficient for various integration of reactive power supplying units, without deteriorating the performance of the AQR.

7.1.2 Plant System with Time Delays

As mentioned in previous section, the plant transfer function $G_{Q_{out}^{WPP}Q_{PCC}}(s)$ normally includes some system delays, which are expressed by $F_{del}(s)$ according to Eq. 5.32 in chapter 5.5. Hence, the time delays need to be handled by the AQR. Fig. 7.4 shows how the Q step response is affected by various time delays. The maximum time delay of

$T = 0.2\,\mathrm{s}$ being considered corresponds to the allowed delay time of reactive power output response stated in the UK grid code requirements (cp. chapter 4.2).

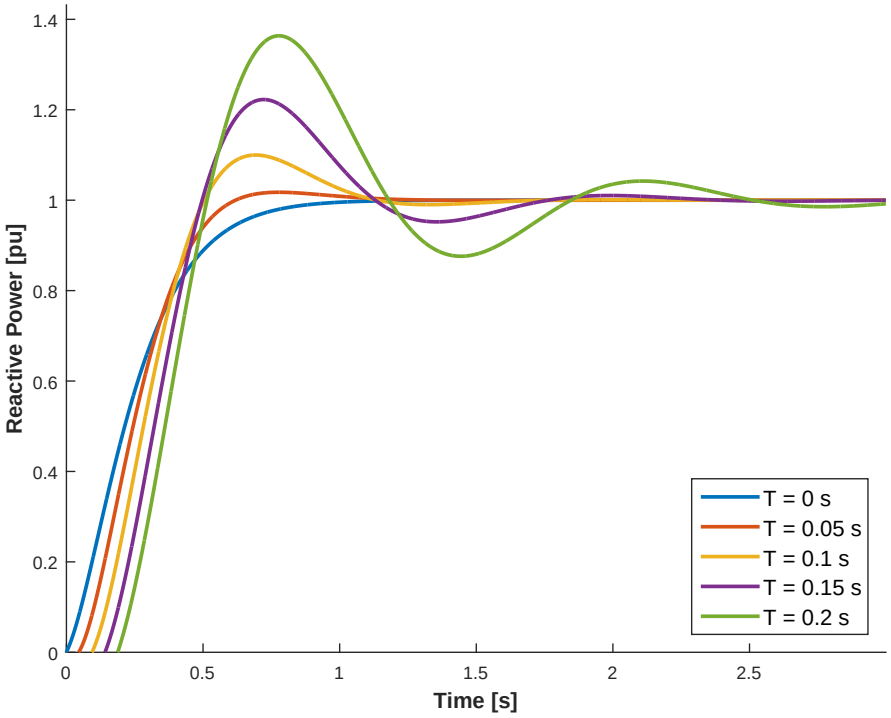

Fig. 7.4: Reactive power step response of closed-loop system with wind power plant AQR for different time delays

It can be clearly seen that rising time delays increase both overshoot and settling time of the system response. Long dead times severely limit the performance of the PI controller, which is due to the fact that it has no knowledge of the delay time. Hence, the controller reacts too abrupt, when the output reactive power Q_{PCC} does not match the desired reference Q_{ref}^{WPP}.

A common approach to overcome process dead times is to use a so called *Smith Predictor*, a type of predictive controller for systems with pure time delays. It uses an internal model to predict the response of the process [49]. The *Smith Predictor* control structure applied for the AQR is sketched in Fig. 7.5. It contains an internal plant model G_p, representing the delay-free response, and a delay estimate e^{-sT}. Thus, the AQR takes into account the dead time in order to compute the output setpoint Q_{out}^{WPP}.

To compare the performance of an AQR design with and without *Smith Predictor*, a Q step response with $T = 0.1\,\mathrm{s}$ is shown in Fig. 7.6. It can be observed that for this exemplary test case the implementation of the *Smith Predictor* increases the rise time by $\Delta t_r = 0.17\,\mathrm{s}$, but on the other hand eliminates the overshoot of $OS = 9.98\,\%$ and reduces the settling

time by $\Delta t_s = -0.18\,\mathrm{s}$. Comparable improvements can be obtained for the remaining test cases that have been considered in Fig. 7.2.

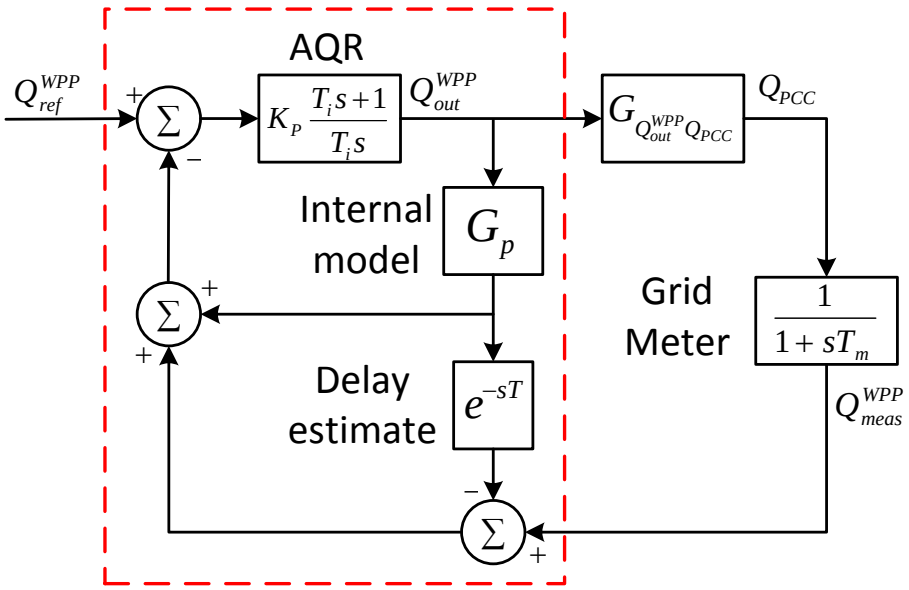

Fig. 7.5: Extended control structure of wind power plant AQR with *Smith Predictor*

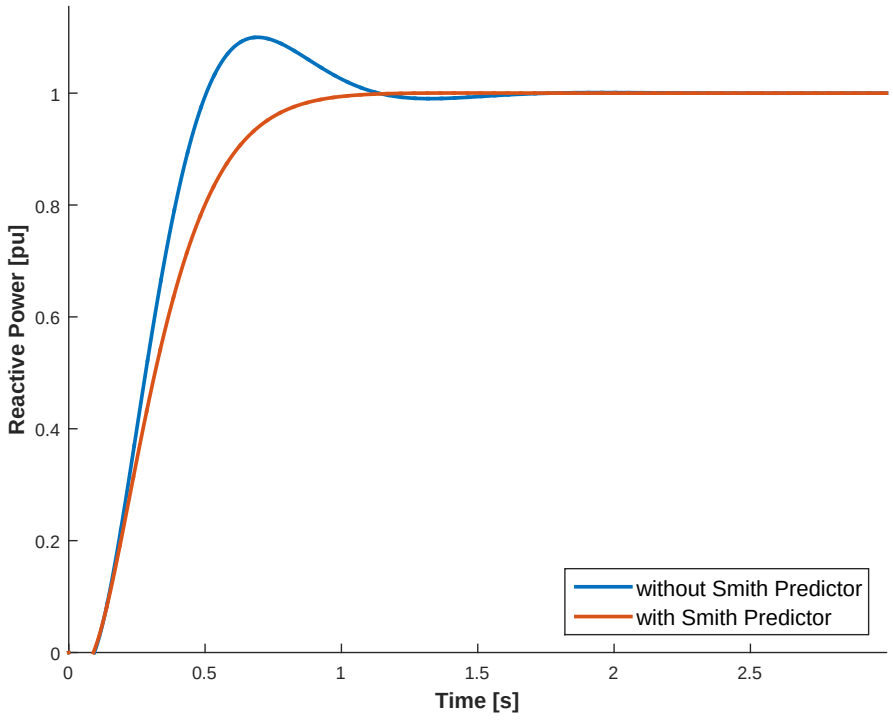

Fig. 7.6: Reactive power step response of closed-loop system with wind power plant AQR with and without *Smith Predictor* for $T = 0.1\,\mathrm{s}$

Thus, it is proved that the predictive controller enhances the system performance, so that similar AQR responses as for a plant without time delays can be achieved.

However, one might claim that using a *Smith Predictor* requires a set of internal plant models representing various WPP configurations and operating conditions. Hence, it is worth analyzing whether one particular internal model can be applied for different actual plant behaviours. In Fig. 7.7 step responses of 7 test cases are depicted, where the internal model of the *Smith Predictor* is developed for SCR_{max} and $P_{WTG,0} = 0.5\,\text{pu}$.

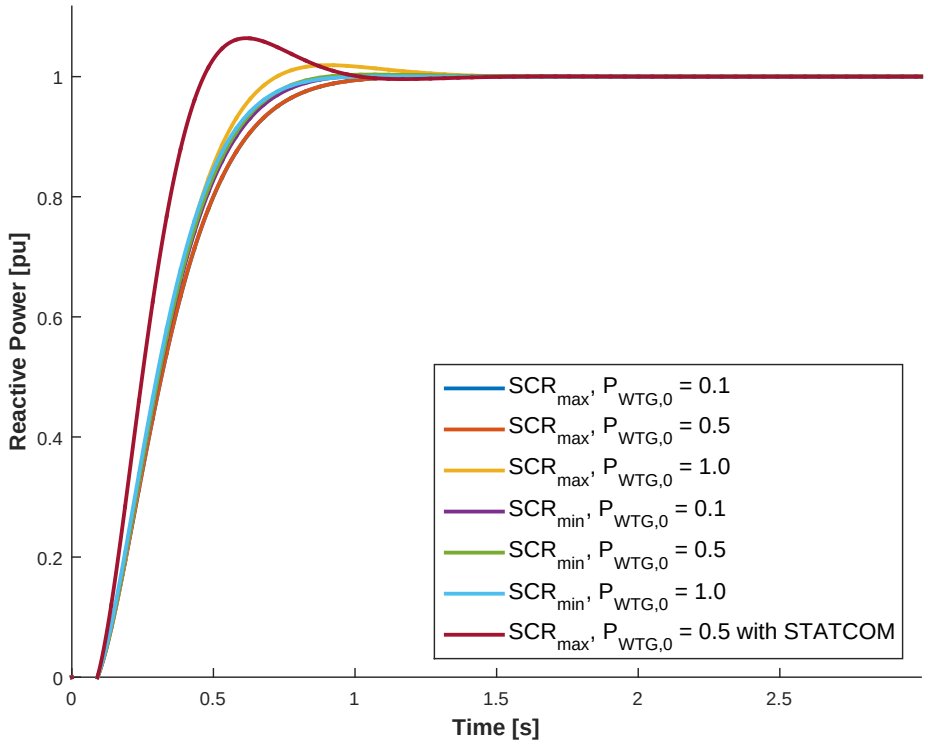

Fig. 7.7: Reactive power step response of closed-loop system with wind power plant AQR including *Smith Predictor* for $T = 0.1\,\text{s}$ and various test cases

The following observations can be made:

- Considering the test case with SCR_{max} and $P_{WTG,0} = 0.5\,\text{pu}$, a smooth system response is ascertained without overshoot, a rise time of $t_r = 0.62\,\text{s}$ and a settling time of $t_s = 0.82\,\text{s}$.
- The remaining test cases without STATCOM implementation exhibit a maximum overshoot of $OS = 1.9\,\%$, which is within an acceptable range. For all those 6 test cases the rise time stays within the range of $t_r = 0.54...0.62\,\text{s}$ and the settling time within the range of $t_s = 0.65...0.82\,\text{s}$. All in all, the results of Fig. 7.7 show that a unique internal plant model is sufficient for various WPP configurations and operating conditions.

- For the last test case with STATCOM implementation the rise time is improved with $t_r = 0.40\,\text{s}$, while the settling time with $t_s = 0.83\,\text{s}$ is closed to the previous range. However, an overshoot of $OS = 6.4\,\%$ is obtained, which exceeds the specified limit of $OS > 5\,\%$. It changes the AQR performance significantly, leading to the conclusion that the incorporation of STATCOMs should be regarded for designing the AQR. An unique internal plant model may not be sufficient in this case.

7.2 Design of AVR

The outer voltage controller is described by the transfer function $F_{AVR}(s)$, where the slope gain K_{PO} defines the ratio between measured voltage and injected reactive power (cp. Fig. 2.4b of chapter 2.2). Since $F_{AVR}(s)$ is not characterized by PI control, the AVR cannot be tuned according to the SO method being applied for the AQR. Moreover, for slope control there are no generic design methods available in the standard literature. However, the AVR determines the overall system behaviour of the WPP voltage control, which has to fulfill the requirements stated in the grid code.

7.2.1 Determination of Time Constant T_{PO}

According to [2, p. 12] the time constant „T_{PO} should be used to respect the bandwidth of the inner loop controllers“. Thus, in order to design the AVR, the bandwidth of the closed-loop AQR system needs to be obtained. As it has been outlined in previous section, different test cases are considered in order to assess the overall system behaviour, such as various WPP configurations and operating conditions as well as various time delays. In Fig. 7.8 the frequency response of the closed-loop AQR system is depicted, where a bandwidth range is gained for all considered test cases.

For all test cases without implementation of STATCOM the bandwidth frequency stays within the interval of $\omega_b = 4.63...5.48\,\frac{\text{rad}}{\text{s}}$ or $f_b = 0.74...0.87\,\text{Hz}$. It can be concluded that this bandwidth range falls below the maximum allowed bandwidth of 5 Hz stated in UK grid code. This fact implies that outer AVR does not require further slowdown in order to prevent system oscillations in a higher frequency range. On the other hand, the overall WPP control cannot be accelerated by advancing the speed of the outer AVR, as the system response depends on its slowest time constants. Hence, it seems reasonable to adjust the AVR time response in order to maintain the current bandwidth.

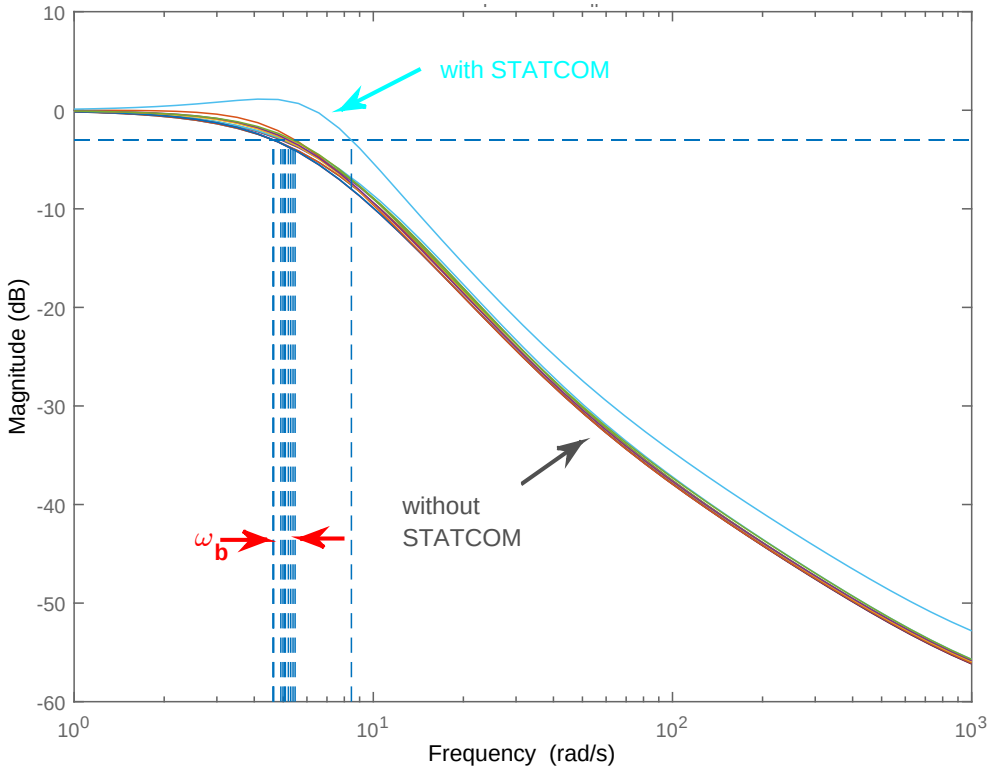

Fig. 7.8: Frequency response of closed-loop AQR system and bandwidth range ω_b for various test cases

Then, for first-order systems such as $F_{AVR}(s)$ the time constant T_{PO} can be calculated according to Eq. 7.5 [28, p. 132].

$$T_{PO} = \frac{1}{\omega_b} \tag{7.5}$$

In Fig. 7.8 the lowest bandwidth of $\omega_b = 4.63\,\frac{rad}{s}$ corresponds to the test case with SCR_{max} and $P_{WTG,0} = 0.5\,\text{pu}$. Likewise for the AQR, the AVR is designed for this particular test case as a starting point, so that a time constant $T_{PO} = 0.22\,\text{s}$ is obtained.

However, in Fig. 7.8 it can be observed that the bandwidth deviates significantly for the implementation of STATCOMs ($\omega_b = 8.45\,\frac{\text{rad}}{\text{s}}$ or $f_b = 1.34\,\text{Hz}$). This is due to the fact that the AQR has been designed with respect to a WPP operation without STATCOMs. Hence, the integration of STATCOMs leads to a deviating system performance (cp. Fig. 7.7). Still, the obtained value for T_{PO} is used as a default AVR design and it is checked later on, whether it can be applied for a WPP operation with STATCOMs.

7.2.2 Definition of Slope Gain K_{PO}

According to the UK grid code the voltage slope is defined by „the percentage change in voltage, based on nominal, that results in a change of reactive power from 0 to Q_{min}

or 0 to Q_{max}“ [6]. As the required reactive capability corresponds to 0.95 leading or lagging power factor, the maximum reactive power supply for this WPP amounts to $\Delta Q_{PCC} = \pm 69.02\,\text{Mvar}$. With a default slope setting of 4 %, imposed by *National Grid*, the slope gain will be according to Eq. 7.6.

$$K_{PO} = \frac{100}{slope\,[\%]} = \frac{\Delta Q_{PCC}}{\Delta V} = \frac{69.02}{0.04} = 2301\,\frac{\text{Mvar}}{\text{pu}} \tag{7.6}$$

However, the UK grid code requires flexible voltage slope changes in a range of 2 - 7 % depending on the WPP location. Hence, it is necessary to evaluate the system performance for various slope gains K_{PO}.

7.3 Performance Analysis of Voltage Control

The performance of voltage control with the previously designed AQR and AVR can be evaluated by a step response of the system. Fig. 7.9 shows the results of voltage control for a default slope of 4 % and two different grid stiffnesses SCR_{max} and SCR_{min}. The PCC voltage is stepped down from 1 to 0.95 pu at a time equal to 1 s. The dynamic behaviour of the voltage and reactive power at the PCC is depicted in Fig. 7.9.

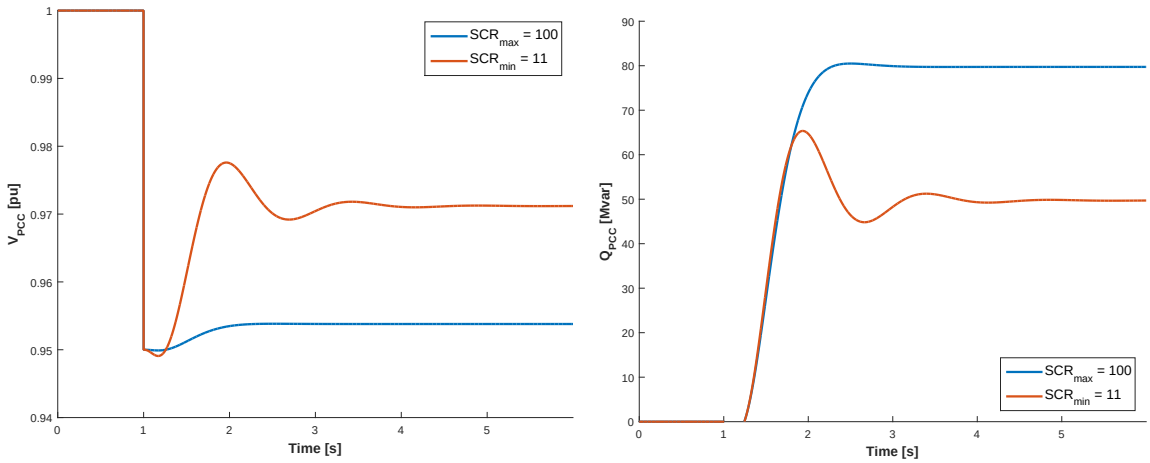

Fig. 7.9: Voltage control performance for a slope of 4 % and different grid stiffnesses SCR_{max} and SCR_{min}

Following observations are made:

- Compensating voltage disturbances by slope control is less affected in strong grids (SCR_{max}), where the PCC voltage is improved towards $V_{PCC} = 0.954\,\text{pu}$, compared to weak grids (SCR_{min}), where the PCC voltage is improved towards $V_{PCC} = 0.971\,\text{pu}$.

- Voltage control in weaker grids requires less reactive power ($Q_{PCC} = 50\,\text{Mvar}$) compared to stronger grids ($Q_{PCC} = 80\,\text{Mvar}$) to eliminate the voltage error to a greater extent (in this way „apply less and achieve more“).

Regarding the dynamic behaviour, it can be seen that the performance with SCR_{min} is degraded compared to SCR_{max} with respect to overshoot and settling time.

Now, in order to assess the relative stability of the system with regard to the slope gain K_{PO}, the open-loop frequency characteristic is shown in Fig. 7.10 for SCR_{max} and SCR_{min}.

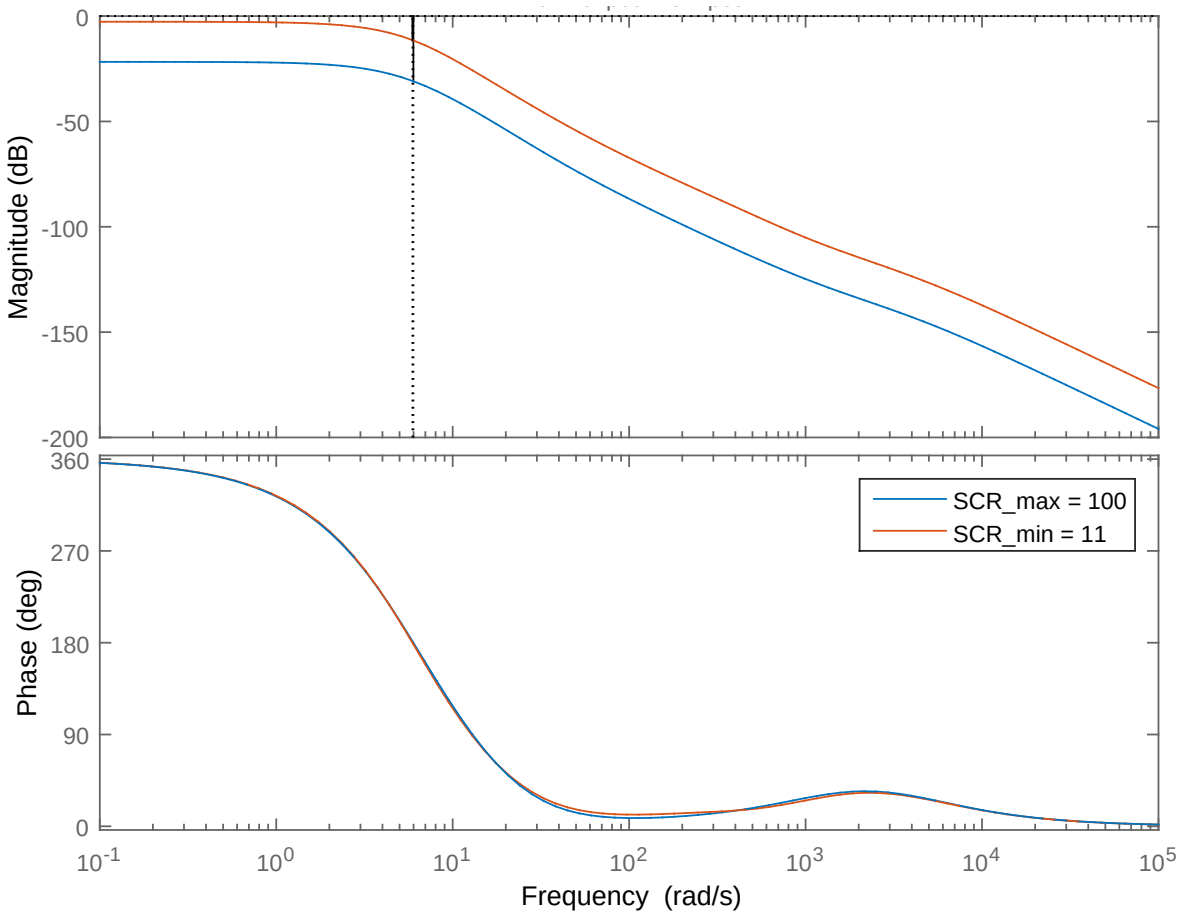

Fig. 7.10: Open-loop frequency characteristic of the overall WPP voltage control system for SCR_{max} and SCR_{min}

Besides an infinite phase margin for both grid stiffnesses, there are differences regarding the gain margin. A system with SCR_{max} has a larger gain margin ($G_m = 30.9\,\text{dB}$) compared to a system with SCR_{min} ($G_m = 11.4\,\text{dB}$). This implies that the overall open-loop gain of the system is not only affected by K_{PO}, but also by the grid stiffness.

In [2, p. 27 ff.] it is ascertained that the open-loop gain K_T of the system can be obtained according to Eq. 7.7, where X_{grid} is the external grid reactance, which is inversely

proportional to SCR, when the grid resistance is neglected (cp. Eq. 5.20 - 5.22 in chapter 5.3).

$$K_T = X_{grid} \cdot K_{PO} = \frac{X_{grid}}{slope} \tag{7.7}$$

Thus, for a certain SCR_1 with a certain $slope_1$, there will always exist another $slope_2$ for another SCR_2, that leads to the same open-loop gain K_T. Systems for equal open-loop gains, where the remaining parameters such as the time constant T_{PO} are unchanged, would exhibit the same frequency characteristic and in this way similar dynamic performance. This relationship is described by Eq. 7.8 and illustrated by Fig. 7.11.

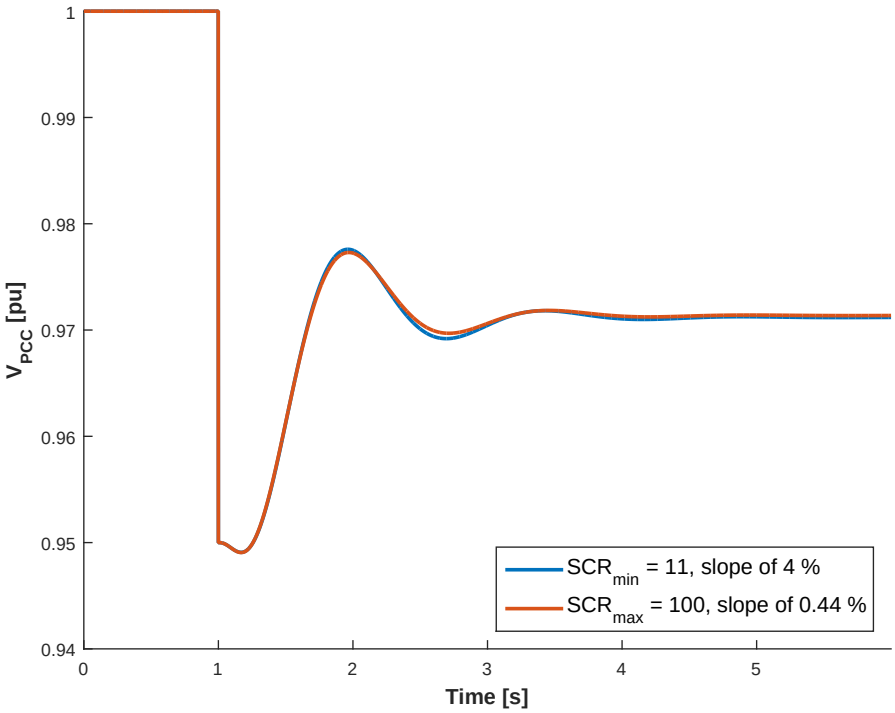

Fig. 7.11: Voltage control performance for different grid stiffnesses and different slopes leading to similar dynamic performance

It shows a step down of PCC voltage from 1 to 0.95 pu, where for SCR_{min} a slope of 4 % is used and for SCR_{max} a corresponding slope of 0.44 % is calculated.

$$SCR_x \cdot slope_x \sim K_T \tag{7.8}$$

The dynamic behaviour is relatively similar, where a maximum error of only 0.05 % is obtained. Hence, the coherence of SCR and voltage slope by Eq. 7.8 is approved. It is applied in the following section for tuning the AVR in order to meet the grid code requirements for various SCRs.

7.4 Tuning of AVR

In the next stage the design specifications such as overshoot, rise and settling time, which are stated in chapter 4.3, are considered for evaluating the dynamic performance of the system. There are decent software tools available in order to perform control design and tuning for extended systems as the one considered in this study. *Mathworks* offers a platform called *SISO Design Tool*, which is applied for the tuning process being realized for the following operating conditions:

- System time delay of $T = 0.2\,\mathrm{s}$, as it acts as worst-case consideration for a maximum permitted commencement of reactive power supply
- Reactive power contribution by only WTGs with initial active power of $P_{WTG,0} = 0.5\,\mathrm{pu}$
- Different grid stiffnesses $SCR_{max} = 100$ and $SCR_{min} = 11$

The default control architecture is shown in Fig. 7.12, where $G_{Q_{ref}^{WPP} V_{PCC}}(s)$ is the plant transfer function, which covers both AQR, time delay and WPP network.

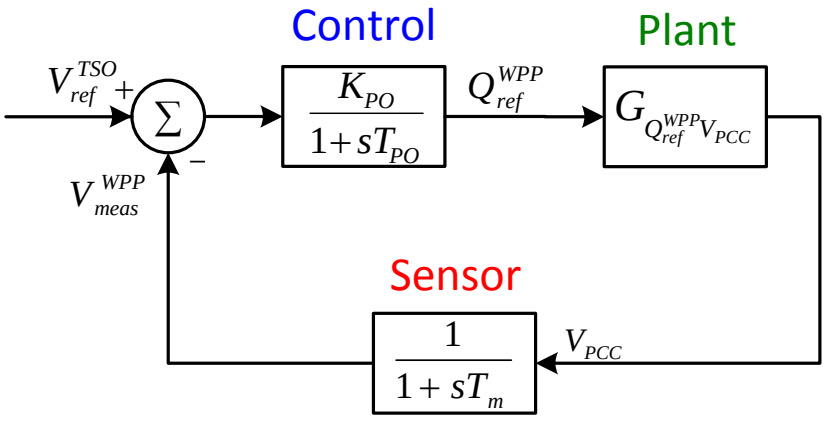

Fig. 7.12: Control architecure used for AVR tuning

Due to the extent of the WPP including all individual WTGs, the plant transfer function is characterized by a high-order model and requires further order reduction in order to be used for *SISO Design Tool*. Noticing that WPP behaves like a first-order system (cp. chapter 6.2) and considering one pole introduced by the AQR and the time delay respectively, it seems reasonable to reduce $G_{Q_{ref}^{WPP} V_{PCC}}(s)$ to a third-order system.

As illustrated by the Bode plots in Fig. 7.13, the reduced transfer function displays the same characteristics within the bandwidth of interest compared to the original transfer function and hence can be used for AVR tuning.

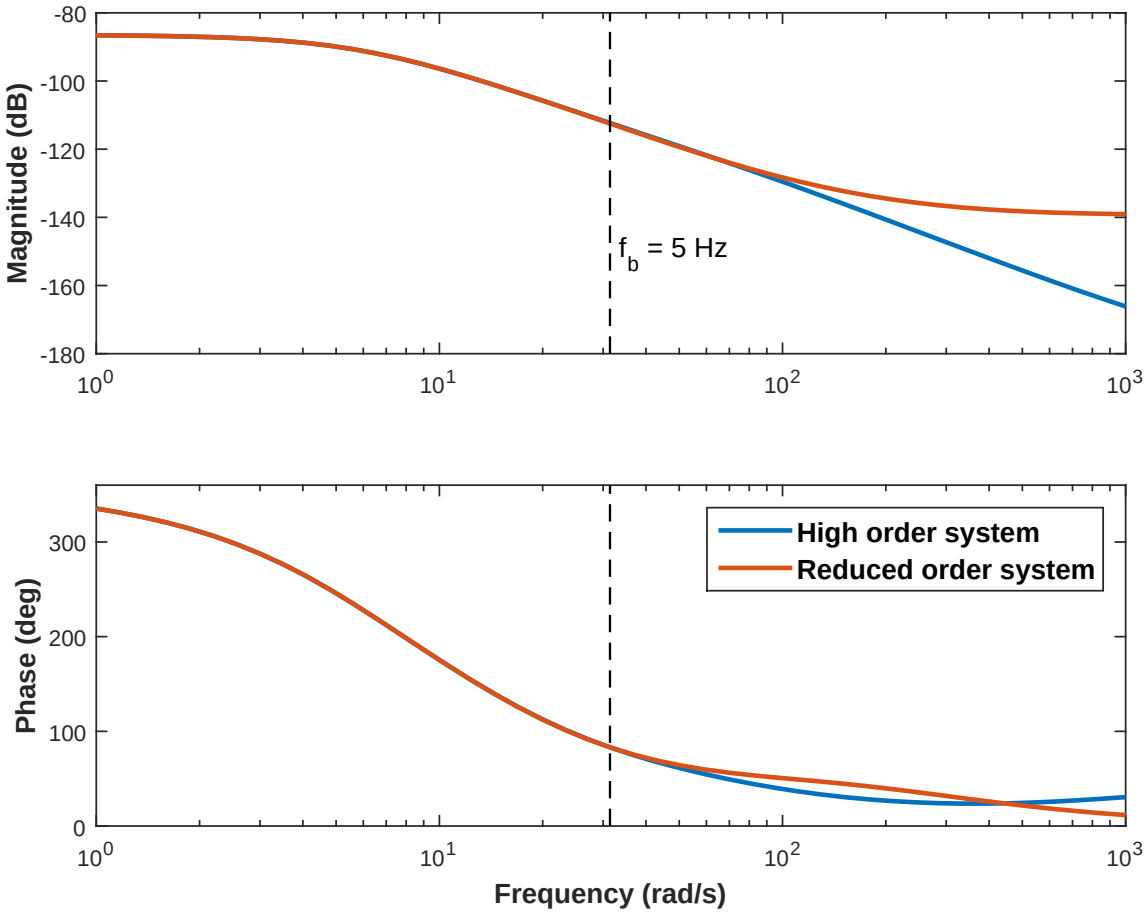

Fig. 7.13: Frequency response of $G_{Q_{ref}^{WPP}V_{PCC}}(s)$ for high-order system and reduced-order system

Now, the closed-loop poles of the system are analyzed by plotting the root locus of the open-loop system. In Fig. 7.14 the colored areas delimit the forbidden area for placing the poles of the system in order to fulfill the design criteria. The vertical line is associated with the settling time value t_s provided. The two rays, starting at the root locus origin, specify the allowed percent of overshoot (OS). The rise time cannot be directly displayed in root locus. However, for the following test cases with a default time constant of $T_{PO} = 0.22\,\mathrm{s}$ it does not constitute a crucial constraint and hence does not require thorough investigation.

For the case with SCR_{max} it can be seen in Fig. 7.14 that the requirements can be fulfilled for a default slope of 4 %, when observing the encircled closed-loop poles, which are located closest to the imaginary axis.

However, moving those poles to the right by gain adjustment provides the boundary value of K_{PO} before violating the design criteria. In Fig. 7.15 the gain is constrained by the overshoot criteria and leads to corresponding minimum slope of 0.7 %. Further reduction

of the slope would cause a too large overshoot of the system response and at a certain point also to non-compliance regarding the settling time.

For the case with SCR_{min} it is observed in Fig. 7.16 that the design criteria are violated. While the settling time constraint is just fulfilled, the system response will show too large overshoot.

Again, the gain can be adjusted to meet the specifications, which is illustrated in Fig. 7.17. The resulting K_{PO} reveals that a corresponding voltage slope of 6.3 % must not be deceeded in order to remain grid code compliant.

However, depending on the connection agreements with the TSO the WPP operator must be able to control the PCC voltage with flatter slope characteristics, at the extreme by a slope setting of 2 %.

It is ascertained that lower slope values are achievable, if the time response of the AVR is prolonged. Fig. 7.18 depicts such a case for a slope of 4 %, where the time constant is increased to $T_{PO} = 0.6\,\mathrm{s}$. Moving the corresponding open-loop pole (encircled in red) to the right modifies the root locus, so that the closed-loop poles is kept inside the permitted area.

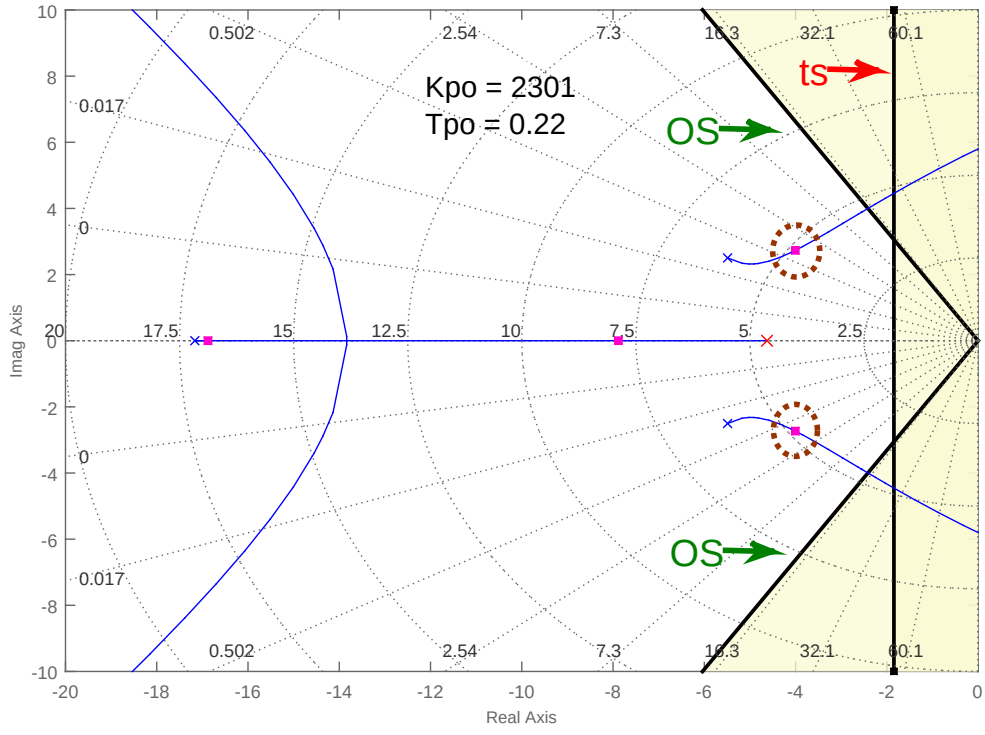

Fig. 7.14: Root locus plot of AVR open-loop system with SCR_{max} and slope of 4 %

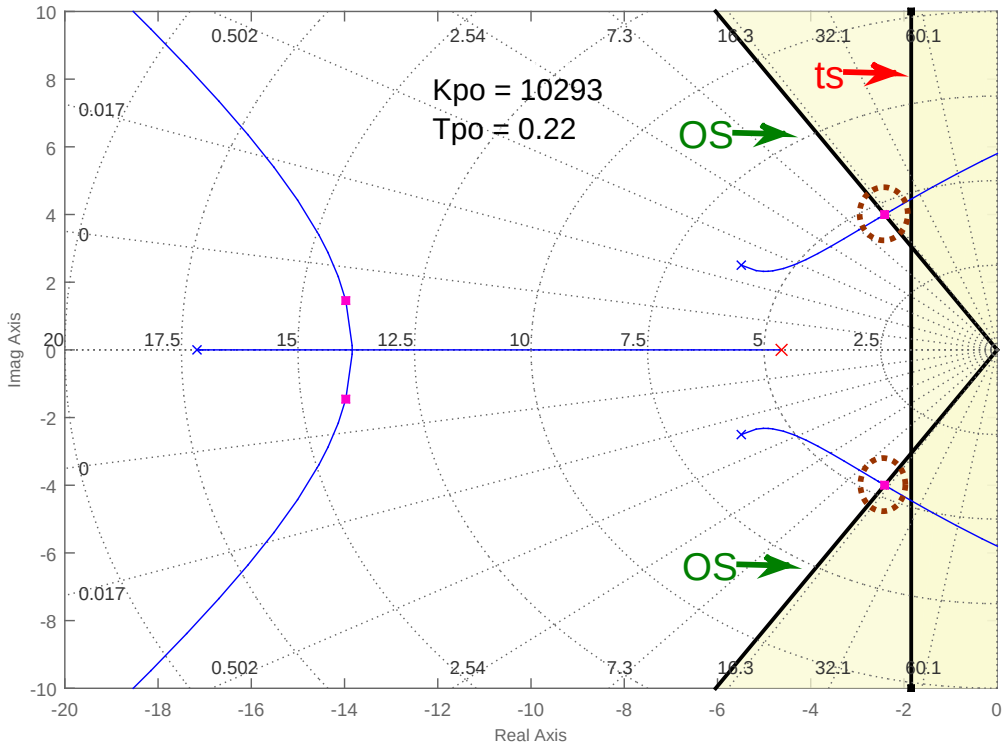

Fig. 7.15: Root locus plot of AVR open-loop system with SCR_{max} and slope of 0.7 %

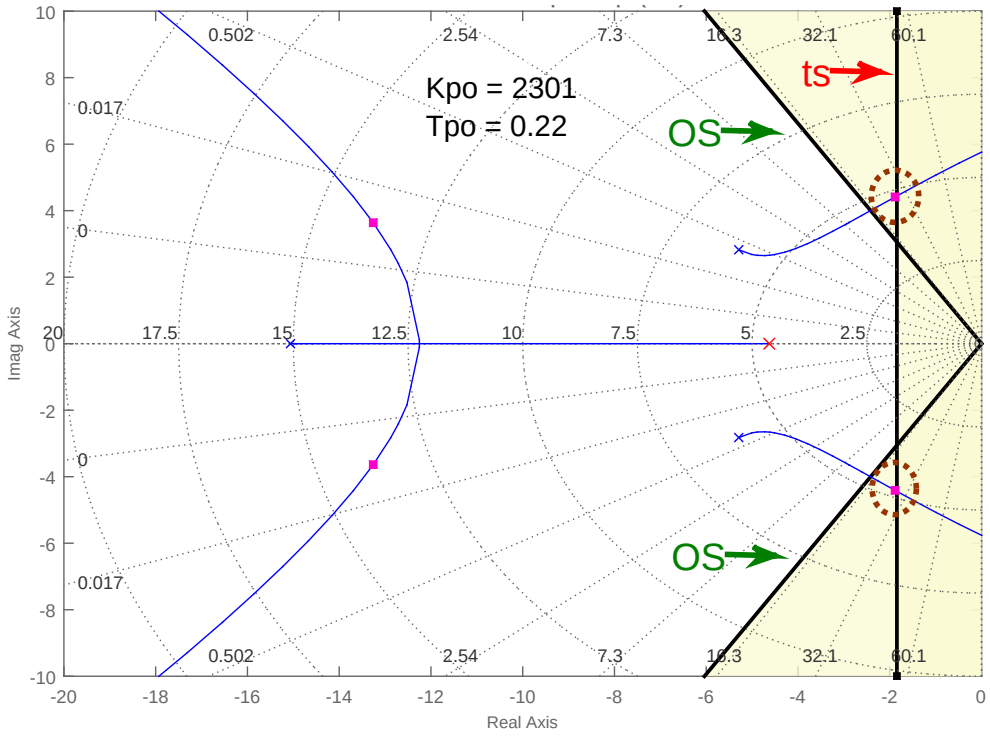

Fig. 7.16: Root locus plot of AVR open-loop system with SCR_{min} and slope of 4 %

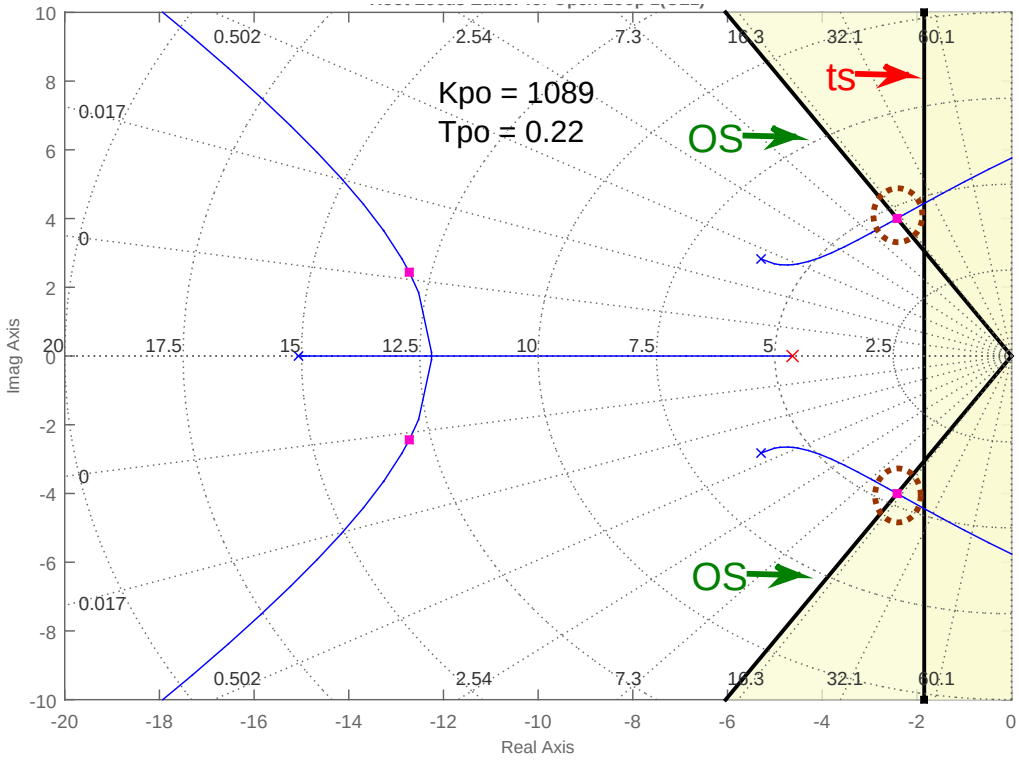

Fig. 7.17: Root locus plot of AVR open-loop system with SCR_{min} and slope of 6.3 %

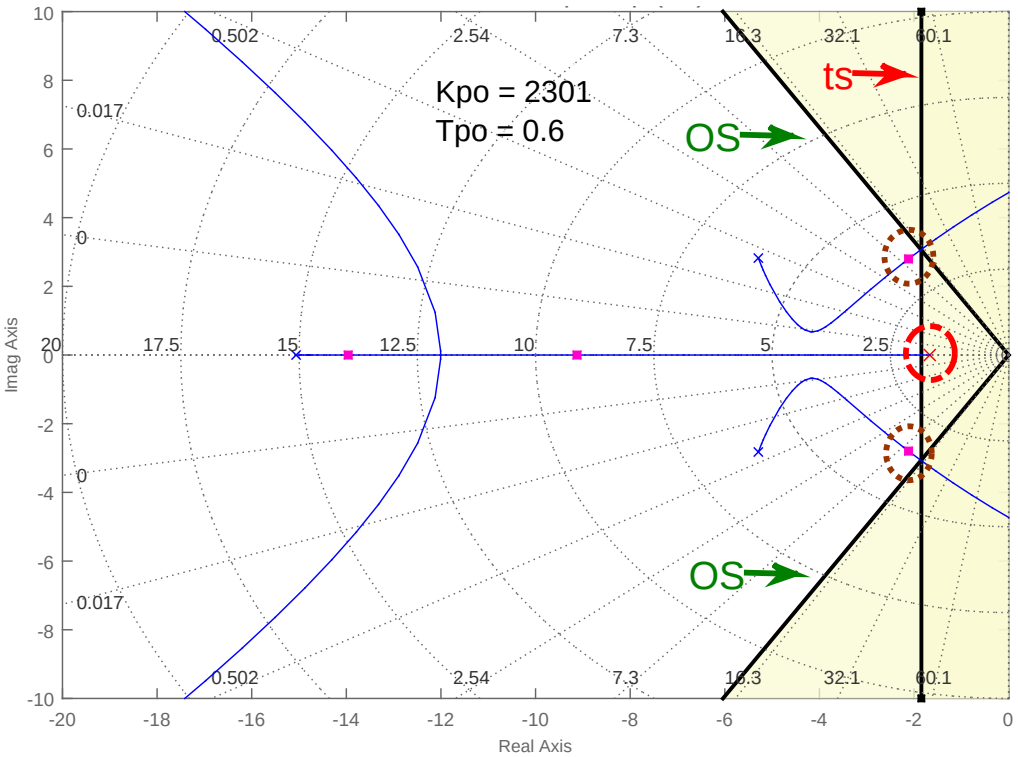

Fig. 7.18: Root locus plot of AVR open-loop system with SCR_{min} and slope of 4 % and an increased time constant of $T_{PO} = 0.6\,\mathrm{s}$

However, it needs to be clearly stated that decelerating the time response of the AVR augments the rise time of the output signal. Hence, its constraint has to be regarded when adjusting the time constant in order to enable lower slope values for low SCR.

Finally, the observations made in this section regarding design specifications for various SCRs can be connected to the relationship between SCR vs. slope that has been outlined in section 7.3. In this way, it is possible to obtain a boundary SCR value that still fulfills the performance criteria for a specified slope setting under the default design parameters of the AVR.

An exemplary study case is provided, where the WPP voltage control has to adjust its slope setting to a minimum value of 2 %. Knowing from Fig. 7.15 that for $SCR_{max} = 100$ a slope value of 0.7 % will still meet the performance criteria, one can determine the minimum SCR^*_{min}, for which a slope value of 2 % can be applied with present AVR settings. The relation of Eq. 7.8 is applied in Eq. 7.9.

$$SCR^*_{min} = \frac{SCR_{max} \cdot 0.7\,\%}{2\,\%} = \frac{100 \cdot 0.7\,\%}{2\,\%} = 35 \tag{7.9}$$

It implies that the designed AVR can operate for short-circuit ratios of $35 < SCR < 100$, while a WPP connection to grids with $SCR < 35$ requires further adjustment of the AVR time constant T_{PO} in order to fulfill the design criteria made in this study.

However, it should be noted that the tuning process is performed under certain conditions stated in the beginning of this section. Subsequently, the WPP voltage control is assessed for various test cases, based on the present AVR design and tuning process.

7.5 Verification of Design and Tuning Process

To verify the main conclusions of previous sections and to show the impact of different operating conditions of the WPP, the step responses for a PCC voltage change of $\Delta V_{PCC} = -5\,\%$ are performed. The following figures show the step response of the system when the PCC voltage is stepped down at time equal to 0 s. The curves show the WPP reactive power output and the red coloured areas highlight the forbidden points defined by overshoot, rise and settling time requirement. The dashed line at $t = 0.2\,\mathrm{s}$ indicates the delay time constraint.

Fig. 7.19 shows the system response for various initial active power values of the WTGs.

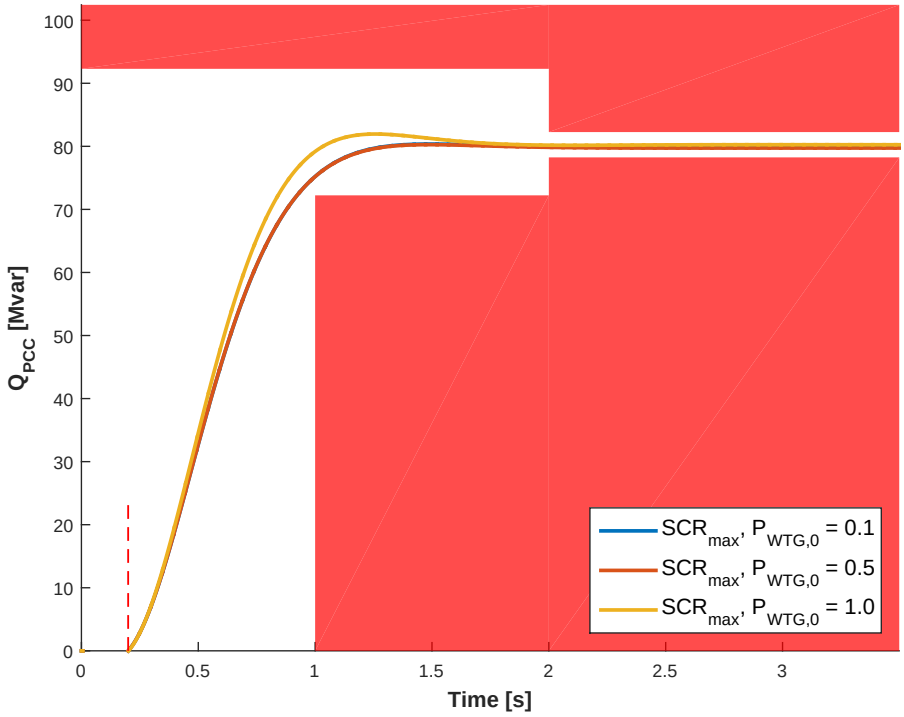

Fig. 7.19: System step response ($\Delta V_{PCC} = 5\,\%$) for a slope of 4 %, SCR_{max} and various operating conditions of the WTGs

For $P_{WTG,0} = 0.1\,\text{pu}$ and $P_{WTG,0} = 0.5\,\text{pu}$ similar performances are observed, while the scenario of rated WTG power ($P_{WTG,0} = 1\,\text{pu}$) leads to more overshoot ($\Delta OS = 1.4\,\%$). Hence, when performing control design and tuning for average wind conditions ($P_{WTG,0} = 0.5\,\text{pu}$), it needs to be regarded that voltage control performance changes slightly for other wind conditions. In this way, it seems reasonable to include some margins in the tuning process to fulfill the requirements for all operating conditions.

Fig. 7.20 compares a case with and without implementation of STATCOM for voltage control.

The system response is accelerated by the integration of STATCOMs, as additional reactive power is initiated compared to the test case with only WTGs contributing. The settling time is comparable for both test cases. However, the overshoot is increased significantly by $\Delta OS = 3.7\,\%$. Similar deviations of those two test cases have already been observed during the AQR designing process (cp. Fig. 7.3 in section 7.1). Thus, for the most suitable control design it is recommended to regard whether the WPP will incorporate the STATCOMs into voltage control permanently or not. Depending on this decision, the parameters of both AQR and AVR should be selected during the design process.

However, both Fig. 7.19 and 7.20 illustrate that the grid code requirements are fulfilled, which has been ascertained by the root locus plot of Fig. 7.14.

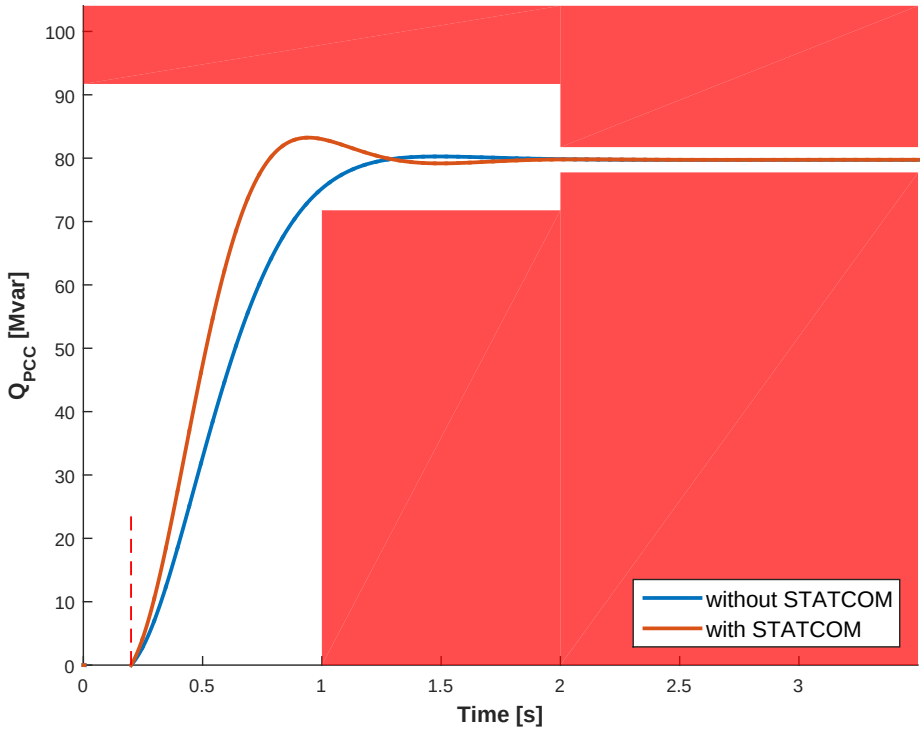

Fig. 7.20: System step response ($\Delta V_{PCC} = 5\,\%$) for a slope of 4 %, SCR_{max} with and without implementation of STATCOM

Now, the step response in Fig. 7.21 aims to validate the observations made during the tuning process for SCR_{min} and a slope of 4 %. As analyzed by the root locus plot of Fig. 7.16, an AVR with $T_{PO} = 0.22\,\mathrm{s}$ produces too large overshoot, which is sufficiently reduced by adjusting the time constant towards $T_{PO} = 0.6\,\mathrm{s}$ (cp. Fig. 7.18). This improvement can be confirmed by comparing both graphs in Fig. 7.21.

Finally, it is checked whether a step response with $SCR^{*}_{min} = 35$, calculated as boundary value by Eq. 7.9 in previous section, fulfills the performance criteria for a minimum slope of 2 %. In Fig. 7.22 the reactive power output response stays within the permitted area, just fulfilling the overshoot and settling time criteria. Hence, the mathematical determination of SCR^{*}_{min} is confirmed.

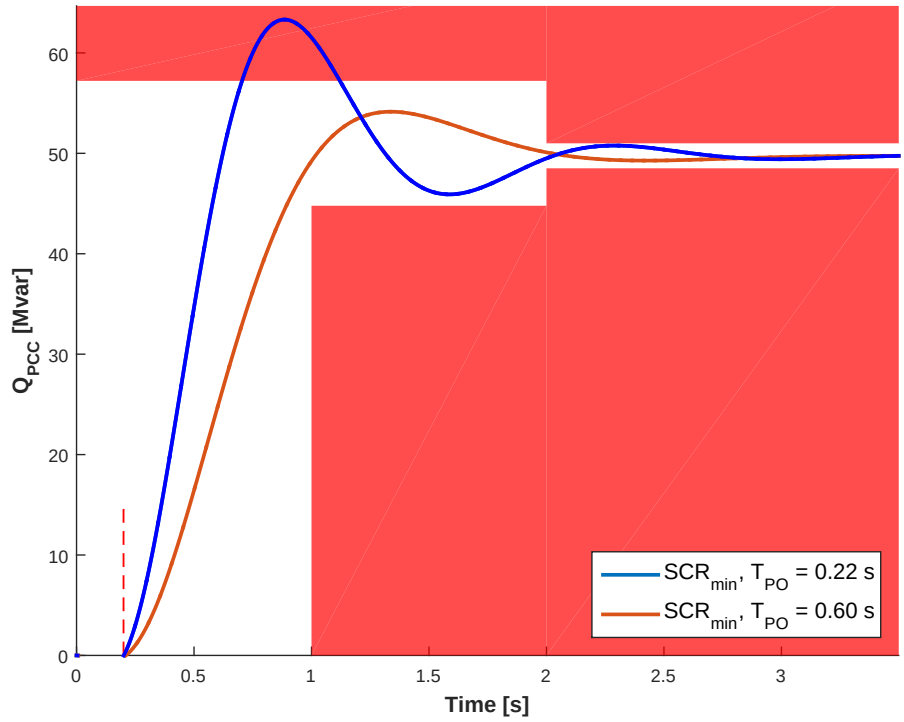

Fig. 7.21: System step response ($\Delta V_{PCC} = 5\,\%$) for a slope of 4 %, SCR_{min} for different AVR time constants

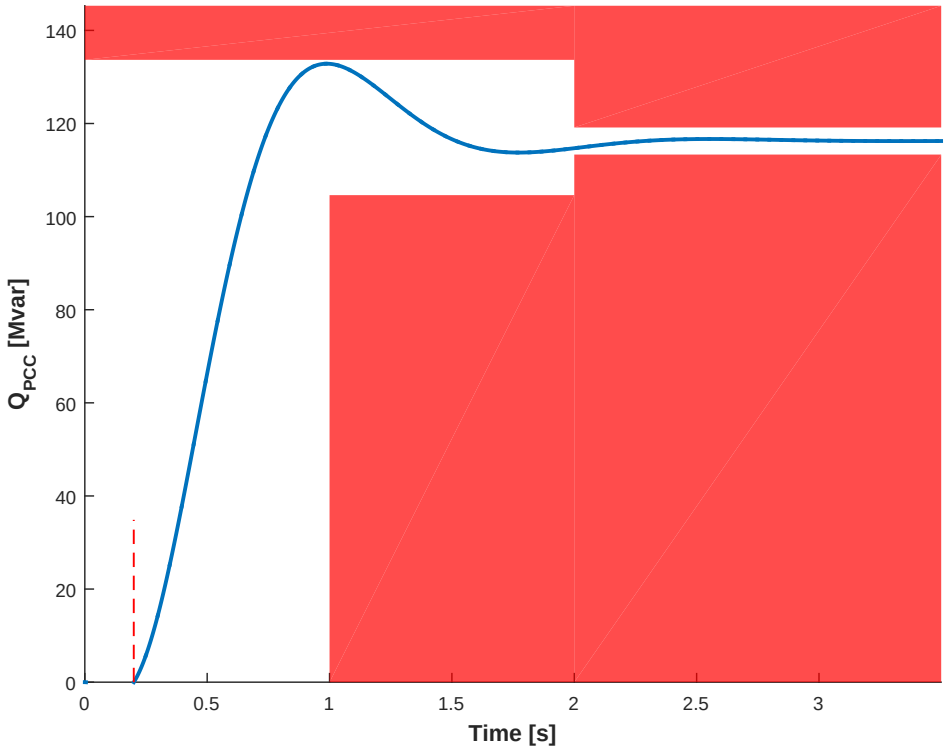

Fig. 7.22: System step response ($\Delta V_{PCC} = 5\,\%$) for a slope of 4 % and $SCR = 35$

7.6 Guidelines for Control Design and Tuning

Based on the results presented in the previous sections some guidelines regarding the design and tuning of the voltage controller of a WPP can be provided. The aim of this guidance is to summarize the outcomes of the assessment studies and in equal measure serve as a basic manual to parametrize the voltage control architecture considered in this project.

Prior to setting up the individual design and tuning steps, following information is required for the particular WPP under consideration:

- As it is crucial for the slope control performance, the stiffness of the external grid should be provided. The corresponding grid impedance may suffer unexpected changes, hence the TSO normally provides a minimum and maximum short-circuit ratio SCR_{min} and SCR_{max} being valid for a particular point of connection.
- A fixed slope setting of the voltage controller is defined by the TSO and should be provided. However, the TSO may decide to modify the predefined slope, in this case a range of possible slope values is necessary to be regarded.
- As it constitutes a major concern for the control performance, the system delays need to be obtained. The controller sampling time and the downstream communication delays from the WPP controller to the WTGs can be aggregated to one value used for control design.
- It has been ascertained during the assessment studies that the presence of STATCOMs affects the voltage control performance significantly, in particular for present time delays. Hence, it needs to be known for the design process whether STATCOMs are incorporated permanently for reactive power contribution or not.

A linearized model of the WPP system needs to be developed in order to obtain the plant transfer functions. The model has to be initialized for a certain operating point of the WPP. Average wind speed conditions of all WTGs may serve as frequently occurring active power production of the WPP. As a starting point for the control design, it is sufficient to regard a maximum grid stiffness SCR_{max}. Then, the following design and tuning steps are proposed:

Design of inner control loop (AQR):

1. The plant function $G_{Q_{out}^{WPP}Q_{PCC}}(s)$, linking demanded and actual WPP reactive power supply without regarding present system delays, needs to be reduced to a second-order system to enable the usage of *Symmetrical Optimum* method.

2. The *Symmetrical Optimum* method is applied to parametrize the PI components of the AQR.
3. A *Smith Predictor* is implemented by using the plant function $G_{Q_{out}^{WPP}Q_{PCC}}(s)$ and the estimated time delays to enhance the AQR performance with due regard to present system delays.

Design of outer control loop (AVR):

4. The plant function $G_{Q_{ref}^{WPP}V_{PCC}}(s)$, linking reactive power setpoint and PCC voltage, needs to be reduced to a third-order system to reflect the dominant dynamics of AQR, system delays and WPP network.
5. The time constant of the slope control (AVR) is obtained by considering the bandwidth of the upstream system, which is defined by AQR, system delays and WPP network.
6. The gain of the slope control (AVR) is calculated by the predefined slope setting and the maximum reactive power capability of the WPP.

Tuning of outer control loop (AVR):

7. Root locus analysis is applicable in order evaluate the control performance according to the grid code requirements, for the demanded slope values and the grid parameters SCR_{max} and SCR_{min}.
8. In case of non-compliance for any of those cases in step 7., the AVR time constant is adjusted to enhance the control performance. The tuning process should account for some margins regarding the fulfillment of overshoot, rise and settling time requirement, since the system behaviour varies for different operating conditions.
9. The design and tuning process is concluded by performing step responses for various operating conditions of the WPP in order to validate the performance of the voltage control.

8 Conclusion and Outlook

8.1 Conclusion

This project has dealt with the topic of voltage control assessment in large WPPs, with the main focus on embedded application of both WTGs and STATCOM. With the aim of evaluating voltage control performance for various grid and operating conditions of WPPs, two main topics are elaborated: the development of a small-signal model for the system and the design and tuning process for a WPP voltage controller.

The selected control architecture is based on a centralized system, where the voltage control is managed only on WPP level and the WTGs and STATCOMs regulate their reactive power supply to fulfill the central control target. The voltage at the PCC is controlled according to a slope characteristic (AVR) and an additional reactive power control loop is applied for taking into account the reactive power losses within the WPP (AQR). The present work considers a relatively large offshore WPP located in UK, where the main point of interest is, besides different possible grid stiffnesses, to incorporate both WTGs and STATCOMs for voltage control.

The WPP consists of full-scale converter connected WTGs and two STATCOMs, which are represented by a state-space model. It is proved by Eigenvalue analysis that only the dynamics of the outer reactive power controller are relevant with respect to the bandwidth of the overall voltage control. The model functionality is successfully validated against a numerical EMT model, with the outcome that the linearized state-space model provides adequate results, even in the case of larger reactive power changes.

The constructed small-signal model of the whole WPP is successfully validated by means of load flow simulations, thus it delivers satisfying outcomes regarding the voltage states of the whole network. In this way, the dynamic behaviour within the WPP is assessable with respect to voltage control, which enables the implementation of various dispatch strategies to analyze reactive power contribution of the individual WTGs and STATCOMs.

The final design and tuning process of the WPP voltage controller provides qualitative outcomes regarding the impact of system delays, grid conditions and various operating

conditions of the WPP. Time delays caused by the communication network deteriorate the performance of the PI controller (AQR) and can be improved sufficiently by use of predictive controllers such as a *Smith Predictor*. The influence on different grid stiffnesses needs to be studied in combination with the specified slope characteristic of the voltage controller, as both of them determine the open-loop gain of the control system and in this way the control performance regarding overshoot, rise and settling time. The time constant of the AVR should be selected according to the bandwidth of the remaining system in order to provide a decent response time of voltage control. However, tendentially low values of SCR and flat slope characteristics complicate the fulfillment of overshoot and settling time requirement of the reactive power output response of the WPP. In this case, enhancing the AVR time constant can compensate for those concerns, though the rise time demand will be the crucial criteria to bear in mind. Different operating conditions of the WPP affect the control performance in minor ways, so that the tuning process should account some margins to ensure grid code compliance for all operating scenarios. However, it should be regarded for the control design and tuning whether voltage control is realized with or without STATCOMs, since both scenarios exhibit significant differences regarding overshoot of reactive power output.

The main contributions presented in this work can be concluded by the accomplishment of the three main objectives:

1. Various possible voltage control philosophes in WPPs have been characterized. It has been observed that the coordination of various strategies depends on factors such as grid stiffness and communication delays and the optimal voltage control strategy cannot directly be ascertained;
2. A small-signal model for the whole WPP system has been developed from scratch without usage of already built-in models. It is appropriate for analyzing various voltage control structures and dispatch strategies;
3. All the observations made during the assessment studies have been collected to provide a first guidance of how to design and tune the particular voltage control architecture considered in this study.

8.2 Outlook

The work presented in this project has approached the topic voltage control in WPPs by many aspects, but in particular the outcomes concluded from the state-of-the-art studies (chapter 2) reveal a lot of other important perspectives within this topic. Hence, future work should be pointed in the following direction:

Implementation in real-time digital simulator:

The results obtained by the state-space model of this project are to be verified by numerical simulations. All components like WTGs, plant layout and external grid can be represented in a real-time digital simulator, which is available in the laboratory facilities at Aalborg University (*Smart Energy Systems Laboratory*). Moreover, it is possible to implement the designed and tuned voltage control in a decicated wind power plant controller for validation purposes. In this way, control assessment is achievable under various conditions including realistic communication networks and data traffic. [50]

In this context, the results of this project will be used in the Danish *RePlan* project „Ancillary Services from Renewable Power Plants“ (PSO Project number: 2015-12347).

Various control strategies:

In chapter 2 various control strategies have been introduced for both WPP main controller and WTG level. As this project has only used a *centralized* voltage control approach with Q compensator for design and tuning purpose, it seems reasonable to investigate alternative architectures with the same target and analyze how they influence the overall performance of the voltage control. As outlined in chapter 2.5, various combinations for control coordination on WPP and WTG level are possible. On WTG level, it has already been shown in [14] that a *distributed* control strategy can benefit the performance for present communication delays and low SCR. On WPP level, the reactive power feed-forward option (Fig. 2.5 II.c) seems auspicious with regard to reduce the system response in the presence of long communication delays. Moreover, on the fly changes of control modes on WPP level can be of relevance for different operating conditions and should be scrutinized.

Dispatch function:

In this project the function of dispatching reference signals to the individual units (WTGs and STATCOMs) in different ways has not been paid attention to. However, various approaches have been presented in chapter 2.3, which should be considered and possibly extended in order to optimize the incorporation of reactive power providing units.

It is one of the great advantages of the developed WPP model in this project to enable such studies by assessing important information (i.e. voltage limits, Q capability) within the WPP network. In particular, the supportive function of STATCOMs regarding reactive power supply, depending on certain operating conditions, can be worth to investigate.

Control interactions:

If multiple WPPs are connected to one PCC, it is important to study the interactions that could occur between different slope controls of different WPPs. In this particular case a master-master configuration could lead to hunting effects between the voltage controllers; the alternative of using a master-slave configuration might be challenging in terms of control cascading. It is also of interest to investigate the interaction of different controls of different generations units within the WPP. Problems may occur for a *distributed* control strategy, where all WTGs are regulating the voltage at their respective POC independent from each other.

Bibliography

[1] Müfit Altin, Remus Teodorescu, Birgitte Bak-Jensen, Pedro Rodriguez, Florin Iov, and Philip C Kjær. Wind power plant control-an overview. In *9th International Workshop on Large-Scale Integration of Wind Power into Power Systems*, 2010.

[2] Jorge Martinez Garcia. *Voltage control in wind power plants with doubly fed generators*. Aalborg University, The Faculty of Engineering and Science, Department of Energy Technology, 2010.

[3] Remus Teodorescu, Marco Liserre, and Pedro Rodriguez. *Grid converters for photovoltaic and wind power systems*, volume 29. John Wiley & Sons, 2011.

[4] Bindeshwar Singh. Introduction to facts controllers in wind power farms: A technological review. *International Journal of Renewable Energy Research (IJRER)*, 2(2):166–212, 2012.

[5] National Grid - Guidance Notes - Power Park Modules, 2012.

[6] National Grid Electricity Transmission The Grid Code. Issue 5. Revision 13 2015.

[7] ANALOG DEVICES. Adsp-21990: Reference frame conversions. Technical report, Analog Devices Inc., 2012.

[8] Prabha Kundur, Neal J Balu, and Mark G Lauby. *Power system stability and control*, volume 7. McGraw-hill New York, 1994.

[9] Stephen J Chapman. Electric machinery fundamentals. 2004.

[10] Taruziwa Madangombe. *Integration of Wind Energy Systems Into the Grid: Power Quality and Technical Requirements*. PhD thesis, University of Cape Town, 2010.

[11] Ieee guide for identification, testing, and evaluation of the dynamic performance of excitation control systems. *IEEE Std 421.2-1990*, pages 1–44, Aug 1990.

[12] E Muljadi and CP Butterfield. Wind farm power system model development. In *World Renewable Energy Congress VIII, Colorado*, 2004.

[13] Z Saad-Saoud, ML Lisboa, JB Ekanayake, N Jenkins, and G Strbac. Application of statcoms to wind farms. *IEE Proceedings-Generation, Transmission and Distribution*, 145(5):511–516, 1998.

[14] Jorge Martinez, PC Kjar, Pedro Rodriguez, and Remus Teodorescu. Comparison of two voltage control strategies for a wind power plant. In *Power Systems Conference and Exposition (PSCE), 2011 IEEE/PES*, pages 1–9. IEEE, 2011.

[15] Jorge Martinez and Philip C Kjaer. Fast voltage control in wind power plants. In *Power and Energy Society General Meeting, 2011 IEEE*, pages 1–7. IEEE, 2011.

[16] Jens Fortmann, Michael Wilch, Friedrich W Koch, and István Erlich. A novel centralised wind farm controller utilising voltage control capability of wind turbines. In *PSCC Power System Computation Conference*, 2008.

[17] Thomas Ackermann et al. *Wind power in power systems*, volume 140. Wiley Online Library, 2012.

[18] Anca D Hansen, Poul Sørensen, Florin Iov, and Frede Blaabjerg. Centralised power control of wind farm with doubly fed induction generators. *Renewable Energy*, 31(7):935–951, 2006.

[19] Rogério G de Almeida, Edgardo D Castronuovo, and JA Peas Lopes. Optimum generation control in wind parks when carrying out system operator requests. *Power Systems, IEEE Transactions on*, 21(2):718–725, 2006.

[20] Mark E Cardinal, Robert W Delmerico, Nicholas W Miller, and Reigh A Walling. Windfarm collector system loss optimization, August 9 2011. US Patent 7,994,658.

[21] Andrzej Grzegorz Adamczyk. *Damping of Low Frequency Power System Oscillations with Wind Power Plants*. PhD thesis, Aalborg University, The Faculty of Engineering and Science, 2012.

[22] Cuiqing Du, Ambra Sannino, and Math HJ Bollen. Analysis of the control algorithms of voltage-source converter hvdc. In *Power Tech, 2005 IEEE Russia*, pages 1–7. IEEE, 2005.

[23] JL Rodriguez-Amenedo, S Arnaltes, and MA Rodriguez. Operation and coordinated control of fixed and variable speed wind farms. *Renewable energy*, 33(3):406–414, 2008.

[24] H Huang, C Mao, J Lu, and D Wang. Small-signal modelling and analysis of wind turbine with direct drive permanent magnet synchronous generator connected to power grid. *IET Renewable Power Generation*, 6(1):48–58, 2012.

[25] Jorge Martinez, Philip C Kjær, Pedro Rodriguez, and Remus Teodorescu. Design and analysis of a slope voltage control for a dfig wind power plant. *Energy Conversion, IEEE Transactions on*, 27(1):11–20, 2012.

[26] Xiao-Ping Zhang, Christian Rehtanz, and Bikash Pal. *Flexible AC Transmission Systems: Modelling and Control: Modelling and Control*. Springer Science & Business Media, 2012.

[27] Jian Sun. Small-signal methods for ac distributed power systems–a review. *Power Electronics, IEEE Transactions on*, 24(11):2545–2554, 2009.

[28] Charles L Phillips and John M Parr. *Feedback control systems*. Pearson, 2011.

[29] Jerzy MosHcinHski and Zbigniew Ogonowski. Advanced control with matlab and simulink, 1999.

[30] R.W. Brockett. Poles, zeros, and feedback: State space interpretation. *Automatic Control, IEEE Transactions on*, 10(2):129–135, Apr 1965.

[31] National Electricity Transmission System Security and Quality of Supply Standard, 2012.

[32] EN 50160 - Voltage characteristics of electricity supplied by public distribution systems.

[33] Z Li, H.; Chen. Overview of different wind generator systems and their comparisons. *Renewable Power Generation, IET , vol.2, no.2, pp.123,138*, 2008.

[34] Bo Wen, Dushan Boroyevich, Rolando Burgos, Paolo Mattavelli, and Zhe Shen. Analysis of dq small-signal impedance of grid-tied inverters.

[35] DIgSILENT GmbH. Technical documentation - two-winding transformer (3-phase).

[36] DIgSILENT GmbH. Technical documentation - three-winding transformer (3-phase).

[37] Bhavik.N Suthar Manish J. Chauhan, Jigar S. Sarda and Viren B. Pandya. Enhancement of low voltage ride through capability of dfig based wind farm using mechanically switched capacitor. *Journal of Information, Knowledge and Research in Electrical Engineering.*, 01-02, Nov 11-Oct 12.

[38] National Grid. Electricity ten year statement (etys) 2012 - appendix d - fault levels.

[39] Technical regulation 3.2.5 for wind power plants with a power output greater than 11 kW, 2010.

[40] TN Preda, K Uhlen, DE Nordgard, and T Toftevaag. External grid representation for assessing fault ride through capabilities of distributed generation units. In *Innovative Smart Grid Technologies (ISGT Europe), 2012 3rd IEEE PES International Conference and Exhibition on*, pages 1–9. IEEE, 2012.

[41] Giddani O Kalcon, Grain P Adam, Olimpo Anaya-Lara, Stephen Lo, and Kjetil Uhlen. Small-signal stability analysis of multi-terminal vsc-based dc transmission systems. *Power Systems, IEEE Transactions on*, 27(4):1818–1830, 2012.

[42] IEEE. Ieee recommended practice for industrial and commercial power systems analysis. 1997.

[43] Saioa Buruchaga Laza Volodymyr Myagkov, Lennart Petersen. Parametric variation for detailed model of external grid in offshore wind farms. *Aalborg Universitet*, 2014.

[44] Vestas Wind Systems A/S. General specification - v112 3.0 mw 50/60 hz. Technical report, 2011.

[45] Dierk Schröder. *Elektrische Antriebe-Regelung von Antriebssystemen*, volume 10. Springer Science & Business Media, 2009.

[46] Chandra Bajracharya, Marta Molinas, Jon Are Suul, Tore M Undeland, et al. Understanding of tuning techniques of converter controllers for vsc-hvdc. In *Nordic Workshop on Power and Industrial Electronics (NORPIE/2008), June 9-11, 2008, Espoo, Finland*. Helsinki University of Technology, 2008.

[47] E Ceanga, C Nichita, L Protin, and N Antonio Cutululis. Theorie de la commande des systemes. *Ed. Tehnica, Bucuresti*, 2001.

[48] Math Works Incorporation. Matlab user manual version 7.1 r14. *Math Works Incorporation, Natick, MA*, 2005.

[49] Ari Ingimundarson and Tore Hägglund. Robust tuning procedures of dead-time compensating controllers. *Control Engineering Practice*, 9(11):1195–1208, 2001.

[50] Aalborg University. Smart energy systems laboratory. *http://www.et.aau.dk/department/laboratory-facilities/smart-energy-systems-lab/*.

A Appendix

A.1 Small-Signal Model of WTG

A.1.1 Linearized Differential Equations

According to Eq. 5.1 to 5.9 of chapter 5.1 the linearized differential equations are obtained as follows. It should be noted that the mathematical description of the WTG in chapter 5.1 is performed in peak-values and has to be transformed to per-unit expressions prior to the linearization process.

$$\frac{d\Delta\varphi_1}{dt} = \Delta V_{DC} - \Delta V_{DC}^* \tag{A.1}$$

$$\frac{d\Delta\varphi_2}{dt} = K_{I,DC}\Delta\varphi_1 - \Delta i_{ACd} + K_{P,DC}\Delta V_{DC} - K_{P,DC}\Delta V_{DC}^* \tag{A.2}$$

$$\frac{d\Delta\varphi_3}{dt} = -V_{POC,0}\Delta i_{ACq} - \Delta Q_{WTG}^* - i_{ACq,0}\Delta V_{POC} \tag{A.3}$$

$$\begin{aligned}\frac{d\Delta\varphi_4}{dt} &= K_{I,Q}\Delta\varphi_3 - (K_{P,Q}V_{POC,0} + 1)\cdot\Delta i_{ACq} \\ &\quad - K_{P,Q}\Delta Q_{WTG}^* - K_{P,Q}i_{ACq,0}\Delta V_{POC}\end{aligned} \tag{A.4}$$

$$\begin{aligned}\frac{d\Delta i_{ACd}}{dt} &= \frac{K_{P,id}K_{I,DC}}{L\cdot t_b}\Delta\varphi_1 + \frac{K_{I,id}}{L\cdot t_b}\Delta\varphi_2 - \frac{K_{P,id}}{L\cdot t_b}\Delta i_{ACd} \\ &\quad + \frac{K_{P,id}K_{P,DC}}{L\cdot t_b}\Delta V_{DC} - \frac{K_{P,id}K_{P,DC}}{L\cdot t_b}\Delta V_{DC}^*\end{aligned} \tag{A.5}$$

$$\begin{aligned}\frac{d\Delta i_{ACq}}{dt} &= \frac{K_{P,iq}K_{I,Q}}{L\cdot t_b}\Delta\varphi_3 + \frac{K_{I,iq}}{L\cdot t_b}\Delta\varphi_4 - \frac{K_{P,iq}(K_{P,Q}V_{POC,0}+1)}{L\cdot t_b}\Delta i_{ACq} \\ &\quad - \frac{K_{P,iq}K_{P,Q}}{L\cdot t_b}\Delta Q_{WTG}^* - \frac{K_{P,iq}K_{P,Q}i_{ACq,0}}{L\cdot t_b}\Delta V_{POC}\end{aligned} \tag{A.6}$$

$$\begin{aligned}\frac{d\Delta V_{DC}}{dt} &= -\frac{V_{POC,0}}{C\cdot t_b\cdot V_{DC,0}}\Delta i_{ACd} - \frac{V_{POC,0}i_{ACd,0}}{C\cdot t_b\cdot V_{DC,0}^2}\Delta V_{DC} \\ &\quad - \frac{i_{ACd,0}}{C\cdot t_b\cdot V_{DC,0}}\Delta V_{POC} + \frac{1}{C\cdot t_b}\Delta I_{SG}\end{aligned} \tag{A.7}$$

$$\Delta i_{AC,Re} = (1 - \frac{\delta_{POC}^2}{2})\Delta i_{ACd} - \delta_{POC}\Delta i_{ACq} - (i_{ACd,0}\delta_{POC,0} + i_{ACq,0})\Delta\delta_{POC} \tag{A.8}$$

$$\Delta i_{AC,Im} = (1 - \frac{\delta_{POC}^2}{2})\Delta i_{ACq} + \delta_{POC}\Delta i_{ACq} + (i_{ACd,0} - i_{ACq,0}\delta_{POC,0})\Delta\delta_{POC} \tag{A.9}$$

$$\Delta Q_{WTG} = -V_{POC,0}\Delta i_{ACq} - i_{ACq,0}\Delta V_{POC} \tag{A.10}$$

Consequently matrices $\boldsymbol{A}$, $\boldsymbol{B}$, $\boldsymbol{C}$ and $\boldsymbol{D}$ are given as follows:

$$\boldsymbol{A} = \begin{bmatrix} 0 & 0 & 0 & 0 & 0 & 0 & a_{17} \\ a_{21} & 0 & 0 & 0 & a_{25} & 0 & a_{27} \\ 0 & 0 & 0 & 0 & 0 & a_{36} & 0 \\ 0 & 0 & a_{43} & 0 & 0 & a_{46} & 0 \\ a_{51} & a_{52} & 0 & 0 & a_{55} & 0 & a_{57} \\ 0 & 0 & a_{63} & a_{64} & 0 & a_{66} & 0 \\ 0 & 0 & 0 & 0 & a_{75} & 0 & a_{77} \end{bmatrix}$$

$a_{17} = 1$

$a_{21} = K_{I,DC}$, $a_{25} = -1$, $a_{27} = K_{P,DC}$

$a_{36} = -V_{POC,0}$

$a_{43} = K_{I,Q}$, $a_{46} = -(K_{P,Q}V_{POC,0} + 1)$

$a_{51} = \frac{K_{P,id}K_{I,DC}}{L \cdot t_b}$, $a_{52} = \frac{K_{I,id}}{L \cdot t_b}$, $a_{55} = -\frac{K_{P,id}}{L \cdot t_b}$, $a_{57} = \frac{K_{P,id}K_{P,DC}}{L \cdot t_b}$

$a_{63} = \frac{K_{P,iq}K_{I,Q}}{L \cdot t_b}$, $a_{64} = \frac{K_{I,iq}}{L \cdot t_b}$, $a_{66} = -\frac{K_{P,iq}(K_{P,Q}V_{POC,0}+1)}{L \cdot t_b}$

$a_{75} = -\frac{V_{POC,0}}{C \cdot t_b \cdot V_{DC,0}}$, $a_{77} = -\frac{V_{POC,0}i_{ACd,0}}{C \cdot t_b \cdot V_{DC,0}^2}$

$$\boldsymbol{B} = \begin{bmatrix} 0 & 0 & b_{13} & 0 & 0 \\ 0 & 0 & b_{23} & 0 & 0 \\ b_{31} & b_{32} & 0 & 0 & 0 \\ b_{41} & b_{42} & 0 & 0 & 0 \\ 0 & 0 & b_{53} & 0 & 0 \\ b_{61} & b_{62} & 0 & 0 & 0 \\ 0 & b_{72} & 0 & b_{74} & 0 \end{bmatrix}$$

$b_{13} = -1$

$b_{23} = -K_{P,DC}$

$b_{31} = -1,\ b_{32} = -i_{ACq,0}$

$b_{41} = -K_{P,Q},\ b_{42} = -K_{P,Q} i_{ACq,0}$

$b_{53} = -\frac{K_{P,id} K_{P,DC}}{L \cdot t_b}$

$b_{61} = -\frac{K_{P,iq} K_{P,Q}}{L \cdot t_b},\ b_{62} = -\frac{K_{P,iq} K_{P,Q} i_{ACq,0}}{L \cdot t_b}$

$b_{72} = -\frac{i_{ACd,0}}{C \cdot t_b \cdot V_{DC,0}},\ b_{74} = \frac{1}{C \cdot t_b}$

$$\boldsymbol{C} = \begin{bmatrix} 0 & 0 & 0 & 0 & c_{15} & c_{16} & 0 \\ 0 & 0 & 0 & 0 & c_{25} & c_{26} & 0 \\ 0 & 0 & 0 & 0 & 0 & c_{36} & 0 \end{bmatrix}$$

$c_{15} = 1 - \frac{\delta_{POC}^2}{2},\ c_{16} = -\delta_{POC}$

$c_{25} = \delta_{POC},\ c_{16} = 1 - \frac{\delta_{POC}^2}{2}$

$c_{36} = -V_{POC,0}$

$$\boldsymbol{D} = \begin{bmatrix} 0 & 0 & 0 & 0 & d_{15} \\ 0 & 0 & 0 & 0 & d_{25} \\ 0 & d_{32} & 0 & 0 & 0 \end{bmatrix}$$

$d_{15} = -i_{ACd,0} \delta_{POC,0} - i_{ACq,0}$

$d_{25} = i_{ACd,0} - i_{ACq,0} \delta_{POC,0}$

$d_{32} = -i_{ACq,0}$

A.1.2 Initialization of Small-Signal Model

The small-signal model is initialized according to the steady-state values of the state variables $\mathbf{x_0}$. The initial values being used for matrices $\boldsymbol{A}$, $\boldsymbol{B}$, $\boldsymbol{C}$ and $\boldsymbol{D}$ are obtained as follows.

The actual active power $P_{WTG,0}$ and reactive power output $Q_{WTG,0}$ of the individual WTG as well as the voltage magnitude $V_{POC,0}$ and angle $\delta_{POC,0}$ at the POC are calculated by load flow simulation of the whole WPP network. Then the initial currents in dq-reference frame emerge according to Eq. A.11.

$$\begin{cases} i_{ACd,0} = \frac{P_{WTG,0}}{V_{POC,0}} \\ i_{ACq,0} = -\frac{Q_{WTG,0}}{V_{POC,0}} \end{cases} \tag{A.11}$$

The initial DC-link voltage is at its nominal value of $V_{DC,0} = V_{DC,n} = 1\,\text{pu}$.

A.2 Parameters of WTG

Tab. A.1 lists the parameters for type-4 WTG being used for the studied case. It shows both the absolute values used for the PLECS model as well as the per-unit values for the state-space model.

Tab. A.1: Parameters of type-4 WTG for the studied case

Parameter		Absolute value		Per-unit value [pu]
Rated power	$P_{WTG,r}$	1.5	MW	1
Rated AC voltage (LN)	$V_{AC,r}$	$\frac{690}{\sqrt{3}}$	$\mathrm{V_{RMS}}$	1
Rated current	$I_{AC,r} = \frac{P_{WTG,r}}{3 \cdot V_{AC,r}}$	1255	$\mathrm{A_{RMS}}$	1
Nominal DC voltage	$V_{DC,n}$	1200	V	1
Base AC impedance	$Z_{AC,b} = \frac{V_{AC,r}}{I_{AC,r}}$	0.3174	Ω	1
Base DC impedance	$Z_{DC,b} = \frac{V_{DC,n}}{I_{AC,r}}$	0.9562	Ω	1
Rated frequency	f	50	Hz	-
Base angular velocity	$\omega_b = 2\pi f$	314.16	$\frac{\mathrm{rad}}{\mathrm{s}}$	-
Base time	$t_b = \frac{1}{\omega_b}$	0.0032	s	-
Base inductance	$L_b = \frac{Z_{AC,b}}{\omega_b}$	1.01	mH	1
Base capacitance	$C_b = \frac{1}{\omega_b Z_{DC,b}}$	3.33	mF	1
Converter inductance	L_C	0.4879	mH	0.4830
Transformer inductance	L_T	0.1733	mH	0.1751
Series inductance	$L = L_C + L_T$	0.6612	mH	0.6680
DC-link capacitor	C	1.9782	mF	0.5942
DC voltage controller	$K_{P,DC}$	0.74	$\frac{\mathrm{A}}{\mathrm{V}}$	0.5
	$K_{I,DC}$	29.58	$\frac{\mathrm{A}}{\mathrm{Vs}}$	$20/s$
Q controller	$K_{P,Q}$	$5.92 \cdot 10^{-4}$	$\frac{\mathrm{A}}{\mathrm{var}}$	0.5
	$K_{I,Q}$	0.02367	$\frac{\mathrm{A}}{\mathrm{var \cdot s}}$	$20/s$
Current controller	$K_{P,id}$	5	$\frac{\mathrm{V}}{\mathrm{A}}$	15.75
	$K_{I,id}$	500	$\frac{\mathrm{V}}{\mathrm{As}}$	1575.31/s
	$K_{P,iq}$	2	$\frac{\mathrm{V}}{\mathrm{A}}$	6.30
	$K_{I,iq}$	500	$\frac{\mathrm{V}}{\mathrm{As}}$	$1575.31/s$

A.3 Small-Signal Model of WPP Network

A complete functional diagram of the WPP network model is given in Fig. A.1. For the sake of illustration, real components are marked green and imaginary components are marked red, while the remaining variables are marked blue. Each block represents a state-space function, which are finally linked together by decent MATLAB functions to form an overall state-space function with specified input and output variables.

Blocks $ssQ_{ref}I_{Re/IM}$, $ssVI_{Re/IM}$ and $ss\delta I_{Re/IM}$ represent the WTG model by linking Q reference, voltage magnitude and angle respectively to the current injections of the network. Their individual contribution are added up by $\sum I_{Re/Im}$.

Power flow Eq. 5.23 is represented by blocks $ssZ_{diagRe/Im}$, $ssY_{ndiagRe/Im}$ and $\sum I_{Re/Im} + I_{ndiagRe/Im}$, yielding in the respective bus voltages.

Linearizing Eq. 5.26 leads to Eq. A.12, which is represented by blocks $ssV_{Re/Im}\delta$ and $ssV_{Re/Im}V$.

$$\begin{cases} \Delta V = \frac{2 \cdot V_{Re,0}}{\sqrt{V_{Re,0}^2 + V_{Im,0}^2}} \Delta V_{Re} & + \frac{2 \cdot V_{Im,0}}{\sqrt{V_{Re,0}^2 + V_{Im,0}^2}} \Delta V_{Im} \\ \Delta \delta = -\frac{V_{Im,0}}{V_{Re,0}^2} \Delta V_{Re} & + \frac{1}{V_{Re,0}} \Delta V_{Im} \end{cases} \tag{A.12}$$

Finally, Eq. 5.27 requires linearization being expressed by Eq. A.13, where $V_{PCC} = V_2$ and $\delta_{PCC} = \delta_2$, and in Fig. A.1 represented by blocks $ss\delta Q_{Pcc}$ and $ssVQ_{PCC}$.

$$\Delta Q_{PCC} = \frac{2V_{PCC,0} - V_{grid,0}(1 - \frac{1}{2}\delta_{PCC,0}^2)}{X_{grid}} \Delta V_{PCC} + \frac{V_{grid,0} V_{PCC,0} \delta_{PCC,0}}{X_{grid}} \Delta \delta_{PCC} \tag{A.13}$$

Likewise for the WTG state-space model, the initial steady-state values are obtained by load flow simulations.

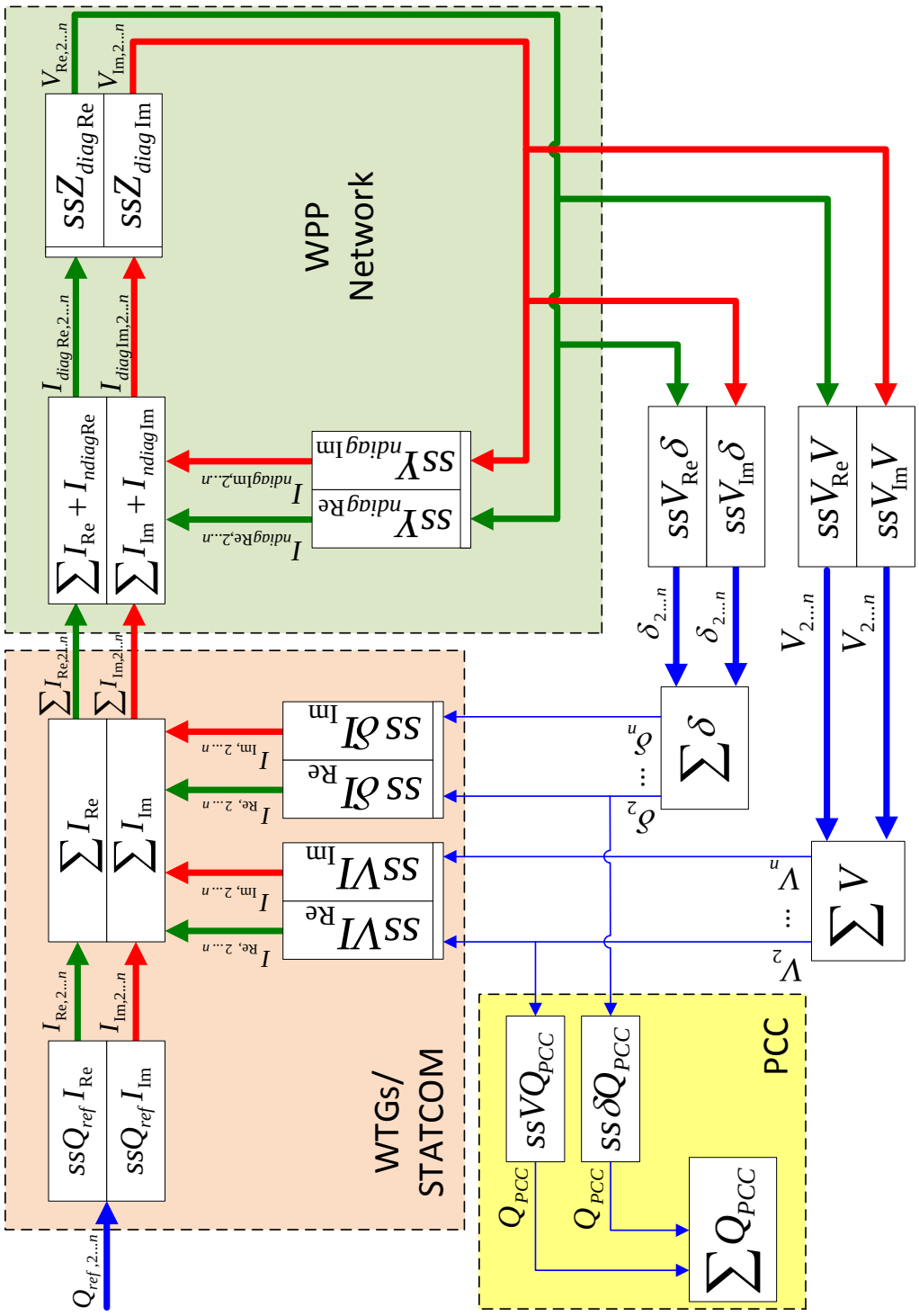

Fig. A.1: Detailed functional diagram of wind power plant network model

A.4 Power Flow Studies

Power flow studies are carried out in the simulation tool *DIgSILENT PowerFactory* in order to assess whether the WPP can fulfill the steady-state reactive power capacity requirements. According to the UK grid code the WPPs are required to supply certain reactive power at certain active power outputs at PCC as outlined in the WPP performance chart in Fig. A.2 Its boundary PQ levels are evaluated, as they represent the extreme cases of reactive power supply.

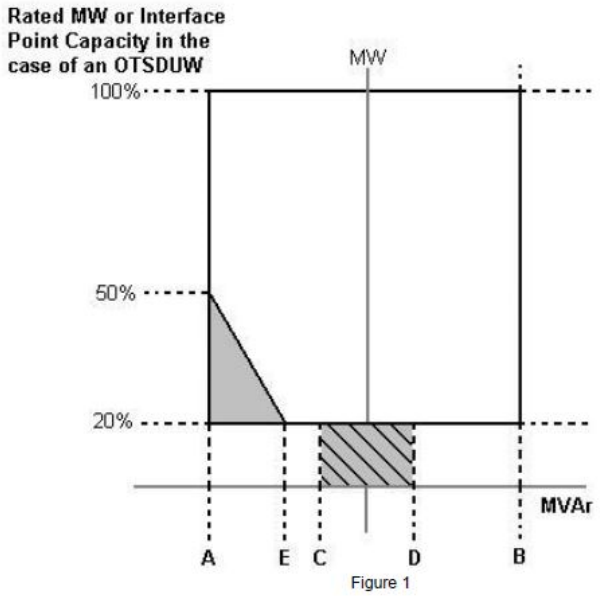

Point A is equivalent (in MVAr) to	0.95 leading Power Factor at Rated MW output or **Interface Point Capacity** in the case of **OTSDUW Plant and Apparatus**
Point B is equivalent (in MVAr) to:	0.95 lagging Power Factor at Rated MW output or **Interface Point Capacity** in the case of **OTSDUW Plant and Apparatus**
Point C is equivalent (in MVAr) to:	-5% of Rated MW output or **Interface Point Capacity** in the case of **OTSDUW Plant and Apparatus**
Point D is equivalent (in MVAr) to:	+5% of Rated MW output or **Interface Point Capacity** in the case of **OTSDUW Plant and Apparatus**
Point E is equivalent (in MVAr) to:	-12% of Rated MW output or **Interface Point Capacity** in the case of **OTSDUW Plant and Apparatus**

Fig. A.2: Wind farm PQ performance chart according to UK grid code [6]

The minimum and maximum required reactive power capacity is evaluated for an active power injection of 100 %, 50 %, 20 % and 0 % of rated WPP power. In Tab. A.2 the respective points, that need to be considered, are depicted. Each simulation in the Tab. A.2 is performed for short-circuit power levels corresponding to $SCR_{min} = 3.5$ and $SCR_{max} = 100$ (cp. chapter 5.3). It is worth mentioning that for assessing the steady-state performance the reactive power is provided only by the WTGs, since the Q capacity of the STATCOMs should be fully available for dynamic voltage control.

Tab. A.2: Reactive power requirements and corresponding wind turbine power output for example wind farm

Point in PQ chart	Rated output of $P_{WPP,r}$ [%]	Required Q capacity	Active Power $P_{WPP,r}$ [MW]	Reactive Power Q_{WPP} [Mvar]	WTG output P_{WTG} [MW]
Point A1	100	0.95 lead PF	210	-69.02	6
Point A2	50	0.95 lead PF	105	-69.02	3
Point E	20	-12% of $P_{WPP,r}$	42	-25.2	1.2
Point C	0	-5% of $P_{WPP,r}$	0	-10.5	0
Point D	20	+5% of $P_{WPP,r}$	0	10.5	0
Point B1	50	0.95 lag PF	105	69.02	3
Point B2	100	0.95 lag PF	210	69.02	6

According to [43] there are two crucial scenarios determining the largest voltage rise and drop along the the network busses:

- Point A2 with SCR_{min} for maximum voltage drop
- Point B2 with SCR_{min} for maximum voltage rise

The assessment studies show that the voltages at MV busses within the feeder exceed their limits of ± 10% for a minimum short-circuit ratio of $SCR_{min} = 3.5$. However, the voltage limits are just maintained, when the external grid is chosen to have a short-circuit power corresponding to $SCR_{min} = 11$. Hence, the assessment studies for dynamic voltage control are performed for the range of $SCR = 11...100$.

Another purpose of the power flow studies is to evaluate the effect of the MSR on reactive power supply of the individual WTGs under normal operating condtions, where $V_{PCC} = 1\,\text{pu}$. As the reactor banks of the MSR can be switched on and off, three exemplary steps of 0 %, 50 % and 100 % of the rated power of 50 Mvar are regarded. Tab. A.3 shows the WTG reactive power supply Q_{WTG} for those test cases and for SCR_{min} and SCR_{max}.

Tab. A.3: Calculated maximum error between state-space and load flow simulations

MSR rating	Q_{WTG} [Mvar] for SCR_{max}	Q_{WTG} [Mvar] for SCR_{min}
0 %	-1.74	-1.54
50 %	-1.12	-0.91
100 %	-0.48	-0.26

It can be concluded that for 100 % MSR rating the WTGs participate least in maintaining

the PCC voltage of $V_{PCC} = 1\,\text{pu}$. Hence, the assessment studies for dynamic voltage control are performed for this scenario, since this will allow the WTGs to contribute most during dynamic responses.

B Digital Appendix

A.1 Project Report

A.2 Figures

A.3 References